UiT
THE ARCTIC UNIVERSITY OF NORWAY

Faculty of Science and Technology
Department of Chemistry

Ligand Noninnocence In Manganese, Iron, and Cobalt Corroles

—

Sumit Ganguly

A dissertation for the degree of Philosophiae Doctor – November 2017

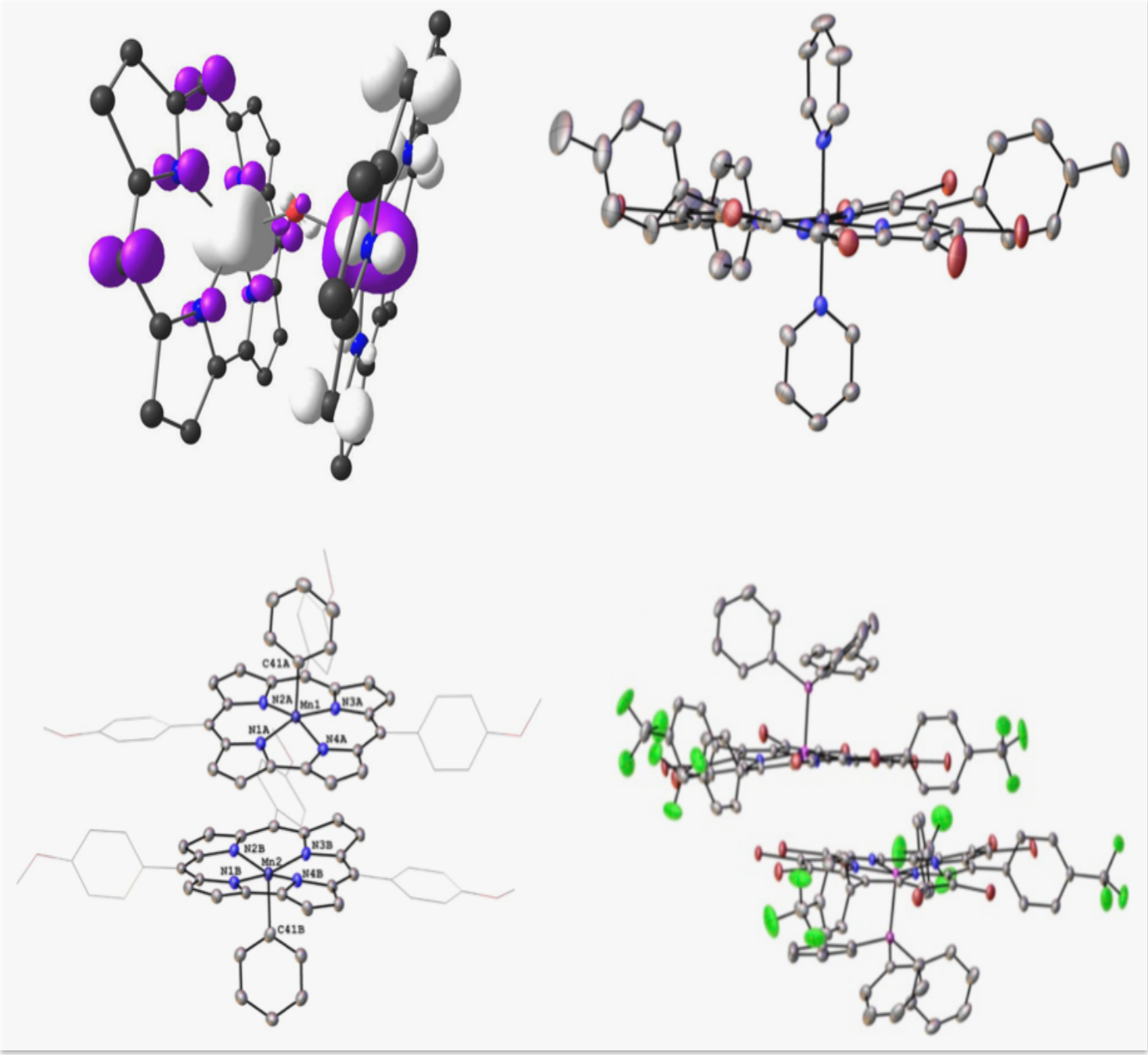

UNIVERSITY OF TROMSØ

A dissertation for the degree of Philosophiae Doctor

Ligand Noninnocence In Manganese, Iron, and Cobalt Corroles

Sumit Ganguly

Department of Chemistry

Faculty of Science and Technology

UiT – The Arctic University of Norway

Tromsø, Norway

Acknowledgements

First and foremost, I am deeply indebted to my mentor Prof. Abhik Ghosh for giving me the opportunity to explore the wonders of corrole chemistry and to conduct the research described herein. His scientific expertise and unfailing moral support have motivated me through the many challenging periods of my PhD years.

My sincere thanks also go to the two senior postdocs in our group, Dr. Kolle Thomas and Dr. Abraham Alemayehu, for their constant support and advice. They have been true friends, indeed elder brothers, to me these past years. I thank my fellow group members – Jan, Hugo, Hans-Kristian, Simon, Ivar, Rune, and Diemo – for their company and friendship both at and away from the laboratory. I am also thankful to our external collaborators, especially Prof. Jeanet Conradie, Dr. Ritimukta Sarangi, Dr. Kevin J. Gagnon, and Dr. Laura J. McCormick.

I am grateful to Valentina Vollan and Ronny Helland for their assistance with administrative matters and for organizing additional financial support on various occasions. I am also grateful to Jostein for his assistance with many mass spectrometric measurements.

I wish to thank my family in India for their unstinting support through my entire PhD journey. Likewise, I also wish to thank my in-laws in Bangladesh. Finally, my heartfelt thanks go to my wife Smritikana for being the rock of my life – without her unconditional support and constant encouragement, I would not have accomplished much of what I have described in the following pages.

Abstract

In recent years, first-row metallocorroles have provided some of the most instructive examples of noninnocent ligands. This thesis presents a study of some 50 iron, manganese, and cobalt corrole complexes with different axial ligands (including approximately 30 new compounds and 6 new X-ray structures) with emphasis on their noninnocent/innocent character. UV-vis spectroscopy has for some time provided a convenient empirical probe of ligand noninnocence in transition metal *meso*-tris(*para*-X-phenyl)corrole (T*p*XPC) complexes. Redshifts of the Soret maxima with increasing electron-donating character of the *para*-substituent X have indicated noninnocent systems, while substituent-insensitive Soret maxima have indicated innocent corrole ligands. I have greatly expanded the scope of this optical probe of noninnocence and used it to identify new classes of noninnocent metallocorroles.

The *μ*-oxo diiron corroles have long been thought of as true Fe(IV) complexes. However, as discussed in **Paper A**, a study of the optical spectra of $\{Fe[T\mathit{p}XPC]\}_2O$ derivatives along with DFT calculations have indicated a noninnocent description for these complexes.

Iron-aryl corroles are classic examples of true Fe(IV) species. Several Fe-aryl corroles were synthesized and examined together with other Fe corrole derivatives by means of UV-vis and NMR spectroscopy and electrochemistry in a detailed study for ligand noninnocence in a wide range of Fe corroles (**Paper B**). Analogous studies of Mn-aryl corroles were also carried out (Chapter 3), but these have not yet been written up as a manuscript. A collaborative study with the Stanford Synchrotron Radiation Lightsource also provided the first X-ray absorption spectroscopic analysis of the question of ligand noninnocence in Fe corrole complexes.

Cobalt-triphenylphosphine ($Co\text{-}PPh_3$) corroles have also been thought of as classic low-spin Co(III) complexes until now. An examination of the UV-vis spectra of $Co\text{-}PPh_3$ corroles and DFT calculations again indicated a partially noninnocent Co(II) corrole radical description for these complexes (**Paper C**). In contrast, an innocent description was indicated for $Rh\text{-}PPh_3$ corroles.

Finally, as discussed in **Paper D**, Co corrole pyridine adducts were likewise studied with a variety of spectroscopic techniques and the noninnocent behavior of the monopyridine adducts was elucidated in considerable detail.

Table of Contents

Acknowledgements 2
Abstract 3
Table of Contents 4
List of Abbreviations, Symbols, and Units 7
Conclusion..... 105
References..... 107
List of Papers 125

Chapter 1 – Introduction to Porphyrin and Corroles 10-26
1.1 General Properties 10
1.2 Structural Properties 11
1.3 Optical Properties 14
1.4.1 Synthesis of Porphyrins 16
1.4.2 Synthesis of Corroles 19
1.5 Modifications/Functionalization of Corroles 25

Chapter 2 – Introduction to Ligand Noninnocence 27-50
2.1 Introduction 27
2.2 Some Major Classes of Noninnocent Ligands 28-32
2.2.1 Dithiolene 28
2.2.2 Dioxolene 30
2.2.3 Diiminopyridine 31
2.2.4 Dioxygen 31
2.2.5 Nitric Oxide 32
2.2.6 Tetrapyrrole Ligands 32
2.3 Noninnocence and Innocence in Metallocorroles..... 33-49
2.3.1 Experimental Techniques for Identifying
Noninnocence in Metallocorroles 34
2.3.2 Ligand Noninnocence in Iron Corroles 35

(a) Chloroiron Corroles 35
(b) FeNO Corroles 36
(c) μ-Oxo Diiron Corroles 39
2.3.3 Ligand Noninnocence in Manganese Corroles 39
(a) MnCl Corroles 39
(b) Mn(V) Corroles 39
2.3.4 Noninnocence in Nickel and Platinum Corroles 40
2.3.5 Noninnocence in Copper and Silver Corroles 42
2.3.6 Innocent Metallocorroles 47
2.3.7 Conclusion 49

Chapter 3 – Manganese Corroles 51-68
3.1 Introduction 51
3.2 Manganese(III) Corroles 51
3.3 Chloromanganese Corroles 54
3.4 Manganese-Aryl Corroles 56
3.5 Electrochemistry of Mn(III), MnCl & Mn-aryl Corroles 57
3.6 New Results on Ligand Noninnocence in MnCl and MnPh Corroles 61

Chapter 4 – Iron corroles 69-84
4.1 Introduction 69
4.2 Iron(III) Corroles 69
4.3 Chloroiron Corroles 72
4.4 Iron-Aryl Corroles 77
4.5 μ-Oxo Diiron Corroles 78
4.6.1 Introduction to paper A: Wolves in Sheep's Clothing:
μ-Oxo-Diiron Corroles Revisited 80
4.6.2 Introduction to paper B: Ligand Noninnocence in Iron Corroles:
Insights from Optical and X-ray Absorption Spectroscopies
and Electrochemical Redox Potentials 82

Chapter 5 – Cobalt and Rhodium corroles.....85-104
5.1 Introduction.....85
5.2 Cobalt-Triphenylphosphine Corroles.....85
5.3 Cobalt-Bispyridine Corroles.....89
5.4 Rhodium Corroles 97
5.5.1 Introduction to paper C: Cobalt- and Rhodium-Corrole-
Triphenylphosphine Complexes Revisited:
The Question of a Noninnocent Corrole.....100
5.5.2 Introduction to paper D: Electronic Structure of
Cobalt-Corrole-Pyridine Complexes: Noninnocent
Five-coordinate Co(II) Corrole-Radical States 102

List of Abbreviations, Symbols, and Units

AcOH	acetic acid
Ar	aryl
ATP	adenosine triphosphate
Avg	average
BQ	benzoquinone
Bu	butyl
Cor	corrole
COD	1,5-cyclooctadiene
DCM	dichloromethane
DDQ	2,3-dichloro-5,6-dicyanobenzoquinone
DFT	density functional theory
DIP	diiminopyridine
DMF	*N*,*N*-dimethylformamide
DPM	dipyrromethanes
$E_{1/2}$	half-wave potential
equiv	equivalent
EPR	electron paramagnetic resonance
ESI-MS	electron spray ionization mass spectroscopy
Et	ethyl
$Fe_2(CO)_9$	diiron nonacarbonyl
Hb	hemoglobin
H_2[TPChl]	5,10,15,20-tetraphenylchlorin
H_2[TPP]	5,10,15,20-tetraphenylporphyrin
H_2[TPFPP]	5,10,15,20-tetrakis(pentafluorophenyl)porphyrin
H_3[TPC]	5,10,15-triphenylcorrole
H_3[OEC]	2,3,7,8,12,13,17,18-octaethylcorrole
H_3[OMC]	2,3,7,8,12,13,17,18-octamethylcorrole
H_2[OEP]	2,3,7,8,12,13,17,18-octaethylporphyrin
H_3[TPFPC]	5,10,15-tris(pentafluorophenyl)corrole
H_3[T*p*XPC]	5,10,15-tris(*para*-X-phenyl)corrole
H_3[TDCPC]	5,10,15-tris(2,6-dichlorophenyl)corrole
H_3[Me_8TPC]	2,3,7,8,12,13,17,18-octamethyl-5,10,15-triphenylcorrole

HOMO	highest occupied molecular orbital
ImH	imidazole
IR	infrared
LL'CT	ligand-to-ligand charge transfer
LUMO	lowest unoccupied molecular orbital
M	molar, mol/L; also, a metal atom
MCD	magnetic circular dichroism
Me	methyl
Mes	mesityl or 2,4,6-trimethylphenyl
min	minutes
mM	millimolar
MO	molecular orbital
nm	nanometer
n-Pr	*n*-propyl
NCS	*N*-chlorosuccinimide
NMR	nuclear magnetic resonance
OAc	acetate
Ph	phenyl
PhCN	benzonitrile
PLC	preparative thin-layer chromatography
PPh_3	triphenylphosphine
ppm	parts per million
py	pyridine
S	total spin quantum number
SCE	saturated calomel electrode
SQ	semiquinone
t-4bpa	tris(4-bromophenyl)aminium hexachloroantimonate
TBACl	tetrabutylammonium chloride
TBAP	tetrabutylammonium perchlorate
TDDFT	time-dependent density functional theory
TFA	trifluoroacetic acid
tma	trimethylamine
Tol	4-methylphenyl
Ts	tosyl or *p*-toluenesulfonyl

UV-vis	ultraviolet-visible
V	volt
XAS	x-ray absorption spectroscopy
XANES	x-ray absorption near-edge spectroscopy
Å	angstrom
λ	lambda
μ_B	Bohr magneton

Chapter 1 – Introduction to Porphyrins and Corroles

1.1 General Properties

Porphyrins are an important class of highly colored, aromatic compounds occur pervasively in nature. The unsubstituted porphyrin skeleton is called ‘porphine’ and it consists of four pyrrole rings linked together by ‘methine’ (=CH–) bridges. The macrocycle contains a total of 22 π-electrons including an [18]annulene substructure (shown in Fig. 1.1). The aromaticity of the conjugated π-system is responsible for intense absorption in the visible region of the electromagnetic spectrum, which is responsible for the brilliant deep-purple color of many porphyrins. In fact, the name ‘porphyrin’ originates from ‘*porphyra*’, the Greek word for ‘purple’. The neutral, free-base form of porphyrins contains two acidic protons, which can be deprotonated to yield the dianionic form which occurs as the ligand in many metal ion chelates. Metal complexes of porphyrins serve important roles in biological systems. For example, heme, which is an iron(II) porphyrin (Fig 1.2), acts as the prosthetic groups in many proteins, which are accordingly known as hemoproteins. Hemoproteins carry out many essential biological processes such as: (a) transport of oxygen in blood (hemoglobin), (b) binding and storage of oxygen in muscle (myoglobin), (c) ATP generation via electron transport (cytochromes b and c), and (d) dioxygen activation (cytochrome P450). Further, a reduced porphyrin complexed to a Mg(II) ion is present in the chromophore occurs as the pigment chlorophyll, the photosynthetic pigment in green plants.

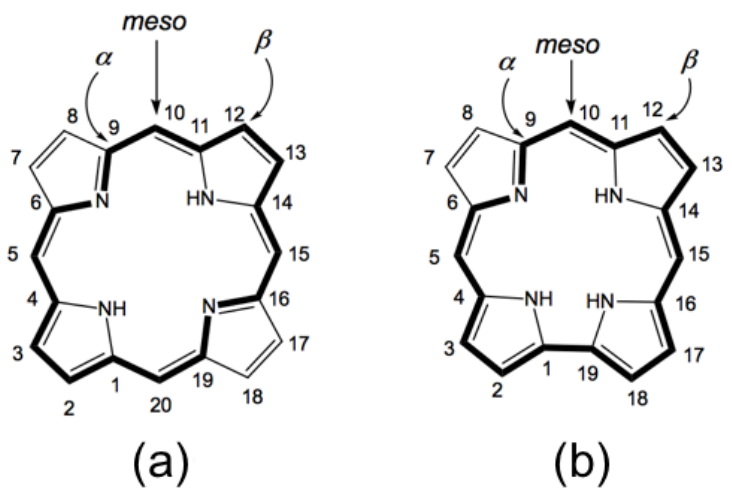

Fig. 1.1 IUPAC numbering for unsubstituted (a) free-base porphyrin or porphine and (b) unsubstituted free-base corrole. The [18]annulene substructure is shown in bold.

Corroles are an important class of porphyrinoid analogues, which have a direct bond (C_1-C_{19} bond) between two adjacent pyrrole units (see Fig. 1.1) and accordingly one less methine bridge. Corroles thus have a smaller coordination cavity than porphyrins. Further, unlike porphyrins, corroles have three pyrrole protons and thus can act as trianionic ligands (corrole^{3-}) towards metal ions. These two features together result in many formally high-valent metal complexes of corroles, where the metal is formally one oxidation unit higher than in related metalloporphyrin congeners. Despite the structural perturbation, corroles also contain an [18]annulene substructure. They are thus aromatic and also absorb strongly in the visible region of the electromagnetic spectrum. Unlike porphyrins, corroles are not known to occur in nature. Vitamin B_{12} contains a nonaromatic tetrapyrrole ring called corrin, which is complexed to a Co ion. A corrole is the fully aromatic counterpart of the naturally occurring corrin macrocycle (Fig. 1.2).

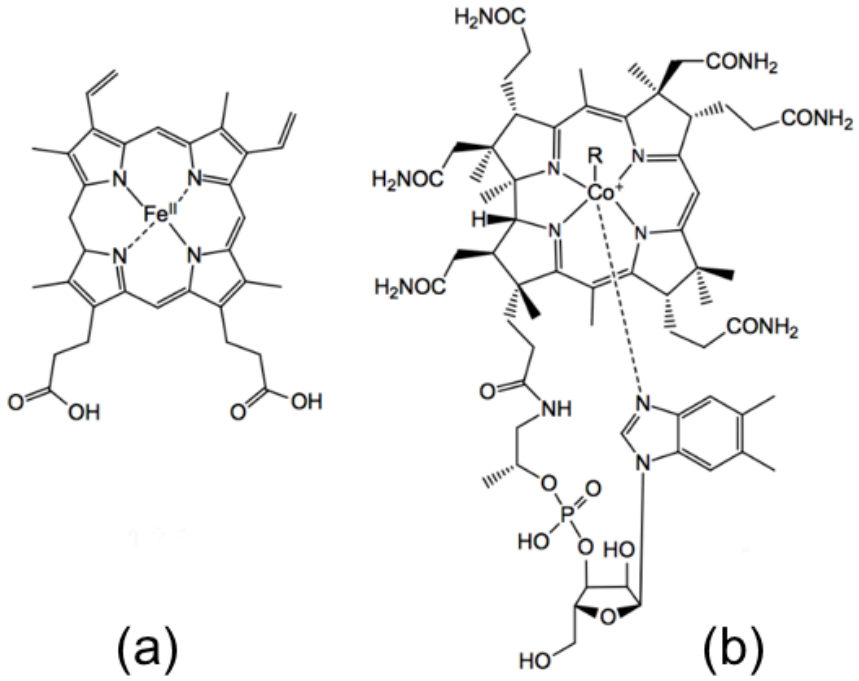

Fig. 1.2 Structures of (a) heme and (b) vitamin B_{12}.

1.2 Structural Properties

As expected for an aromatic system, sterically unconstrained porphyrins adopt planar conformations. Nevertheless, significant deviations from planarity are common and has been observed in many heme prosthetic groups in hemoproteins as well as in synthetic metalloporphyrins.[1] The reasons underlying such nonplanar distortions

include: (a) steric congestion arising from peripheral substituents, (b) size mismatch between the macrocycle cavity and the metal ion, (c) electronic and steric interactions involving the axial ligand, (d) influences of the protein environment, etc.[1a] These distortions influence various chemical and physical properties of porphyrins including their redox potentials, axial ligand binding affinity, UV-vis spectra, etc. Some of the main types of nonplanar porphyrins include the following (Fig. 1.3):[1,2]

(a) Ruffling: Alternate twisting (clockwise and anticlockwise) of pyrrole rings, resulting in alternate displacement of *meso*-carbons above and below the mean porphyrin plane, e.g., $Ni^{II}[Br_8(CF_3)_4P]$[3] and $Ni[Et_8(n\text{-}Bu)_4P]$[4].

(b) Saddling: Alternate tilting of the pyrrole rings above and below the mean porphyrin plane, which leaves all the *meso*-carbons in the mean molecular plane, e.g., $H_2[Br_8TPFPP]$[5] and $Zn[I_8TpCF_3PP]$[6].

(c) Doming: Displacement of the metal ion above the mean porphyrin plane and of the β-carbons below the same plane, typically as a result of an excessively large coordinated ion, e.g., $Tl^{III}[Et_8(NO_2)_4P]Cl$[7] and $Pb^{II}[(n\text{-}Pr)_4P]$[8].

(d) Waving: Upward and downward tilting of two opposite pyrrole rings, relative to the mean macrocycle plane, e.g., $H_2[(4\text{-}F\text{-}Ph)_8TPFPP]$[9].

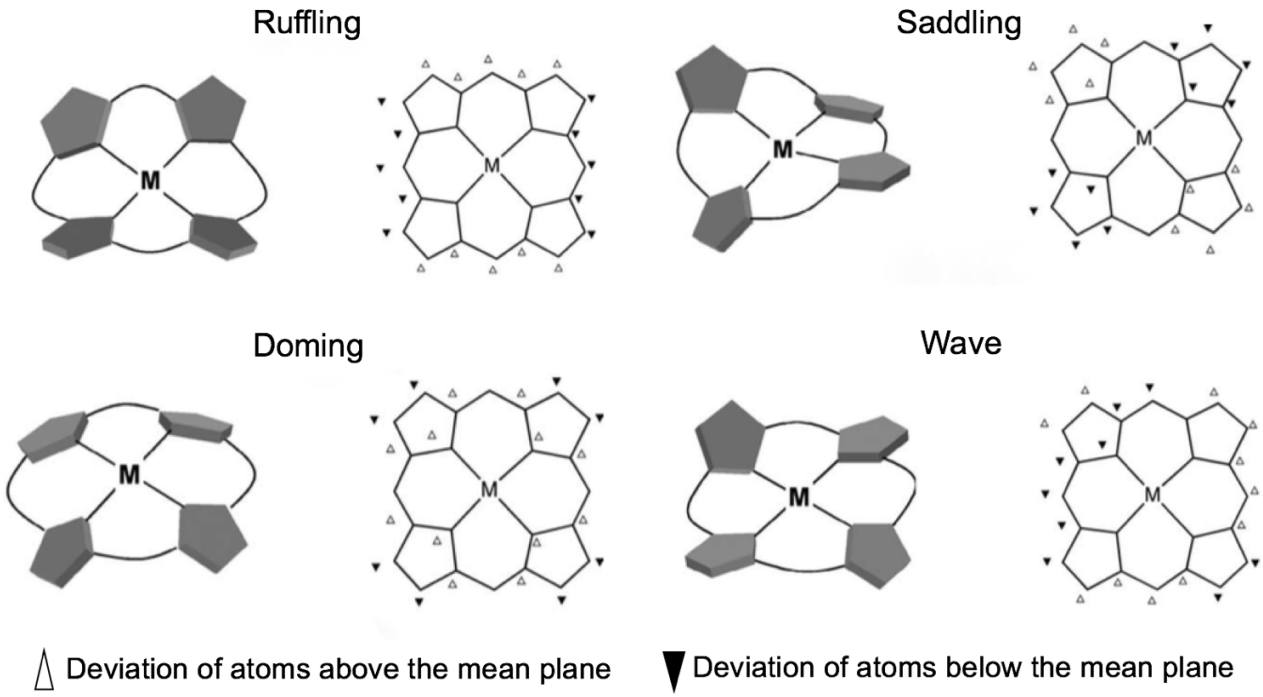

Fig. 1.3 Nonplanar distortion modes in porphyrins. Reproduced with permission from ref 2.

Corroles are structurally less diverse than porphyrins. Free-base corroles undergo significant nonplanar distortion in order to relieve the steric strain arising from the three N-H protons.[10,11] The X-ray structure of the free-base β-octabromocorrole $H_3[Br_8TPFPC]$ exhibits the strongest nonplanar distortion among all free-base corroles reported to date, where two adjacent pyrrole rings were found to be tilted by 98° relative to each other.[12] DFT calculations suggest that the steric interaction among the three central N-H protons is the main cause behind such nonplanarity.

Metallocorroles, on the other hand, exhibit mostly planar structures. Interestingly, even in the presence of highly sterically hindered substituents, metallocorroles such as $Au[(CF_3)_8TpFPC]$[166] or $Ir[Br_8TPFPC](tma)_2$[13], exhibit essentially planar macrocycle conformations.

Saddled conformations are rare for metallocorroles. The only major exception consists of copper corroles which are inherently saddled as a result of a specific $Cu(d_{x2-y2})$-corrole(π) orbital interaction (see sections 2.3.5 for additional details).[144] Sterically hindered substituents can lead to even more intense saddling.[14] Slightly

saddled structures have been observed for Fe[Me_8TPC]Cl[200] and Ag[T*p*MePC][150], while a silver β-octabromocorrole has been found to exhibit a strongly saddled geometry.[152]

A four-coordinate bismuth corrole Bi^{III}[TPFPC] has been recently found to exhibit significant doming.[16] In addition, five-coordinate MoO,[15] Sn^{IV}Ph,[156a] and ReO[160] corroles exhibit pronounced domed conformations, whereas mild doming has been observed for Mn^{V}-(NMes) corrole[17] and Ge^{IV}-μ-oxo biscorroles.[155]

The ruffled conformation is also extremely rare for corroles. DFT calculations predict that ruffling is generally extremely unfavorable for metallocorroles. However, mild ruffling has been recently noted for certain phosphorus corroles.[18]

The wave conformation has not yet been observed for corroles.

1.3 Optical Properties

The presence of an extended conjugated π-system in porphyrins and corrole results in strong absorption in the visible region of electromagnetic spectrum, which is the reason behind their bright colors. A typical UV-vis spectrum of a free-base porphyrin or corrole consist of a sharp and strong Soret band in the near UV-region around 400 nm and two to four less intense Q bands in the visible region around 500-700 nm (Fig. 1.4).

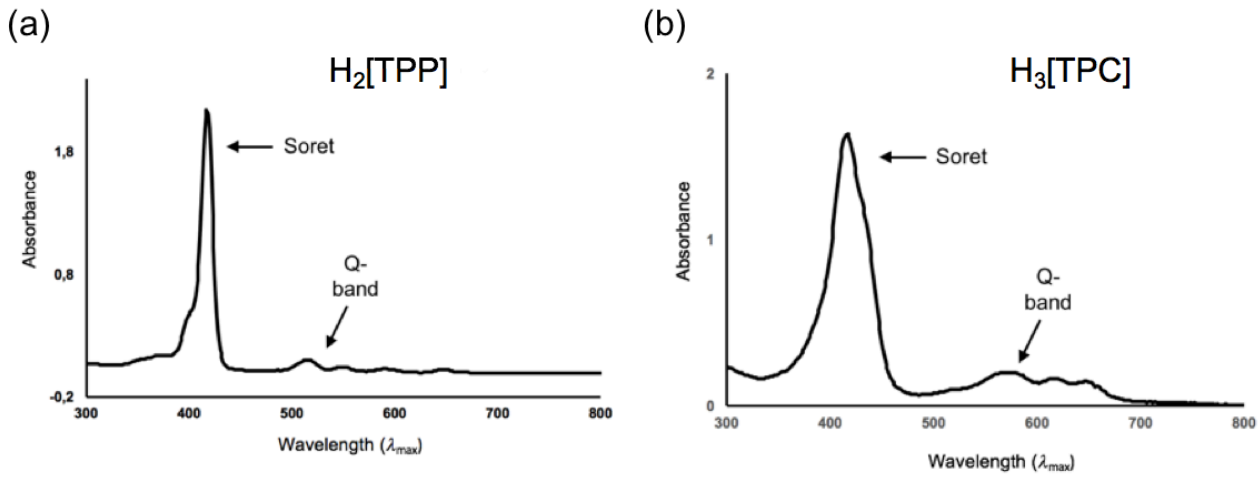

Fig. 1.4 UV-vis spectra of (a) H_2[TPP] and (b) H_3[TPC] in DCM.

The electronic spectra of porphyrins can be explained by Gouterman's four-orbital model.[19] According to the model, the two near-degenerate HOMOs {$b_1(a_{2u})$ and $b_2(a_{1u})$ respectively} and the two degenerate LUMOs {$c_1(e_g)$ and $c_2(e_g)$

respectively} of a porphyrin (D_{4h}) are energetically well separated from all other occupied and unoccupied molecular orbitals. The possible transitions involving these four frontier MOs give rise to the Soret and Q bands of porphyrins,[20] where intense Soret bands correspond to the 'allowed transitions' and lower intensity Q bands to the 'forbidden transitions' (Fig. 1.5).

As shown in Fig. 1.5 the a_{2u} HOMO has amplitudes at the *meso*-position and pyrrole nitrogens, whereas a_{1u} HOMO has amplitudes at the α- and β-position. Thus, substitution at the *meso*-position with an electron-donating group or coordination with a more electropositive metal increases the energy of b_1 HOMO, which leads to a redshift of the Soret band. Similarly, substitution at the β-positions by electron-donating alkyl groups or electron-withdrawing bromine group result in increase or decrease in the energy of the b_2 HOMO. Peripheral substituents thus exert a significant influence on the electronic properties and spectra of porphyrins.

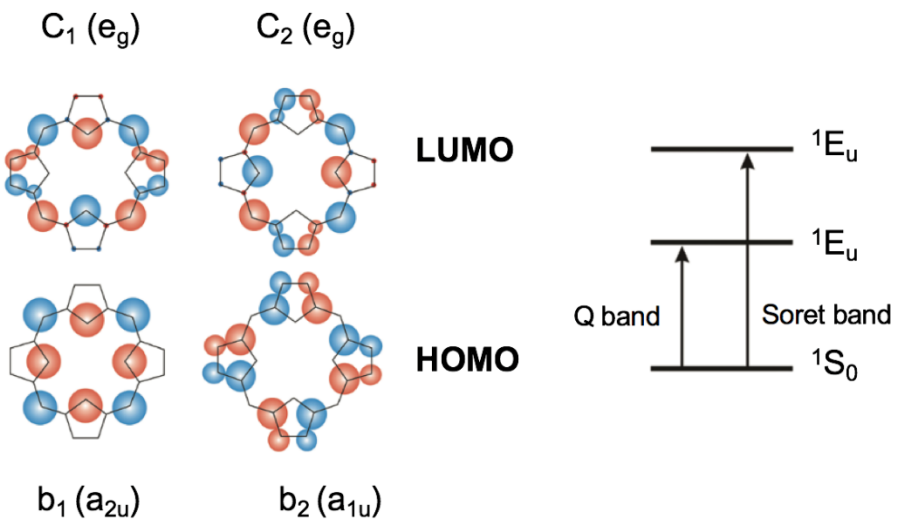

Fig. 1.5 Porphyrin frontier orbitals in the four-orbital model and the possible transitions between energy levels. Reproduced with permission from ref 20.

Gouterman's four orbital model applies also to corroles, as suggested initially by Hush *et al.*[21] and later by Ghosh and co-workers.[22] The absence of one *meso*-carbon results in a lowering of symmetry to C_{2v} for corroles relative to D_{4h} for porphyrins. Thus, in corroles, the a_{2u} HOMO transforms as b_1, and a_{1u} HOMO transforms a_2. The HOMOs and LUMOs of corroles thus are qualitatively similar in shape to those of porphyrins. Accordingly, we may apply the similar substituent effect arguments to corrole derivatives as we do for porphyrin derivatives.

1.4.1 Synthesis of Porphyrins

The pioneering work of H. Fischer in porphyrin synthesis[23] inspired many chemists to seek several efficient methodologies for porphyrin synthesis over almost 60-70 years. In this section, I have discussed the key one-pot procedures available for the synthesis of *meso*-A_4 porphyrins (Figure 1.6).

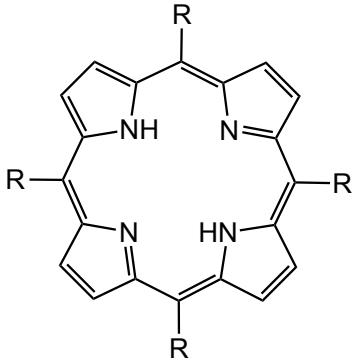

Fig. 1.6 Structure of a *meso*-A_4 free-base porphyrin.

The first one-pot synthesis of porphyrins was reported by Rothemund in 1935-36. A solution of pyrrole (5 M) and formaldehyde (2%) in pyridine was heated in a sealed glass tube for several hours, which after extraction and work-up led to crystalline unsubstituted porphine.[24] This same method was also applicable to other aldehydes such as acetaldehyde, propionaldehyde, *n*-butyraldehyde, benzaldehyde and furfuraldehyde.[25] A modified synthesis of free base *meso*-tetraphenylporphyrin (H_2[TPP]) was also established.[26] The presence of pyridine in the reaction medium in sufficient amounts was necessary for easier crystallization of the porphyrin product while keeping other impurities in solution phase. Formation of two porphyrin-like products was observed during the synthesis of TPP. These two products were chromatographically separated and spectroscopically identified as H_2TPP and H_2[TPChl] (tetraphenylchlorin).[27] Modified procedures were later suggested to improve the yield of free-base TPP, along-with synthesis of new *meso*-tetraarylporphyrin derivatives with different *p*-substituents.[28,29] Other methods for the synthesis of unsubstituted porphine were also discovered around this time.[30]

The Rothemund seal-tube method generally led to poor yields of porphyrins. A new synthesis of tetraphenylporphyrin by Adler and Longo greatly overcame this problem in 1966. In the new method, condensation of benzaldehyde and pyrrole (0.005 mole each) was performed in refluxing acetic acid over 6-8 hours, whereupon

H_2[TPP] was obtained in ~40% yield after purification (~50% in acidified benzene).[31] The yield of H_2[TPP] and the reaction rate was found to depend on several factors such as the acidity of the solvent, temperature, the availability of atmospheric oxygen, and the initial concentrations of the reagents.[32] A simplified one-pot synthesis of H_2[TPP] was later developed where pyrrole and benzaldehyde (0.8 mole each) were refluxed in propionic acid under air for only 30 min, after which H_2[TPP] crystallized out upon cooling and was filtered off.[33] The simple filtration technique led H_2[TPP] in nearly ~20% yield and is clearly a great advantage of the Adler-Longo method. However, tetraphenylchlorin (H_2[TPChl]) was observed to be present as a contaminant (~3-5% by weight) and attempts to remove it via column chromatography and other separation methods have not proved particularly successful. Subjecting the entire H_2[TPP]- H_2[TPChl] mixture to DDQ oxidation provided a convenient solution to the problem, leading to pure H_2[TPP].[34]

The harsh acidic conditions employed in the Adler-Longo method is unsuitable for aromatic aldehydes with sensitive functional groups. Also, many porphyrins do not crystallize out from the solution as readily as H_2[TPP] and accordingly purification via simple filtration of the tarry product mixture can be cumbersome. To overcome these difficulties, Lindsey proposed a new methodology applicable to sensitive aldehydes and amenable to simple purification steps. The synthetic strategy builds on the postulate that the cyclic porphyrinogen, formed via the condensation of pyrrole and aldehyde under appropriate conditions, is thermodynamically favored over linear polypyrrylmethanes. Once generated under equilibrium conditons, the porphyrinogen can be irreversibly oxidized to the porphyrin. In a typical method, equimolar quantities of pyrrole and benzaldehyde (10^{-2} M each) were condensed in dry DCM under a N_2 atmosphere in presence of $BF_3.Et_2O$ (10^{-3} M) as a catalyst for 1 hour, followed by oxidation using *p*-chloranil (reflux, 1 hour), after which pure H_2[TPP] (yield = 45-50%) could be obtained via column chromatography.[35] The maximum yield of porphyrin is achieved with pyrrole and aldehyde concentrations at 10^{-2} M each and the yield declines markedly at higher and lower concentrations.

The question of reversible porphyrinogen formation in the Lindsey synthesis was examined in a key set of experiments.[36] Two different solutions containing different preformed porphyrinogens (i.e., from two separate reactions of two different aldehydes with pyrrole) were mixed together and allowed to react further (exchange

reaction) and the end result was compared with the 'mixed condensation' scenario where both aldehydes were present together and condensed with pyrrole. Both experiments led to very similar product distributions, strongly supporting the reversibility of porphyrinogen formation.[37] Detailed experiments have suggested that the porphyrinogen derives from an open-chain octameric species at equilibrium. Pyrrole and aldehyde concentrations higher or lower than 10^{-2} M were found to reduce the octamer yield by affecting the equilibrium distribution profile of the oligomers, thus compromising the overall yield of the porphyrin.

The major advantage of the Lindsey method is its applicability to a wide range of aldehydes, including those with sensitive functionalities. Thus, a variety of *meso*-tetraalkylporphyrins,[37] *meso*-tetramesitylporphyrin,[38] and several mono- and bis-*ortho*-substituted tetraarylporphyrins[39] were synthesized according to this procedure. However, the small working concentrations of pyrrole and aldehyde is still a drawback in gram-scale preparations of porphyrin, since it requires large volumes of chlorinated solvents. In 1994, Lindsey came up with a modified procedure where 0.1 M pyrrole and benzaldehyde were condensed at a higher Lewis acid concentration ([$BF_3.Et_2O$] = 0.01 M) to afford H_2[TPP] in 20-30% yield.[40] A one-step synthesis involving pyrrole, aldehyde, and the oxidant from the beginning was also devised. In order to account for the poor solubility of the higher amount of oxidant in the reaction medium, an electron-transport chain was devised consisting of catalytic amounts of *p*-chloranil together and Fe(II)-phthalocyanine, with molecular oxygen as terminal electron acceptor. Furthermore, addition of certain salts to the two-flask synthesis of H_2[TPP] improved the yield remarkably. Thus a ~ 50% yield of H_2[TPP] was obtained by using 0.1 equiv NaCl together with pyrrole (0.1 M) and benzaldehyde (0.1 M) and $BF_3.Et_2O$ (0.01 M).[41] The effects of several acid catalysts on yield of H_2[TPP] were also examined.[42] The mechanistic aspects of these protocols were all examined in considerable detail with the help of laser desorption mass spectrometry (LD-MS) as the key tool.[43]

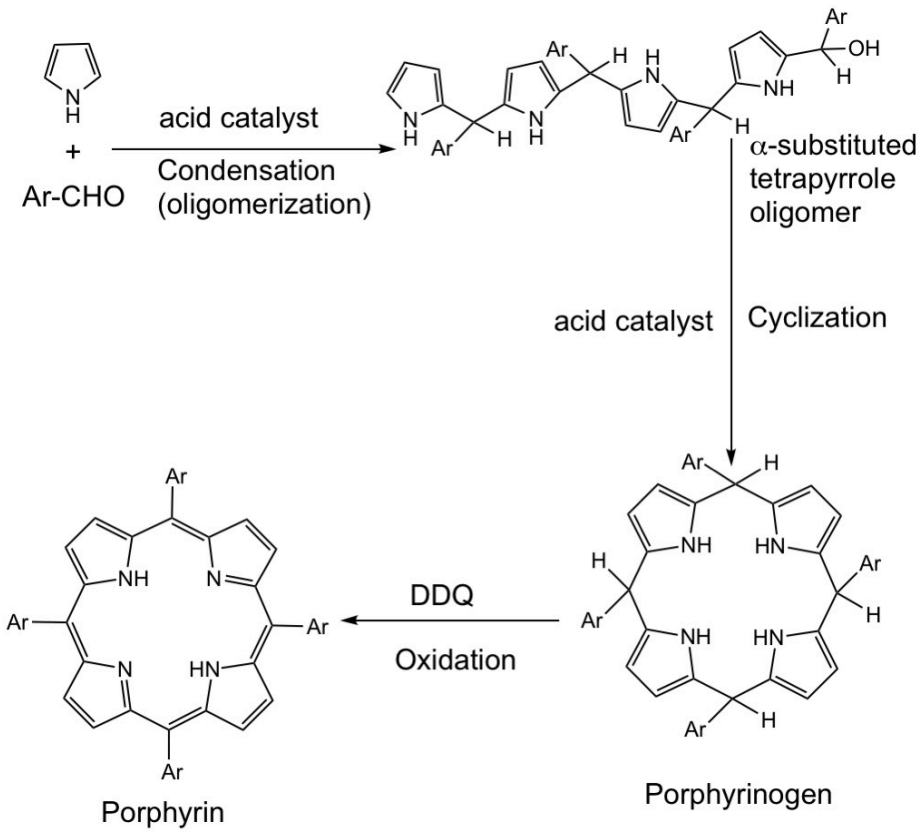

Fig. 1.7 Schematic representation of the key stages of a one-pot porphyrin synthesis. Adapted with permission from ref 43a.

1.4.2 Synthesis of Corroles

The synthesis of corroles has been reviewed recently and is summarized here in somewhat greater detail than the syntheses of porphyrins.[44] The first successful synthesis of corroles was accomplished by Johnson and Kay in 1965 via a photochemical oxidative cyclization of an *a,c*-biladiene. Condensation of either (a) 5,5′-diformyldipyrrane with 3,4-dialkylpyrroles (path A in Fig. 1.8) or (b) 2-formylpyrroles with dipyrrane-dicarboxylic acid (path B in Fig. 1.8) in HBr/AcOH medium yielded the precursor *a,c*-biladienes as crystalline hydrobromide salts, which were then suspended in methanolic ammonia solution and irradiated to afford free-base corroles in about 20-60% yields.[45] Oxidizing agents such as $K_3[Fe(CN)_6]$, $FeCl_3$, and H_2O_2 could at times also be used in lieu of irradiation.[46]

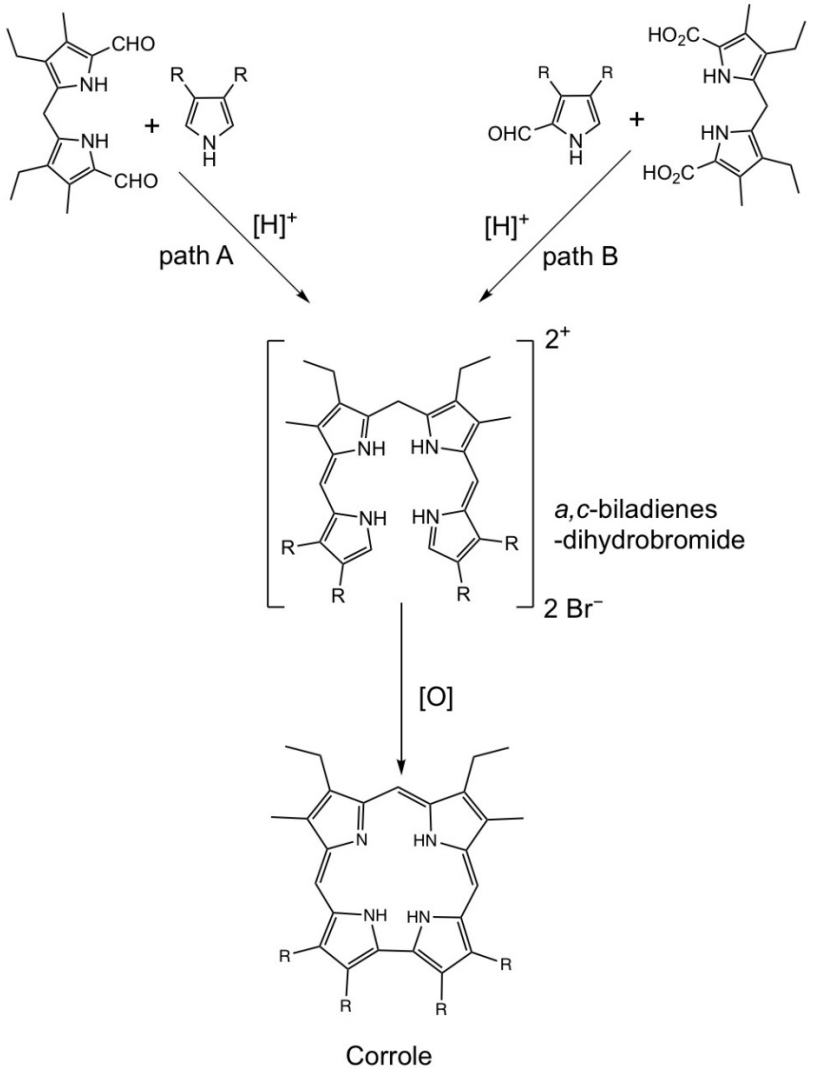

Fig. 1.8 Schematic representation of the corrole synthesis by Johnson and Kay. Adapted with permission from ref 44.

Another useful method for corrole synthesis consists of the metal-assisted cyclization of a tetrapyrrolic precursor such as an *a,c*-biladienes. A Co(II)-mediated template synthesis of a Co^{III}-PPh_3 octaalkylcorrole was attempted by Conlon *et al.*[47] The role of cobalt ion is both to act as the templating agent and to stabilize the various tetrapyrrolic intermediates and the final product. The *in-situ* cyclization and metalation of *a,c*-biladienes was later exploited to synthesize rhodium, iron, and manganese octaalkylcorroles.[48] Metal-assisted cyclization was also reported by Paolesse and co-workers, where they managed to synthesize cobalt-corroles directly from a mono-pyrrolic precursor such as 2-formylpyrrole.[49] Cobalt-coordination was believed to catalyze the ring contraction of the initially formed porphyrinogen species, followed oxidation leading to a *meso*-phenyl-substituted cobalt corrole.[49a] Other

examples of ring contraction of a porphyrinoid leading to a corrole include (a) the ring contraction of a thiaphlorin[50] and (b) the metalation of a porphyrin with a rhenium carbonyl.[51]

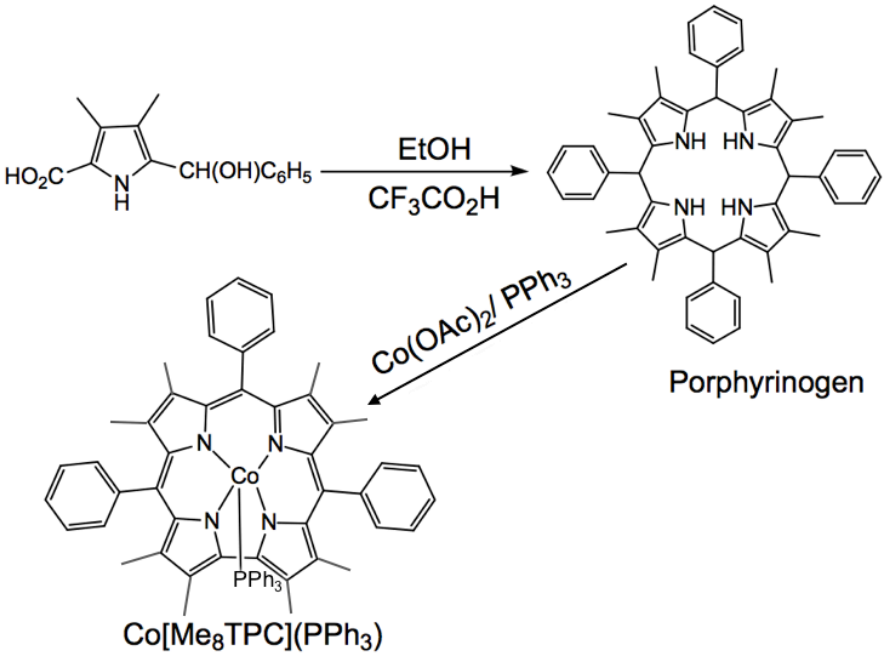

Fig. 1.9 Schematic representation of a corrole synthesis via ring contraction. Adapted with permission from ref 49a.

Until 1999, the synthesis of free base corrole synthesis was mainly limited to the use of *a,c*-biladienes as a precursor. Although improvements were made to the synthesis[52] and cyclization[53] of *a,c*-biladienes, a simple one-pot synthesis of free-base corroles was still lacking. The discovery of new one-pot and quasi-one-pot syntheses of *meso*-triarylcorroles via the reaction of pyrrole and aromatic aldehydes proved to be a game-changer that led to the rapid blossoming of corrole chemistry to the point where it begins to rival porphyrin chemistry in terms of breadth and diversity.

Gross *et al*. reported a solvent-free method of condensing an equimolar mixture of pyrrole and an aromatic aldehyde using basic alumina as a solid support at 100°C for 4 hours, followed by oxidation with DDQ.[54] This method proved successful for synthesizing the electron-deficient *meso*-tris(pentafluorophenyl)corrole, H_3[TPFPC], which was obtained in 11% yield after purification. Given the highly exothermic nature of the reaction, heating and the use of the solid support was later shown to be unnecessary in many cases.[55] Although

initially meant for electron-deficient aldehydes, Gross's method was found to be applicable to synthesizing new A_3-corroles from both electron-rich and electron-poor aldehydes.[77,185]

Also in 1999, Paolesse *et al*. synthesized *meso*-triphenylcorrole, H_3[TPC], by reacting pyrrole and benzaldehyde (3:1) in refluxing AcOH.[56] One drawback of the method was the formation of H_2[TPP] in comparable yields to corrole. Several *meso*-triarylcorroles from different aldehydes (both electron-poor and electron-rich) were synthesized following this procedure, with higher yields of corrole being obtained with electron-poor aldehydes.[57] In another interesting approach, free-base H_3[TPC] was synthesized in good yield (~65%) by oxidation of the corresponding open-chain tetrapyrrane precursor under acid-free conditions and in presence of NH_4Cl or NH_4NO_3 as additive.[58]

Around the same time, new methods for synthesizing A_2B *meso*-triarylcorroles (where one of the three *meso* aryl group is different from the other two) were being developed. Dehaen *et al*. reported an acid-catalyzed [2+2] condensation of dipyrromethane (DPM) with electron-deficient aromatic aldehydes,[59] while Gryko *et al*. reported the synthesis of five new unsymmetrically *meso*-substituted corroles via the reaction of dipyrromethanes with reactive aldehydes (i.e. with electron-withdrawing fluorine atoms) in the absence of any added catalyst.[60] A versatile method was accordingly devised for the synthesis of *trans*-A_2B corroles via the acid-catalyzed condensation of a DPM and an aromatic aldehyde followed by oxidation with DDQ.[61] Gryko and co-workers further refined methods for condensing pyrroles with different classes of aldehydes (categorized according to reactivity and/ or steric bulk) for the synthesis of different A_3-corroles[62] and even managed to synthesize an ABC corrole with three different aryl groups at the *meso*-positions.[63] Specific and optimized methodologies were also suggested for *trans*-A_2B corroles,[62] especially for the ones bearing electron-withdrawing groups.[64]

While searching even higher yielding methods with improved purification steps, Koszarna and Gryko came up with a protocol in 2006 that almost revolutionized the one-pot pyrrole-aldehyde condensation process.[65] The primary strategy was to maximize the yield of bilane, the direct corrole precursor, among the various condensation products (e.g., dipyrromethanes, tripyrrane, and higher oligocondensates), which they accomplished by carrying out the condensation in a water/MeOH mixture. The choice of the solvent mixture came from findings by Kral *et*

al. who developed an effective method dipyrromethane synthesis via pyrrole-aldehyde condensation in water. These authors exploited the solubility difference between the substrates (aromatic aldehyde, pyrrole) and the product (dipyrromethane) in water and managed to essentially stop the reaction at the dipyrromethane stage by precipitating it out from the reaction medium.[66] A notable point was that when the condensation was conducted in a 1:1 mixture of aqueous HCl and methanol, the yield of dipyrromethanes decreased significantly (probably because of higher oligomerization). This observation prompted Gryko to run the pyrrole-aldehyde condensation in water/methanol mixtures to allow better solubility of both the substrates and the DPM and thereby promote further reaction leading to the formation of the bilane, which could be precipitated out from the system due to poor solubility. Thus, condensation of benzaldehyde (5 mM) with pyrrole (molar ratio 1:2) in 1:1 water/methanol in presence of HCl (0.25 mM) for 3 hours, followed by extraction with $CHCl_3$ and subsequent oxidation by *p*-chloranil (reflux, 1 hour), yielded free-base H_3[TPC] in 27% yield.[65] Additional A_3 *meso*-triarylcorroles with were synthesized by the same method in moderate to good yields (10-25%), with relatively low yields observed for electron deficient aldehydes. For the oxidation step, $CHCl_3$ and *p*-chloranil were found to be the best solvent-oxidant combination, which facilitated the purification and avoided over-oxidation. This same water/methanol/HCl method was also found to be applicable to the synthesis of *trans*-A_2B corroles from DPMs (both sterically hindered and unhindered) and different aldehydes. However, sterically hindered DPMs were found to require a higher MeOH to H_2O ratio, a higher acid-concentration, and longer reaction times relative to sterically unhindered DPMs. In this thesis, I have used Gryko's standard water/methanol/HCl method[65] to synthesize free-base *para*-substituted triarylcorroles, H_3[T*p*XPC] (X = CF_3, H, Me, OMe) in good yields.

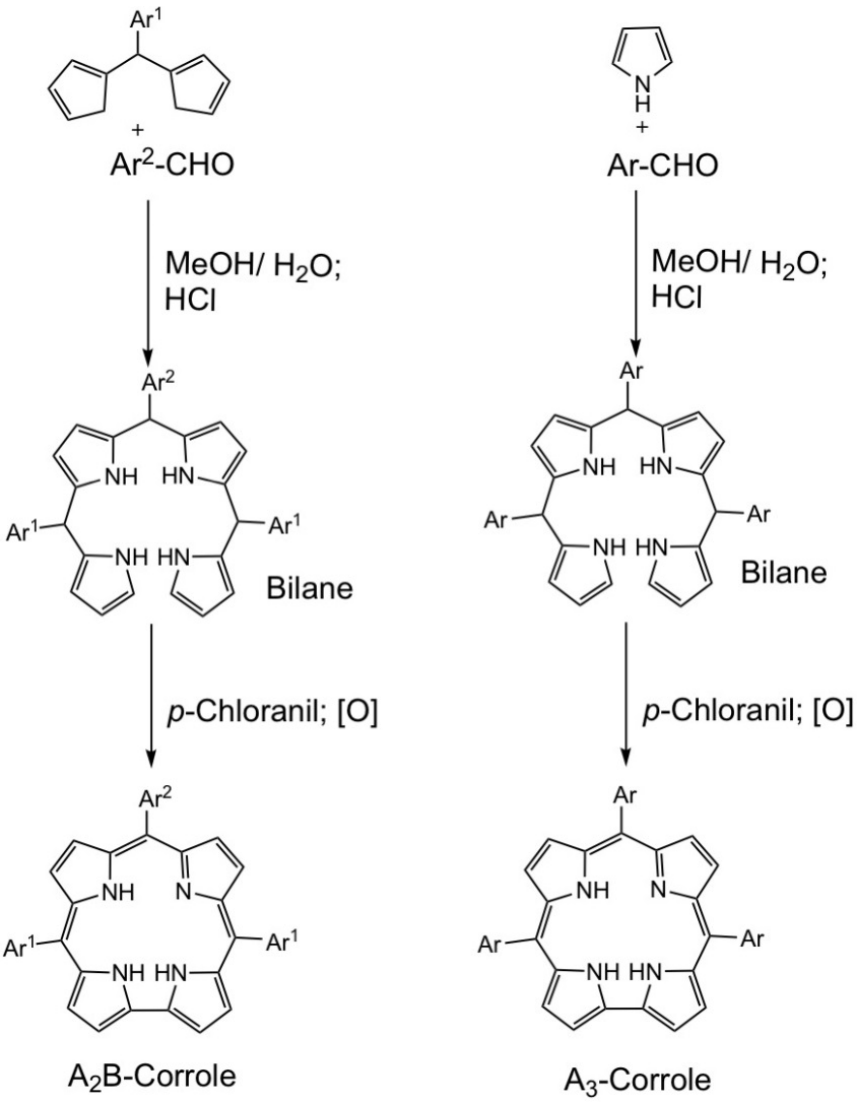

Fig. 1.10 Schematic representation of the syntheses of *meso*-A_3 and *meso*-A_2B corroles via the water/MeOH method.

Other notable methods of corrole synthesis include:

(a) microwave irradiation of a mixture of pyrrole, aldehyde, and basic alumina in a microwave vial, which leads to an improvement in the yield of several A_3-corroles relative to Gross's conventional heating approach;[67]

(b) pyrrole-aldehyde condensations catalyzed by the cation exchange resin Amberlyst-15, which is advantageous for the reusability of the catalyst;[68]

(c) use of an ionic liquid such as [Bmim][BF_4] ($Bmim^+$ = 1-butyl-3-methylimidazolium cation) for the synthesis of *trans*-A_2B corroles, which effectively reduces the amount of organic solvent required for the synthetic procedure and thereby leads to a "greener" synthesis;[69] and

(d) a large-scale, modified Lindsey synthesis of H_3[TPFPC], via a $BF_3.Et_2O$-catalyzed condensation reaction of pyrrole and C_6F_5CHO in the presence of *p*-formaldehyde.[70]

1.5 Modifications/Functionalization of Corroles

Since the discovery of corroles, several attempts have been made to functionalize corroles. Functionalization at the inner core positions of corroles mainly involve metalation reactions. Corrole ligands are found to form stable complexes with several main-group metals, almost every transition metals, and many f-block metals.[71c,72] Other important functionalization processes include demetallation[73] and N-alkylation reactions.[74]

Peripheral functionalization can be perfomed at both the *meso*- or the β-positions of corrole rings, as described in several review articles including a recent one.[71] Here we will focus on a handful of important β-functionalization methods, with an emphasis on β-halogenation reactions, especially bromination.

β-Octafluorocorroles can only be synthesized via the condensation reaction of aromatic aldehydes with 3,4-difluoropyrrole.[75,236] In contrast, chlorination of all eight β-positions has been accomplished by treating a Cu-corrole with NCS[76] or by exposing a Co-corrole to chlorine gas.[229]

β-Octabromination is also facile in copper corroles, especially with liquid bromine at room temperature.[77] Alternatively, direct bromination can also be carried out on chromium,[78] iridium,[79] alumnium,[80] and gallium corroles,[81] as well as for certain free-base corroles.[57] Methodologies for partial bromination have also been documented.[82,155a] Copper β-octabromocorroles are of particularly value as synthetic intermediates. Thus, Cu[Br_8T*p*XPC] derivatives can undergo a variety of palladium-catalyzed coupling reactions to afford β-octakis(trifluoromethyl)corroles,[147] undecaarylcorroles,[83,84] and triaryltetrabenzocorroles.[85] These new complexes all exhibit interesting electronic and structural properties. The partially brominated corroles also undergo Suzuki coupling with arylboronic acids[82a] or Stille coupling with Sn-acetylene reagents[86] to yield the corresponding substituted products.

Copper or manganese β-octabromocorroles can be demetalated to synthesize corresponding free-base octabromocorroles,[87] which upon metalation yield new classes of sterically hindered metallocorroles.[87b,88,133]

Iodination has been performed for up to four β-pyrrolic positions. 2,3,17,18-Tetraiodinated complexes have been obtained for aluminum and gallium corroles,[89] while for phosphorus corroles a tri-iodinated derivative was synthesized and spectroscopically studied.[90] Quite interestingly, Gross and co-workers recently reported a one-pot metalation and iodination reaction of free-base *meso*-tris(pentafluorophenyl)corrole, affording the tetraiodinated, M[I_4TPFPC] complexes, where M = Cu, Ag and Au.[91]

Other important examples of β-functionalization include: (a) formylation of free-base H_3[TPC][92a] and of Ga[TPFPC](py),[92b] (b) 3-carboxylation of Ga[TPFPC](py)[93a] also synthesis of a series of free-base corrole-3-carboxylic acids and their Cu complexes,[93b] (c) iridium-catalyzed borylation of H_3[TPFPC] to afford 2-borylcorrole,[94] d) fluoroalkylation of H_3[TPFPC],[82a] (e) chlorosulfonation and sulfonation of free-base corroles and metallocorroles,[92b,90,95] and, (f) nitration of free-base, Cu, Ge, or Fe corroles to afford the corresponding mono-3-substituted or bis-3,17-disubstituted products.[96,129]

Chapter 2 – Introduction to Ligand Noninnocence

2.1 Introduction

The assignment of a formal oxidation state to the central metal ion in coordination complexes can at times be tricky. In such cases, strong mixing of metal d and ligand σ or π orbitals can result in a metal oxidation state that differs from one that one might naively predict from an ionic model of metal-ligand bonding. The ligands in such complexes have been termed 'noninnocent' or 'suspect' in such complexes on account of their involvement in the 'uncertainty in oxidation state assignment'.[97]

The 'innocent' and 'noninnocent' terminology was introduced by Jørgensen in his comprehensive review in 1966.[98] According to his definition, ''ligands are innocent when they allow oxidation states of the central atom to be defined''. Werner-type complexes such as $[Co(NH_3)_6Cl_3]$ or $PtCl_2(NH_3)_2$, where the oxidation state of the central metal can be unambiguously determined {Co(III) in the first complex, and Pt(II) in the second one}, are complexes with innocent ligands (Fig. 2.1)

On the other hand, the $Ni(gma)_2$ {gma = glyoxalbis(2-mercaptoanil)} complex (Ni-A) can be considered as a Ni(II)-diradical (Ni-B), or as a Ni(IV) complex (Ni-C), or even as a Ni(0) complex (Ni-D), as a result of extensive interactions of the Ni(II) d-electrons with the gma π-system. Thus, complex Ni-A is best thought of as a Ni-complex with delocalized bonds (Ni-E).[99] Here, an assignment of oxidation state for Ni is ambiguous and the ligand is thus noninnocent (Fig. 2.1).

Although the original definition of 'noninnocence' referred only to the ligands, in reality it is the metal-ligand combination that elicits noninnocent behavior. A specific ligand such as corrole can be innocent in certain complexes, but noninnocent in others. For noninnocence to occur, key frontier MOs of the metal and the ligand need to overlap in a symmetry-allowed manner and also be energetically matched. We shall see (in sections 2.3.5 and 2.3.6) that these conditions explain that corroles are innocent in gold complexes, but noninnocent in copper complexes.

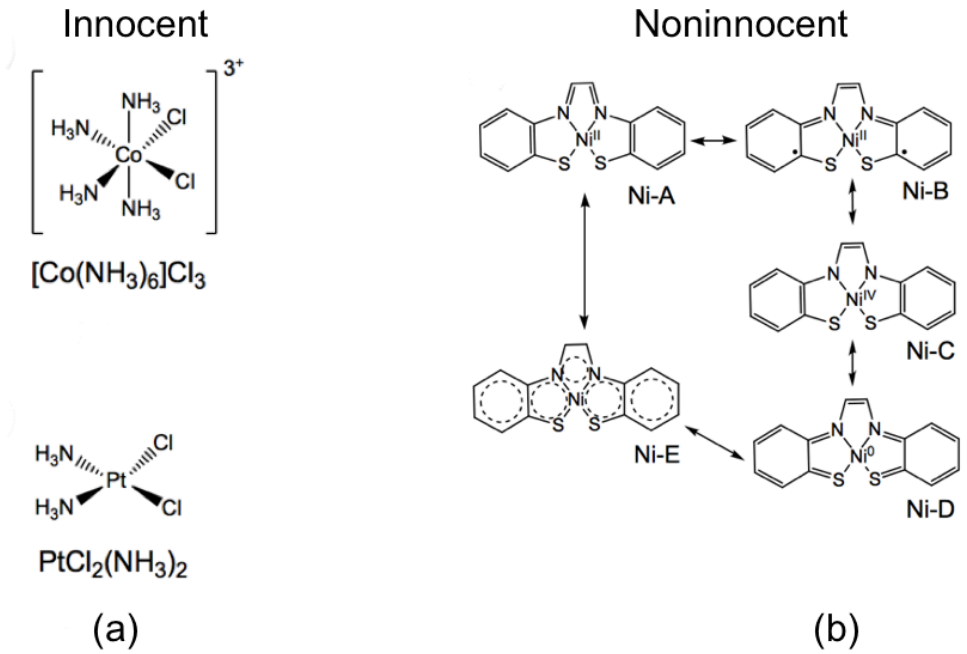

Fig. 2.1 Examples of complexes with (a) innocent and (b) noninnocent ligands. Adapted with permission from ref 99.

In section 2.2, I shall briefly discuss some of the major types of noninnocent ligands. In section 2.3, I shall present the main ideas of this thesis, viz., a detailed discussion of different metallocorroles in respect of their noninnocent/innocent behavior.

2.2 Some Major Classes of Noninnocent Ligands

2.2.1 Dithiolene. Nickel dithiolene complexes were discovered as the first series of complexes to exhibit non-innocent behavior. As shown in Figure 2.2, the oxidation state of the metal might conceivably range from Ni(0) up to Ni(IV). Magnetic measurements revealed the diradical nature of the compounds and helped assign the Ni oxidation state as Ni(II).[100] Each of the two dithiobenzil ligands thus acts as a radical-anion.[101]

Similar square-planar structures were suggested for $M(mnt)_2^{2-}$ [mnt^{2-} = maleonitriledithiolate] complexes (M = Ni, Pd, Pt, Co, Cu), based on their powder X-ray diffraction patterns.[102] Quantum-mechanical calculations revealed that the HOMO of dithiolene complexes is essentially ligand-based and electrochemical studies established the following reversible one-electron oxidation and reduction steps for the complexes (see equation 2.1 and Fig. 2.2):[103]

$$[M(S_2C_2R_2)_2] \underset{e^-}{\overset{e^-}{\rightleftharpoons}} [M(S_2C_2R_2)_2]^{1-} \underset{e^-}{\overset{e^-}{\rightleftharpoons}} [M(S_2C_2R_2)_2]^{2-} \quad \text{(eq. 2.1)}$$

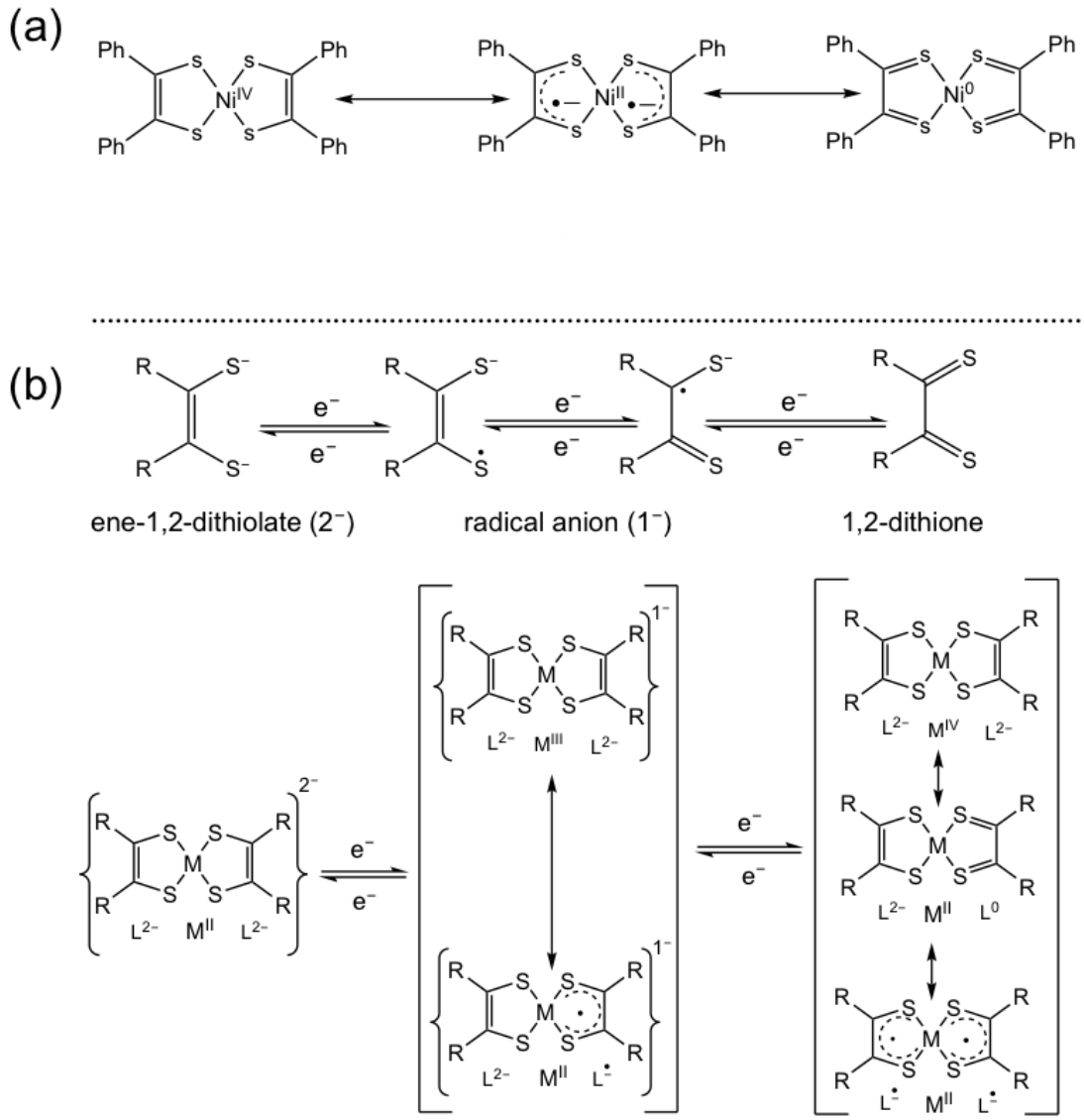

Fig. 2.2 (a) Resonance structures of a Ni-dithiolene complex; (b) representation of three oxidation states of a dithiolene complex connected by electron transfer processes. Reproduced with permission from ref 103.

A dithiolene-like moiety is well-established in bioinorganic chemistry as a part of the molybdopterin or tungstopterin cofactors.[104]

2.2.2 Dioxolene. 1,2-Dioxolene ligands derived from catechol exist in three distinct oxidation states related by single-electron transfer processes[105] (see Fig 2.3). Examples of such ligands include tetrachloro-1,2-semiquinonate (Cl_4SQ) ligands coordinated to 3d metal ions such as Cr and V.[106] A neutral, chromium complex with a 9,10-phenanthraquinone ligand, $Cr^{III}(phenBQ)_3$, exhibits a multistep redox series with electron transfers occurring entirely on the ligand. The neutral form of the complex consists of an S = 3/2 Cr(III) center antiferromagnetically coupled to three chelated semiquinone radical ligands.[107]

In biology, certain iron proteins contain a Fe^{III} center that can be chelated by a catecholate substrate, which then undergoes an intramolecular electron transfer process to form a Fe^{II}-semiquinone complex that subsequently reacts further (Fig. 2.3).[108]

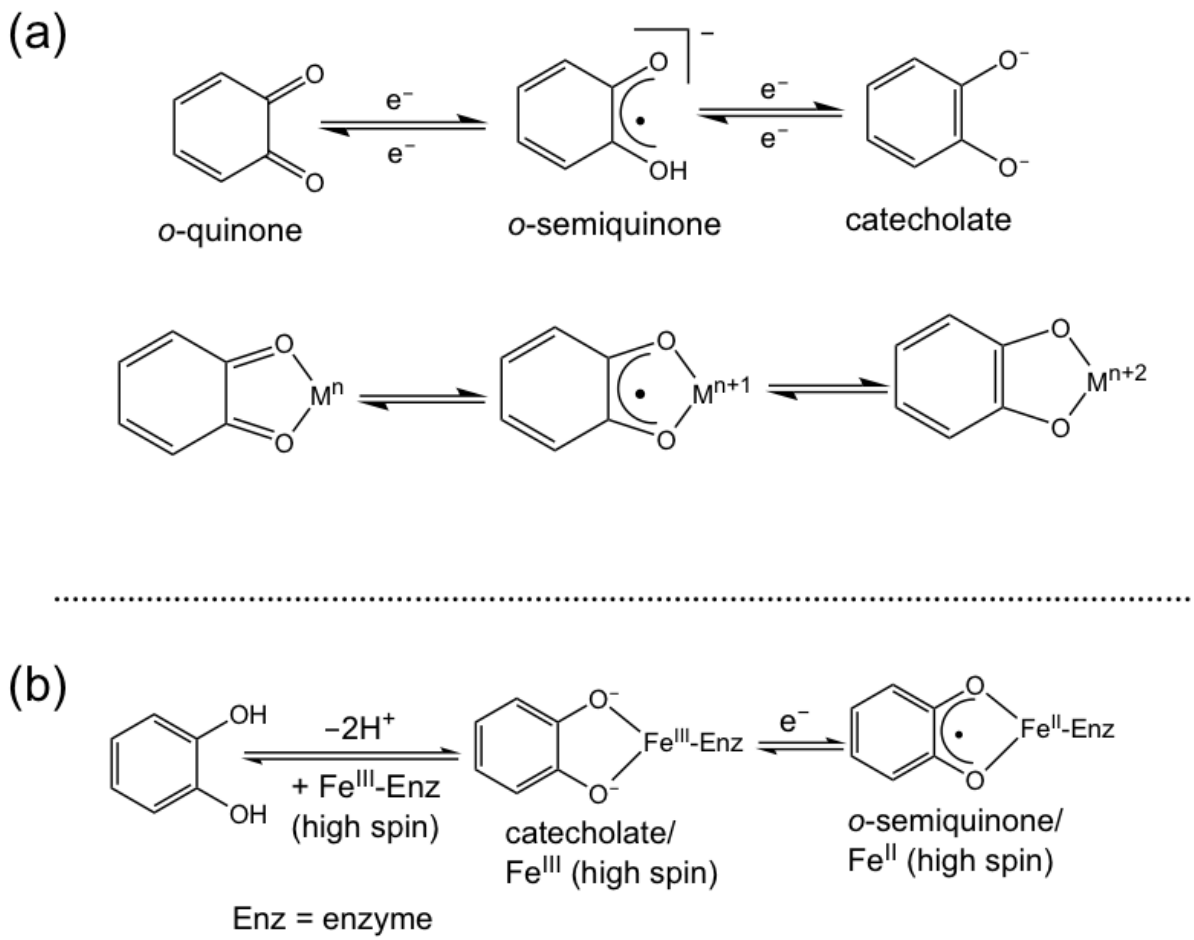

Fig. 2.3 (a) Three oxidation states of a dioxolene ligand and its metal complex. (b) Schematic representation of the noninnocent behavior of an enzymatic iron complex. Reproduced with permission from ref 112.

2.2.3 Diiminopyridine. The neutral complex $Fe(PDI)(N_2)_2$ is best described as an Fe(II) complex with a doubly reduced diradical ligand (Fig. 2.4)[109] and not as an Fe(0) species. This complex serves as a pre-catalyst for hydrogenation, hydrosilylation, and cycloaddition reactions.[110] By serving as a reservoir of electrons, the conjugated diiminopyridine ligand allows Fe-PDI complexes to undergo two-electron oxidative addition of a diene via a cycloaddition reaction.[111]

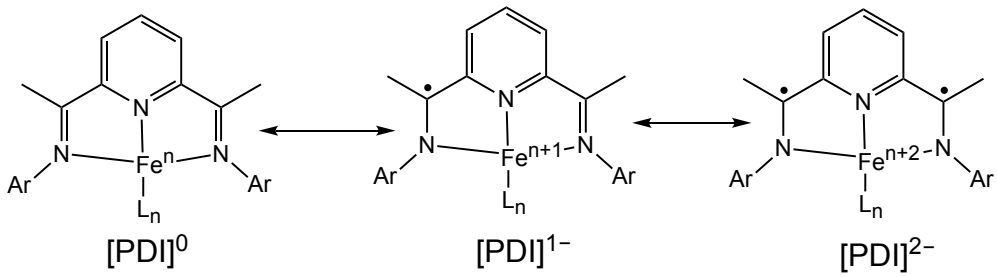

Fig. 2.4 Redox activity of the diiminopyridine ligand in an Fe complex. Reproduced with permission from ref 109.

2.2.4 Dioxygen. The noninnocent behavior of the $O_2/O^{\bullet-}/O_2^{2-}$ series has been well established in biology.[112] Oxygen transport and storage are important biological functions and in many animals involve oxygen binding to the heme centers of hemoglobin (Hb) and myoglobin (Mb). The electronic structure of oxyhemoglobin (and oxymyoglobin) has long been debated. As expected for a high-spin Fe(II) complex, deoxy-Hb is paramagnetic; oxy-Hb, however, is diamagnetic. According to Weiss, the following reaction takes place:[113]

$$Fe^{II} \text{ (high spin, } S = 2) + O_2 \text{ (} S = 1) \rightarrow Fe^{III}\text{–}O_2^{\bullet-}$$

According to this picture, oxygen binding leads to oxidation of the Fe^{II} center to a low-spin Fe^{III} that is antiferromagnetically coupled to a superoxide ligand to afford an overall $S = 0$ ground state. Pauling disfavored this picture and instead suggested an Fe^{II}–(O_2^0) electronic structure for oxy-Hb, where both the heme and O_2 fragments are $S = 0$.[114]

A recent advanced quantum chemical study[115] strongly supports the Weiss picture, whereas certain other studies favor Pauling's description. However, all studies agree as to the fundamentally noninnocent behavior of the dioxygen ligand in these complexes.

2.2.5 Nitric Oxide. Jørgensen described nitric oxide (NO) as the 'simplest case of noninnocent ligand'.[98] The key orbital interactions in transition metal nitrosyls involve the metal d orbitals and the NO π^* orbitals. Some of these orbital electrons can be thought of classic backbonding interactions, others not. In light of these considerations, Enemark and Feltham have suggested that the MNO unit in a metal nitrosyl should be viewed as a single covalent unit with an effective d electron count that is the sum of the metal d electrons and the NO π^* electrons.[117] According to their notation, Fe^{III}-NO, Fe^{II}-NO, Co^{II}-NO complexes are better described as $\{FeNO\}^6$, $(FeNO\}^7$, and $\{CoNO\}^8$, respectively, where the superscripted numeral indicates the effective number of d electrons. For metalloporphyrins, these three Enemark-Feltham counts correspond to highly characteristic MNO angles, which are ~180°, ~140°, and ~120°, respectively (Fig. 2.5).[118,119] Some authors have suggested that a linear MNO unit such as the one in the $\{FeNO\}^6$ complex $[Fe(CN)_5(NO)]^{2-}$ is indicative of an NO^+ ligand.[116] However, a number of nonheme $\{FeNO\}^7$ complexes also exhibit linear FeNO units, where the NO is clearly not describable as NO^+.[120] In our view, there is a clear subjective element in describing a coordinated NO as NO^+, $NO^\bullet$, or NO^-. In these cases, stating the Enemark-Feltham electron count often provides an adequate indication of the electronic structure. As discussed in section 2.3.2 (b), FeNO corroles provide some particularly fascinating examples of nonobvious Enemark-Feltham counts.

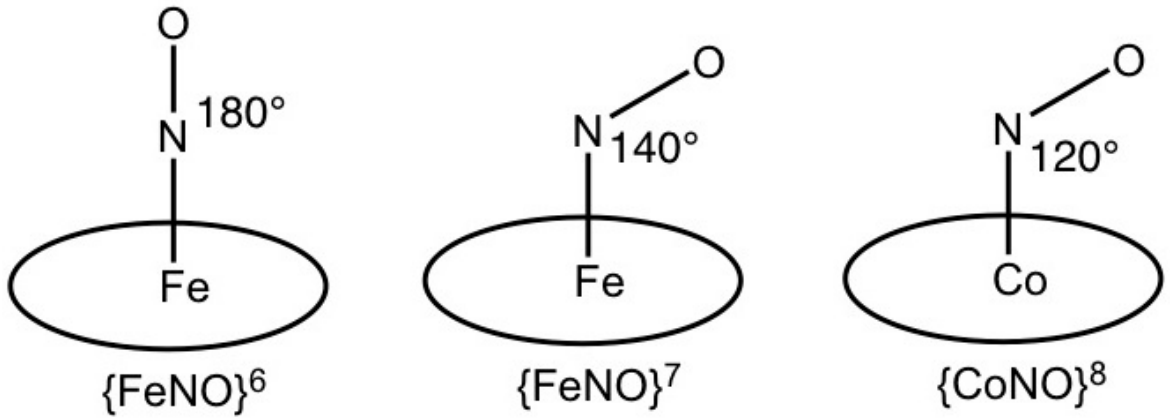

Fig. 2.5 MNO angles in metalloporphyrins.

2.2.6 Tetrapyrrole Ligands. Noninnocent behavior is fairly common for porphyrins and other tetrapyrrole ligands.[121] The critical Compound I intermediate of heme proteins such as the cytochromes P450, chloroperoxidase and other

peroxidases, and catalase provide classic examples of ligand noninnocence. Although these intermediates are sometimes simplistically written as Fe(V), they are better described as S = 1 $Fe^{IV}O$ centers spin-coupled to a ligand radical.[122] The ligand radical may be localized on the porphyrin or in part also on the heme axial ligand. The nature of the spin coupling may range from fairly strongly antiferromagnetic (in the case of heme-thiolate proteins such as chloroperoxidase and the cytochromes P450) to ferromagnetic (for many peroxidases). The compound I (Fig. 2.6) intermediates have been studied in great detail by a variety of spectroscopic techniques, notably EPR and Mössbauer spectroscopy.[123]

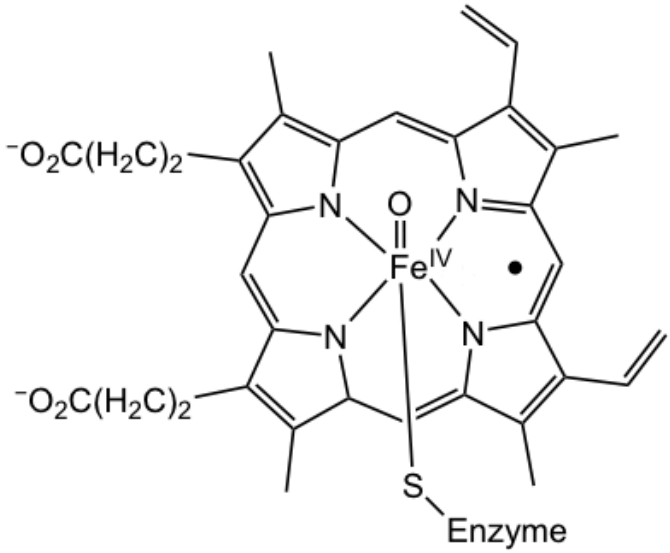

Fig. 2.6 Compound I, an Fe^{IV}-oxo porphyrin radical. Reproduced with permission from ref 123b.

Chlorophylls, which are highly substituted Mg(II)-chlorin complexes, provide another key example of biological metalloradicals. As primary electron acceptors in photosystem I, they form a paramagnetic, EPR-detectable trianionic species:[124]

$$Mg^{II}{-}(Chl^{2-}) + e^{-} \rightarrow Mg^{II}{-}(Chl^{\bullet 3-})$$

Occurrence of this short-lived species is crucial for the charge-separation within the photosynthetic membrane during photosynthesis.

2.3 Noninnocence and Innocence in Metallocorroles

Corroles exhibit unique coordination chemistry relative to porphyrins. Unlike dianionic porphyrins, corroles typically act as formally trianionic ligands toward coordinated atoms. Second, corroles provide a significantly more compressed cavity for the

coordinated atom. These two factors are responsible for the existence of many stable, formally high-valent transition metal corrole complexes. Careful examination, however, shows that many of these complexes do not contain true high-valent metal centers. Instead, the metal atom retains a normal oxidation state, while the corrole ligand assumes an oxidized corrole$^{\bullet 2-}$-like state. The true oxidation state of the central metal is thus ambiguous in many metallocorroles and accordingly the corrole ligands in these complexes may be described as noninnocent. Of course, there are many innocent metallocorrole systems as well. The corrole ligands in the majority of 4d and 5d metallocorroles may be described as innocent. Most main group element corrole complexes are also innocent. Finally, with some metals such as silver, the corrole may be innocent or not depending on the peripheral substituents.[152]

2.3.1 Experimental Techniques for Identifying Noninnocence in Metallocorroles

Ligand noninnocence in metallocorroles can be identified both experimentally and theoretically. UV-vis absorption spectroscopy is arguably the most convenient tool in this regard. A comparative study of the Soret absorption maxima of *meso*-T*p*XPC-complexes [where T*p*XPC = tris(*para*-X-phenyl)corrole] provides a simple yet and reliable probe of the innocence/noninnocence of the corrole ring system. Thus, a strong redshift of the Soret maxima with increasing electron-donating character of *para*-substituent X is indicative of a noninnocent corrole with substantial corrole$^{\bullet 2-}$ character. This is the case for all Cu triarylcorrolates (regardless of β-pyrrole substitution) and several classes of Mn and Fe corroles. Many of the findings in this area are my own, as discussed later in this thesis. On the other hand, substituent-insensitive Soret maxima, as observed for Au, Ru, and Os corroles, are indicative of for innocent, formally corrole^{3-} ligands.

NMR spectroscopy has proved to be another valuable probe for detecting corrole radical character, especially for iron and copper corroles. Temperature-dependent ^{1}H NMR spectroscopy has proven particularly useful for characterizing the singlet-triplet equilibria of Cu corroles. Both ^{1}H and ^{13}C NMR spectroscopy provide detailed information on the spin-density profiles of FeCl and Fe-aryl corroles, wherein the corrole ligand is essentially noninnocent and innocent, respectively.

EPR spectroscopy is also useful in that it can indicate whether a certain radical is metal-centered or corrole-centered. Thus, EPR spectra indicated the

presence a full-fledged corrole radical in certain charge-neutral Pt-diaryl corrole complexes.[140]

X-ray crystallographic structures provide another powerful probe of a noninnocent corrole. For copper corroles, strong macrocycle saddling is indicative of a specific metal(d)-ligand(π) orbital interaction, which results in a noninnocent corrole ligand. For certain other systems such as FeCl corroles, characteristic bond length alternations in and around the bipyrrole part of the corrole skeleton indicate radical character. These bond length alternations can also be probed with IR and resonance Raman spectroscopies.

Very recently, X-ray absorption spectroscopy has been found to yield fairly detailed insights into the oxidation state of the central metal and hence also into the question of ligand noninnocence in metallocorroles.[153]

Finally, quantum chemical calculations, in particular DFT calculations, provide a detailed picture of the spin density profiles (and spin couplings) of metallocorroles and thus shed a great deal of light on the question of ligand noninnocence.

Somewhat surprisingly, electrochemical redox potentials are an unreliable probe for ligand noninnocence. Thus, for a given corrole ligand, both innocent FePh (Fe^{IV}–$corrole^{3-}$) and a noninnocent FeCl (Fe^{III}–$corrole^{\bullet 2-}$) complexes (see paper B) exhibit similar redox potentials and HOMO-LUMO gaps. That said, an electrochemical HOMO-LUMO gap (i.e. the algebraic difference between the first oxidation and the first reduction potentials) of ~2.2 eV, which is the π–π^* energy gap for most closed-shell corroles, is generally indicative of an innocent corrole ligand.

2.3.2 Ligand Noninnocence in Iron Corroles

(a) Chloroiron Corroles. Despite early Fe(IV) assignments, FeCl corroles are best described as noninnocent Fe^{III}–$corrole^{\bullet 2-}$, on the basis of UV-Vis spectra (substituent-sensitive Soret maxima), ^{1}H NMR spectra, and DFT calculations.[125] A detailed discussion of FeCl corroles vis-à-vis the question of ligand noninnocence is provided in section 3.4 and in paper B.

One important observation is that the addition of excess imidazole to a solution of an FeCl octaalkylcorrole leads to a bisimidazole adduct at –50 °C. ^{1}H NMR, EPR, and DFT studies describe these adducts as having low-spin Fe(III) centers that are uncoupled or weakly ferromagnetically coupled to a $corrole^{\bullet 2-}$

radical.[125] Similar behavior is also observed for cyanide addition, although the oxidized biscyanide adduct slowly reduces to the nomal-valent Fe(III) state, $\{Fe[Cor](CN)\}^{-}$.[126]

(b) FeNO Corroles. FeNO corroles are one of the newest additions to the family of noninnocent systems. Ever since Vogel's early report of the Fe[OEC](NO) complx,[127] a large number of FeNO corroles have been synthesized and until recently described as $\{FeNO\}^6$ complexes.[128-131] Ghosh and co-workers, however, have recently proposed a different, noninnocent electronic description for the FeNO corroles, based on experimental and computational studies. According to these authors, FeNO corroles are best described as an $\{FeNO\}^7$ center (low spin, S = 1/2), antiferromagnetically coupled to a corrole$^{\bullet 2-}$ radical, to yield an overall S = 0 ground state.[132]

UV-vis spectroscopic studies provided the first clue to the noninnocent character of FeNO corroles. Thus, the Soret maxima of Fe[T*p*XPC](NO) derivatives were found to exhibit strong redshifts with increasing electron-donating character of the *meso*-aryl *para*-substituent X (see Fig 2.7).[132] Further, IR spectroscopy also appeared to support the new $\{FeNO\}^7$ description of FeNO corroles. The NO stretching frequencies (υ_{NO}) of Fe[T*p*XPC](NO) derivatives range over 1761–1781 cm^{-1} for X = OMe to X = CF_3. These frequencies are substantially lower those of genuine $\{FeNO\}^6$ porphyrins (e.g. υ_{NO} = 1893 cm^{-1} for Fe[TpivPP](NO), which is some 90 cm^{-1} higher than those of analogous $\{FeNO\}^7$ porphyrins). Accordingly, it is reasonable to view FeNO corroles as a resonance hybrid of the form $\{FeNO\}^6$–$Corr^{3-}$ ↔ $\{FeNO\}^7$–$Corr^{\bullet 2-}$, with the latter resonance form contributing substantially.

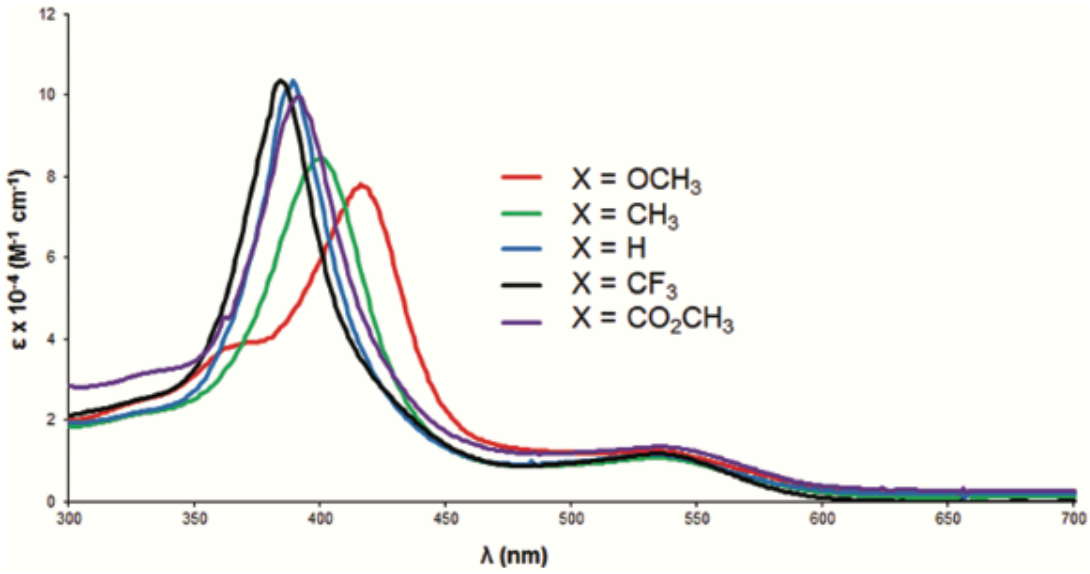

Fig. 2.7 UV-vis spectra of Fe[T*p*XPC](NO) as a function of X. Reproduced with permission from ref 132.

Possibly the most convincing evidence for the noninnocent nature of FeNO corroles came from DFT calculations, where the spin density profile of Fe[TPC](NO) could be clearly attributed to spin-coupled $\{FeNO\}^7$–corrole$^{\bullet 2-}$ fragments. Detailed calculations further suggested that the FeNO unit was best thought of as an Fe(III) center (S = 3/2) antiferromagnetically coupled to a NO^- (S = 1) diradical. It is worth mentioning that the substantial displacement of the Fe atom from the mean corrole N_4 plane (~0.45 Å) favors the antiferromagnetic coupling between Fe d_{z2} electron and corrole a_{2u} radical. Furthermore, the optimized structure of Fe[TPC](NO) exhibits characteristic bond distance alternations in and adjacent to the bipyrrole part of the corrole macrocycle (Fig. 2.8). High quality X-ray crystal structures and IR spectroscopy confirm the presence of these bond-length alternations, which have also been found in noninnocent FeCl corroles.

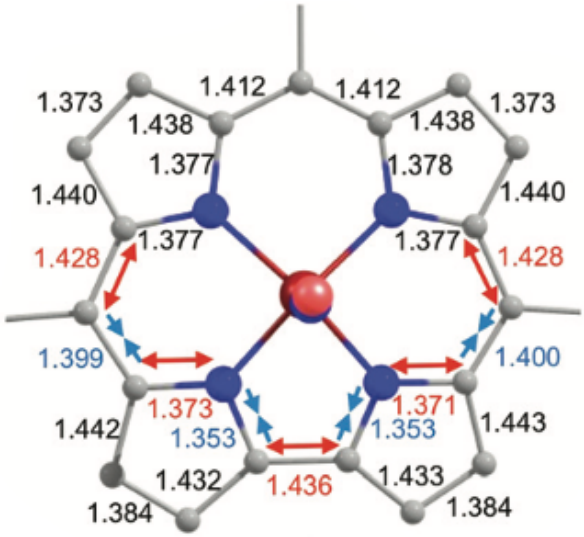

Fig. 2.8 Calculated bond length alteration in Fe[TPC](NO). Reproduced with permission from ref 132.

Ghosh and co-workers also examined the electronic structures of FeNO β-octabromocorroles.[133] The NO stretching frequencies for Fe[Br_8T*p*XPC](NO) complexes were observed to be higher than those of their nonbrominated counterparts. Interestingly, the Soret maxima of the octabromo complexes were found to vary little with increasing electron character of *para*-substituent X (λ_{max} = 394±3 nm), compared to the nonbrominated FeNO corroles. However, this substituent-insensitivity of Soret maxima was attributed to steric inhibition of resonance, whereby the bulky bromine atoms in β-positions force the *meso*-aryl groups to be essentially orthogonal to the corrole ring, thereby exerting smaller electronic effects. DFT calculations on Fe[Br_8TPC](NO) indicated the same non-innocent $\{FeNO\}^7$–corrole$^{\bullet 2-}$ electronic description as for Fe[TPC](NO). Both the crystal structure of Fe[Br_8TFPC](NO) and DFT calculations indicated characteristic bond length alteration in the bipyrrole part of the macrocycle, analogous to what was found for Fe[TPC](NO). Moreover, analogous IR skeletal modes, indicative of a non-innocent corrole ring, were identified for both Fe[TPC](NO) and Fe[Br_8TPC](NO). Overall, despite their electron-deficient nature, FeNO octabromocorroles were found to exhibit the same qualitatively noninnocent electronic structures as their nonbrominated counterparts.[133]

Finally, it is worth noting that FeNO corroles exhibit one reversible oxidation and one reduction[128b,131] in cyclic voltammetry experiments and both are believed to

be ligand-centered processes, according to DFT calculations. The calculated spin density profiles for both the oxidized and reduced states of FeNO corroles indicate a simple S = ½ $\{FeNO\}^7$ center.[134]

(c) μ-Oxo Diiron corroles. In the course of research described in this thesis (see section 4.6.1 and paper A), μ-oxo diiron corroles, which have long been thought of true Fe(IV) species, have been formulated as complex spin-coupled assemblies of intermediate-spin Fe^{III} centers and $corrole^{\bullet 2-}$ radicals. The evidence for this conclusion derived from substituent-sensitive Soret maxima of $\{Fe[T\mathit{p}XPC]\}_2O$ derivatives and broken-symmetry DFT calculations.

2.3.3. Ligand Noninnocence in Manganese Corroles

(a) MnCl Corroles. Substituent-sensitive Soret maxima derivatives and DFT calculations effectively have suggested a noninnocent Mn^{III}–$corrole^{\bullet 2-}$ description for MnCl corroles (see sections 3.3 and 3.6 for a detailed discussion).

(b) Mn(V) Corroles. Several Mn corroles at the formal Mn(V) level are known. Although the majority of these are S = 0 d_{xy}^2 complexes with strongly p-donating oxo or imido axial ligand, there are a few instances of corrole radical states at the formal Mn(V) level.

An interesting case of corrole radical formation has been reported recently by Abu Omar *et al*. The addition of one equiv TFA to the Mn(V)-oxo corrole Mn[TPFPC](O) resulted in the formation of a manganese(IV)-hydroxo corrole cation, $\{Mn^{IV}[TPFPC^{\bullet 2-}](OH)\}^+$ (Fig. 2.9), with a dramatically different UV-vis spectrum relative to the starting material.[135] Also, EPR studies revealed the presence of both an S = 3/2 Mn(IV) center and a corrole radical.[135]

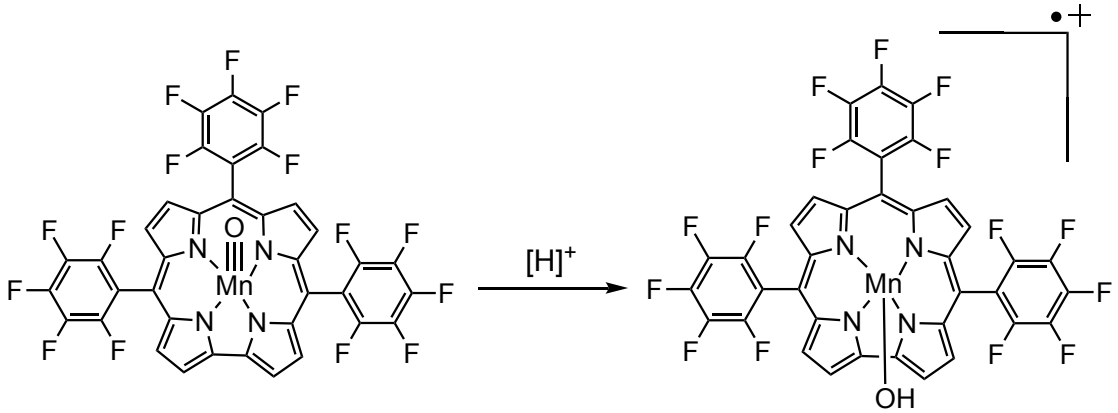

Fig 2.9 Proton-induced corrole radical formation from Mn[TPFPC](O). Reproduced with permission from ref 135.

A second instructive example is provided by the Mn-tosylimido TPFPC complex. Based on magnetic susceptibility measurements, Abu Omar *et al*. reported a high-spin S = 1 ground state for Mn[TPFPC](NTs) complex,[136] which may be contrasted with a clear S = 0 ground state for the analogous mesitylimido complex Mn[TPFPC](NMes).[137] DFT calculations on the model Mn[Cor](NTs) (M_s = 1) revealed a complex spin-density profile suggestive of an $Mn^{III}[Cor^{\bullet 2-}](NTs^{\bullet -})$ description for the complex (see Fig. 2.10).[134]

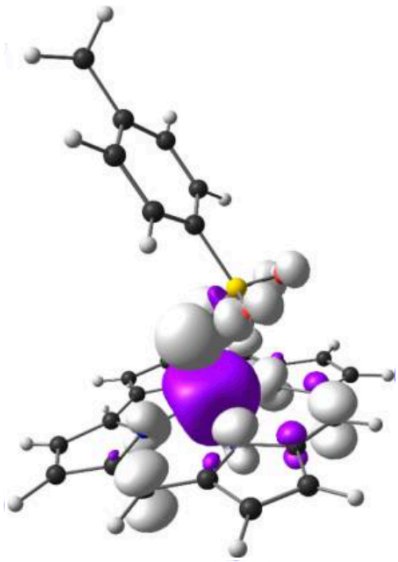

Fig 2.10 DFT spin density plot for Mn[Cor](NTs) (M_s = 1). Reproduced with permission from ref 134.

2.3.4 Noninnocence in Nickel and Platinum Corroles

A nickel corrole was first reported in the legendary publication by Johnson and Kay, who postulated presence of a Ni(II) center, with the corrole acting as a doubly deprotonated, dianionic ligand in the neutral complex.[45b] The Ni corrole exhibited significant UV-vis spectral changes in presence of added base, which was interpreted as indicative of the formation of an anionic Ni(II) complex. A similar observation was also reported by Murakami *et al*., who again invoked a Ni(II) description.[138] However, the X-ray structure of $Ni[Et_4Me_4C]$ reported by Vogel *et al*. tells a different story.[139] The structure reveals a planar macrocycle with short Ni-N bond distances (1.829−1.859 Å) relative to Ni^{II}[OEP] (1.928- 1.958 Å). The structural studies, alongside EI mass spectra and IR spectra, appeared indicative of a formally

trivalent metal center. However, magnetic moment studies and EPR studies of the sample in both solid and in solution phase indicated an S = 1/2 ground state. The EPR spectra were also qualitatively different than spectra of a typical Ni(III) porphyrins. In light of these findings, a noninnocent Ni^{II}–corrole$^{\bullet 2-}$ description was assigned to the complex. DFT calculations also confirmed that the Ni^{II}-corrole$^{\bullet 2-}$ radical states have significantly lower energy than a Ni^{III} state.[22]

Platinum corroles, reported recently by Ghosh and co-workers, present a fascinating story in respect of ligand noninnocence.[140] Insertion of platinum into corroles is a challenging affair and has only been accomplished in benzonitrile solution under microwave irradiation. These conditions afford diamagnetic Pt(IV) corroles with the formula, Pt[T*p*XPC](*o*/*m*/*p*-C_6H_4CN)(PhCN), with a solvent-derived *o*/*m*/*p*-C_6H_4CN ligand. The Soret maxima of these complexes were found not to vary as a function of *para* substituent X, thus indicating an innocent corrole macrocycle (see Fig. 2.11). Treating these Pt(IV) complexes with aryl-Grignard reagent led to air-stable, Pt[T*p*XPC](*o*/*m*/*p*-C_6H_4CN)(*p*-C_6H_4Me) derivatives at the formal Pt(V) level. These oxidized Pt complexes exhibited a strongly split Soret envelope, of which the higher energy peaks were found to redshift significantly (~32 nm on going from X = CF_3 to X = OMe) with increasing electron-donating character of *para* substituent X (see Fig. 2.11), strongly suggesting a Pt^{IV}-corrole$^{\bullet 2-}$ description of the complexes. X-band EPR spectra of the complexes in both solid and frozen-solution state revealed a signal centered around g ≈ 2.00. This observed *g*-value is in agreement with the reported values for other corrole radical derivatives. Also, the hyperfine coupling to Pt, observed only in solution state, was deemed too small for the radical to be Pt-centered. Furthermore, the X-ray structures of the oxidized, Pt-diaryl complexes were found to exhibit characteristic bond length alternations in and adjacent to the bipyrrole part of the corrole ring. Based on all these results, a noninnocent Pt^{IV}–corrole$^{\bullet 2-}$ description could be assigned to these Pt-diaryl corroles.[140]

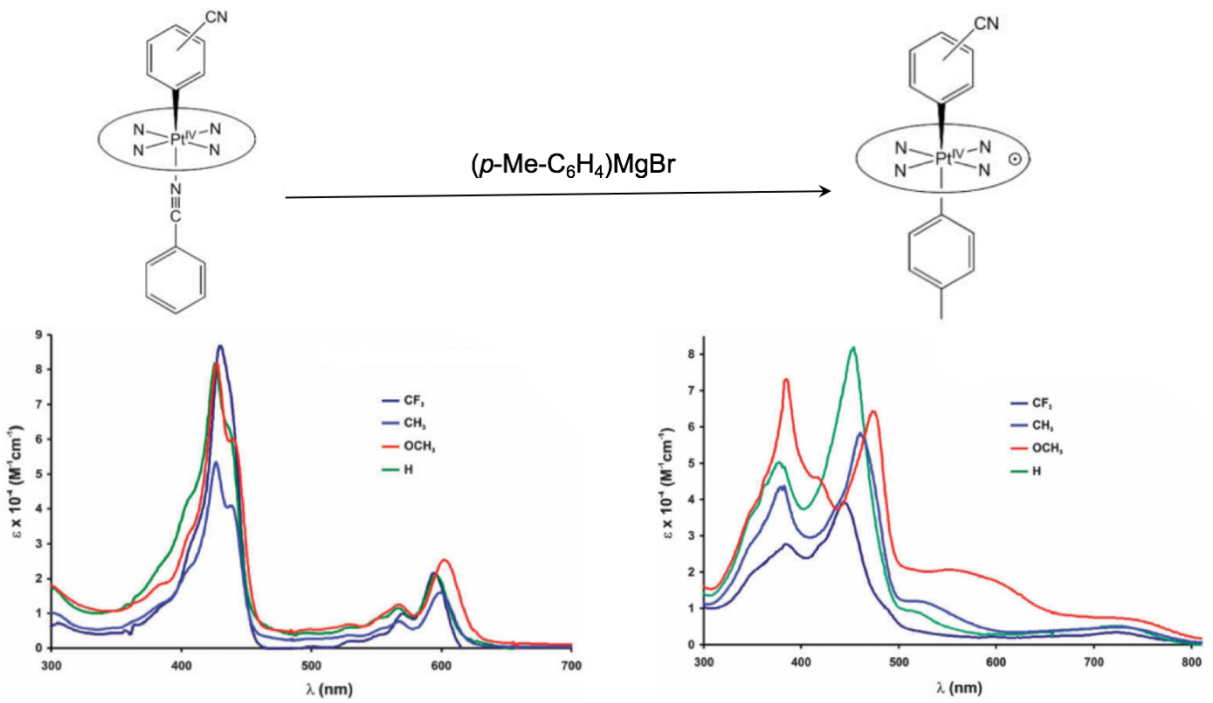

Fig. 2.11 UV-vis spectra of innocent and noninnocent Pt corroles. Reproduced with permission from ref 140.

2.3.5 Noninnocence in Copper and Silver Corroles

Copper corroles have been the subject of some of the most in-depth studies of ligand noninnocence in metallocorroles. The first Cu corrole was synthesized by Johnson and Kay, where it was initially formulated as a Cu(II) species.[45b] A much clearer picture of the electronic structure emerged from Vogel and co-workers' analysis of the Cu[Et_4Me_4C] complex, which was found to be EPR-inactive.[139] Although the crystal structure of the Cu[Et_4Me_4] suggested a trivalent Cu center, the compound exhibited broadening of ^{1}H NMR signals at elevated temperatures and even disappearance of *meso*-proton signals above 386 K. Such behavior could only be interpreted in terms of a thermally accessible, paramagnetic excited state. Indeed, DFT calculations by Ghosh and co-workers confirmed the presence of Cu^{II}–corrole$^{\bullet 2-}$ triplet states, only slightly higher in energy than the S = 0 ground state.[22] Ghosh *et al*. also synthesized of Cu β-octafluorocorrole derivatives, Cu[F_8T*p*XPC], for which temperature-dependent ^{19}F NMR peak (β-F's) also exhibited thermal broadening, consistent with increasing population of a paramagnetic excited at higher temperatures.[75b] Additional confirmation came from the findings of Brückner *et al*. who reported variable-temperature ^{1}H NMR spectra of Cu[TPC] (see Fig. 2.12), and concluded that the equilibrium between the diamagnetic singlet ground state and

paramagnetic triplet excited state is both temperature and solvent-dependent.[141] Gross *et al*. also noted analogous NMR peak broadening of Cu[TPFPC] and Cu[TDCPC] at higher temperature, and they favored the earlier assignment of the paramagnetic excited state as Cu^{II}−corrole$^{\bullet 2-}$ state.[142] Quite interestingly, the copper triphenyltetrabenzocorroles exhibit a paramagnetic ground state.[85b]

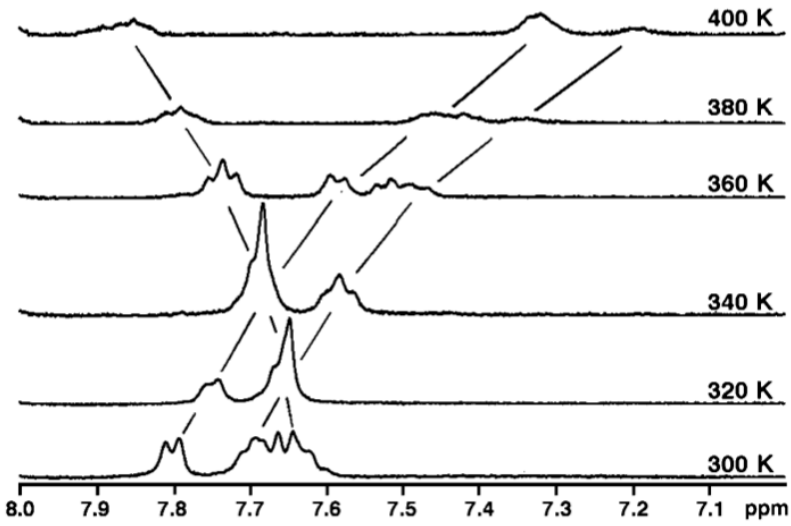

Fig. 2.12 Variable-temperature ^{1}H NMR spectra of Cu[TPC]. Reproduced with permission from ref 141.

Fairly uniquely among metallocorroles, Cu corroles exhibit strongly saddled geometries. Early DFT calculations by Ghosh and co-workers predicted a strongly saddled conformation for Cu[Br_8TPFPC].[77] Such a nonplanar distortion can be attributable to a Cu(d_{x2-y2})−corrole(π) orbital interaction. Subsequently, X-ray structural studies confirmed significantly saddled structures for Cu[TPC][141] as well as for other Cu corroles.[143] In connection with an X-ray structure of a decasubstituted Cu corrole, Bröring *et al*. pointed out the presence of a Cu(d)-corrole(π) orbital interaction and postulated a Cu^{II}−corrole$^{\bullet 2-}$ ground state description.[143] X-ray structural studies by Ghosh and co-workers on two sterically unhindered, *trans*-A_2B Cu triarylcorroles also revealed strongly saddled conformations.[144] Based on DFT calculations, these authors identified a specific Cu(d_{x2-y2})-corrole(a_{2u}) orbital interaction, which becomes symmetry-allowed under saddling, as the driving force for the nonplanar distortion. Thus, according to DFT calculations, even unsubstituted Cu corrole is predicted to be significantly saddled. The Cu(d_{x2-y2})-corrole(a_{2u}) orbital interaction allows the flow of electron density to flow the corrole π-HOMO into the

formally empty d_{x2-y2} orbital of the Cu(III) ion (Fig. 2.13). Accordingly, copper corroles are best viewed as a Cu^{II}–corrole$^{\bullet 2-}$ assemblies rather than as Cu^{III}–corrole^{3-}. It is therefore legitimate to describe the saddling of Cu corroles as driven by the imperative to adopt a noninnocent electronic structure. In an extensive ab initio quantum chemical study, Pierloot *et al*. have supported the idea of a noninnocence-driven, inherently saddled Cu corrole.[145] To our knowledge, the occurrence of noninnocence-driven saddling is unique to Cu corroles and is unprecedented for metalloporphyrins, where saddling occurs primarily due to peripheral steric crowding.

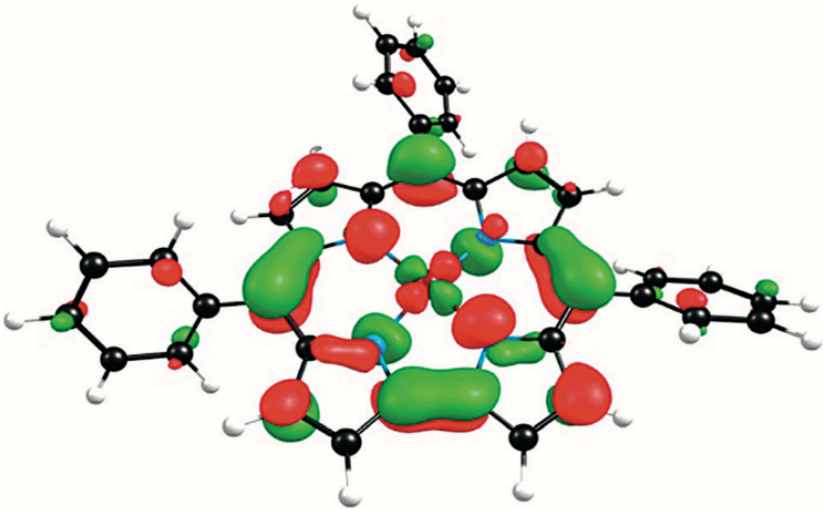

Fig. 2.13 DFT HOMO of Cu[TPC]. Reproduced with permissions from ref 144.

Although all Cu corroles are inherently saddled on electronic grounds, the degree of saddling increases with increasing sterically hindered character of the peripheral substituents. Thus, X-ray structural studies by Ghosh and coworkers indicated saddling dihedrals of χ_3 ~68° for Cu β-octabromo-*meso*-triarylcorroles[146] and χ_3 = 84.5° for a Cu β-octakis(trifluoromethyl)-*meso*-triarylcorrole, Cu[$(CF_3)_8$T*p*FPC]. The latter compound, with nearly orthogonal adjacent pyrrole rings (see Fig. 2.14), is the most strongly saddled metallocorrole reported to date.[147b] Interestingly, Cu undecaarylcorroles are slightly less saddled (χ_3 ~60-66°) than Cu β-octabromo-*meso*-triarylcorroles, but significantly higher than β-unsubstituted Cu[TPC] (χ_3 ~45°).[83c] The higher degree of saddling in the various sterically hindered Cu corroles results in enhanced Cu^{II}–corrole$^{\bullet 2-}$ antiferromagnetic coupling; as a result,

the NMR spectra of these complexes do not show any evidence of thermally accessible paramagnetic excited states.[146,83c]

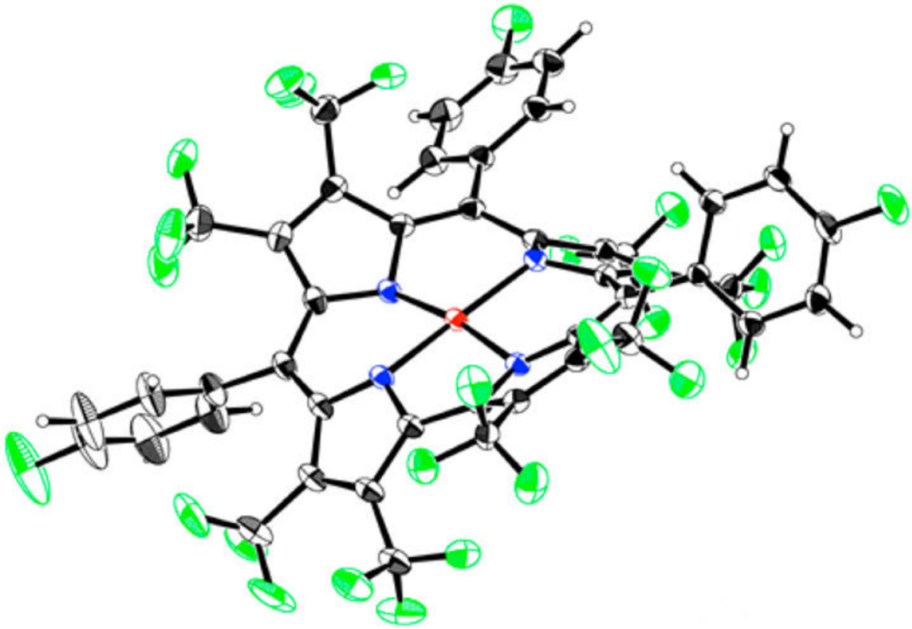

Fig. 2.14 X-ray structure of Cu[$(CF_3)_8$T*p*FPC]. Reproduced with permission from ref 147a.

Optical spectra provide some of the most dramatic illustrations of the noninnocent character of Cu corroles. Thus, Ghosh and co-workers have shown that the Soret maxima of Cu[Y_8T*p*XPC] derivatives (Y = H, Br, F, CF_3) exhibit dramatic redshifts with increasing electron-donating character of the *para* substituent X on *meso*-aryl groups (see Fig. 2.15).[75b,77,147a] Furthermore, for a given *meso* substituent, the Soret maximum redshifts along the following series of β-substituents, Y = H → F → Br → CF_3, which correlates with the increasing degree of saddling along the series. Overall, a 100-nm shift of the Soret maximum has been observed across the entire set of Cu[Y_8T*p*XPC] derivatives, from 407 nm for Cu[T*p*CF_3PC] to 507 nm for Cu[$(CF_3)_8$T*p*OMePC].

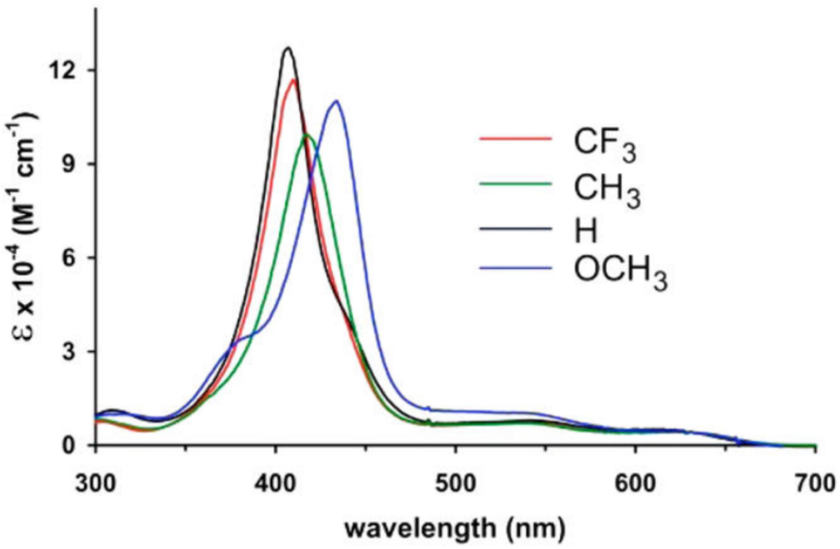

Fig. 2.15 UV-vis spectra of Cu[T*p*XPC] as a function of X. Reproduced with permission from ref 134.

TDDFT calculations by Ghosh and co-workers have provided crucial insight into the substituent-sensitive Soret maxima of Cu corroles. In particular, they showed that the key substituent-sensitive transitions under the composite Soret envelope which indicate that one or more transitions within the Soret envelop have significant aryl-to-corrole charge-transfer character.[148] In another study of a series of *trans*-A_2B Cu triarylcorroles, Ghosh and co-workers showed that only the substituents at 5,15-*meso* positions exert a significant influence on the positions of the Soret maxima.[149]

In contrast to Cu corroles, the Soret maxima of Ag[T*p*XPC] derivatives are found to be insensitive toward the *para*-substituents X.[151] The X-ray structure of a silver corrole also revealed only a slightly saddled Ag corrole core.[150] These findings appear to indicate a relatively innocent Ag^{III}-corrole^{3-} description for Ag triarylcorroles. For the Cu corroles, the relatively low energy of Cu $3d_{x2-y2}$ orbital facilitates the strong Cu(d_{x2-y2})-corrole(a_{2u}) orbital interaction, which is crucial for the corrole radical character. For Ag corroles, an analogous orbital interaction is much less favored because of the higher energy of Ag $4d_{x2-y2}$ orbital, which explains the lower degree of saddling of Ag triarylcorroles. TDDFT calculations also predict much less charge-transfer character in the Soret transitions of Ag[TPC], explaining the substituent-insensitive Soret maxima.

Bromination at β-positions of Ag corroles introduces new twists to the above story, as observed recently by Ghosh and co-workers.[152] Thus, the Soret maxima of β-octabromo series Ag[Br_8T*p*XPC] were found to redshift with increasing electron-donating character of the *para*-substituent X (Fig. 2.16). Also, a crystal structure of Ag[Br_8T*p*MeC] complex revealed a dramatically saddled macrocycle. Together, these results appeared to suggest that Ag[Br_8T*p*XPC] are significantly noninnocent. Ghosh and coworkers postulated that the steric factor, i.e., the increased inclination of Br_8T*p*XPC ligands to undergo saddling, and the electronic factor, i.e., the Ag($4d_{x2-y2}$)–corrole(a_{2u}) orbital interaction, reinforce each other, resulting in a noninnocent corrole with strongly saddled geometry. In other words, unlike simple Ag triarylcorroles, Ag[Br_8T*p*XPC] derivatives appear to be best described as Ag^{II}-corrole$^{\bullet 2-}$.[152] A recent X-ray absorption near-edge spectroscopic (XANES) study on Ag porphyrins and corroles provided additional evidence consistent with this picture.[153]

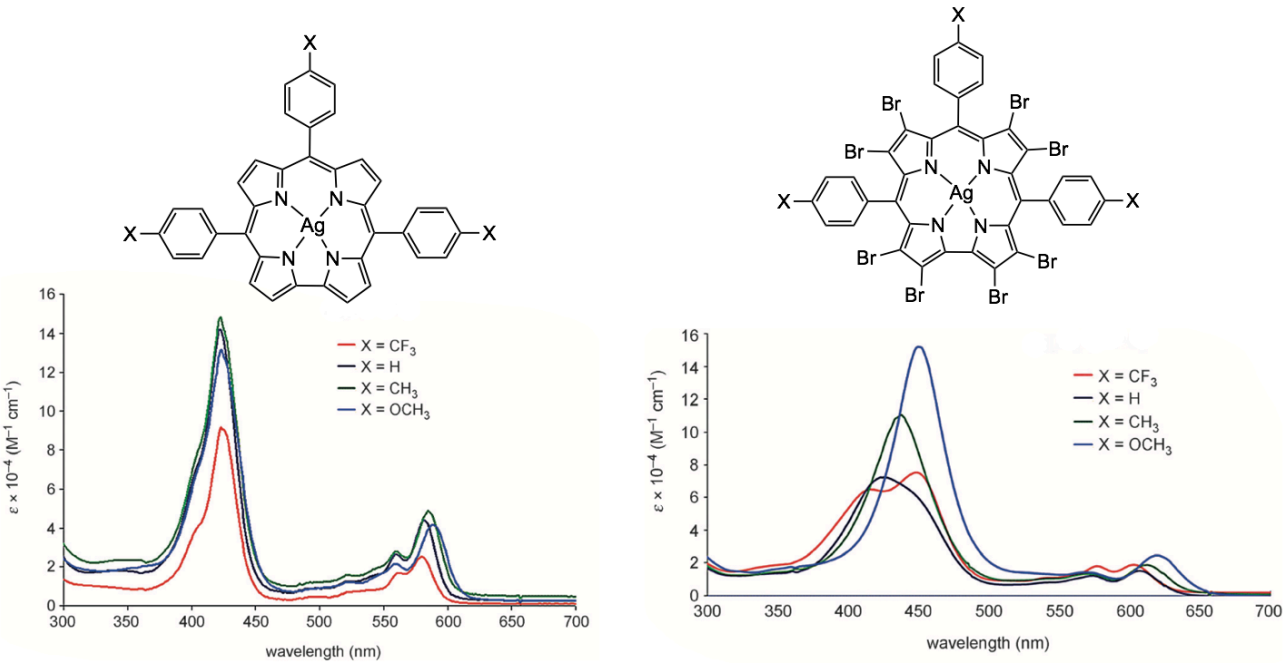

Fig.2.16 UV-vis spectra of two families of Ag corroles. Reproduced with permission from ref 152.

2.3.6 Innocent Metallocorroles

Metallocorroles with main-group elements provide archetypal examples of electronically innocent corrole ligands. Group 13 metallocorroles, including Al(III) and Ga(III) corroles, and Group 14 metallocorroles, including Ge(IV) corroles and Sn(IV)

corroles, exhibit sharp Soret and Q bands, which are explained by Gouterman's four-orbital model. Moreover, high values of electrochemical HOMO-LUMO gaps (~2.1–2.2 V) of these complexes are also indicative of an innocent corrole ligand in these complexes.[154-156] Group 15 corrole derivatives such as P^V *meso*-triarylcorroles,[157] As^{III}[OEC],[158] and Sb^{III}[OEC][158] all exhibit electrochemical HOMO-LUMO gaps of ~2.0-2.1 V, indicating macrocycle-centered redox reactions and hence an innocent corrole ligand.

Several electronically innocent 4d and 5d transition metal corroles have been identified by Ghosh and co-workers and these satisfy nicely the optical test for innocence/noninnocence described above. Thus Au,[151] OsN,[159] ReO,[160] ^{99}TcO,[161] and RuN[162] complexes of *meso*-triarylcorroles all exhibit substituent-independent Soret maxima and high electrochemical HOMO-LUMO gaps (~2.15 ± 0.10 V), which indicate an innocent corrole ligand and a redox-inactive metal center. On the other hand, CrO,[163] MoO,[163] Ag,[151] and RuNO[162] complexes of *meso*-triarylcorroles, together with the newly discovered Mo and W biscorroles,[164] all exhibit substituent-insensitive Soret maxima but relatively low electrochemical HOMO-LUMO gaps (~1.0-1.6 V). Therefore, these complexes thus contain an innocent corrole ligand coexisting with a redox-active metal center.

As archetypal innocent metallocorroles, Au corroles deserve a brief discussion. Compared with Cu and Ag corroles, Au corroles are found to be essentially planar.[151] Even a great deal of peripheral steric crowding does not affect the planarity of Au corroles, as exemplified by the X-ray structures of Au[(*p*CF_3Ph)$_8$TPC],[84c] Au[Br_8TPFPC],[165] and Au[(CF_3)$_8$T*p*FPC].[166] Compared with the nearly perfectly planar Au[(CF_3)$_8$T*p*FPC] complex (Fig. 2.17)., the saddling dihedrals in the analogous Cu complex are up to some 80° higher. This planarity of the Au corroles can be explained in terms of an almost insignificant metal(d_{x2-y2})–corrole(a_{2u}) orbital interaction as a result of the very high energy of the Au $5d_{x2-y2}$ orbital (in significant part due to relativistic effects). These same considerations explain the absence of charge-transfer character in Soret region of Au corroles, which explains the substituent-independent behavior of the Soret maxima of both the Au[T*p*XPC][151] (Fig. 2.18) and Au[Br_8T*p*XPC] series.[167]

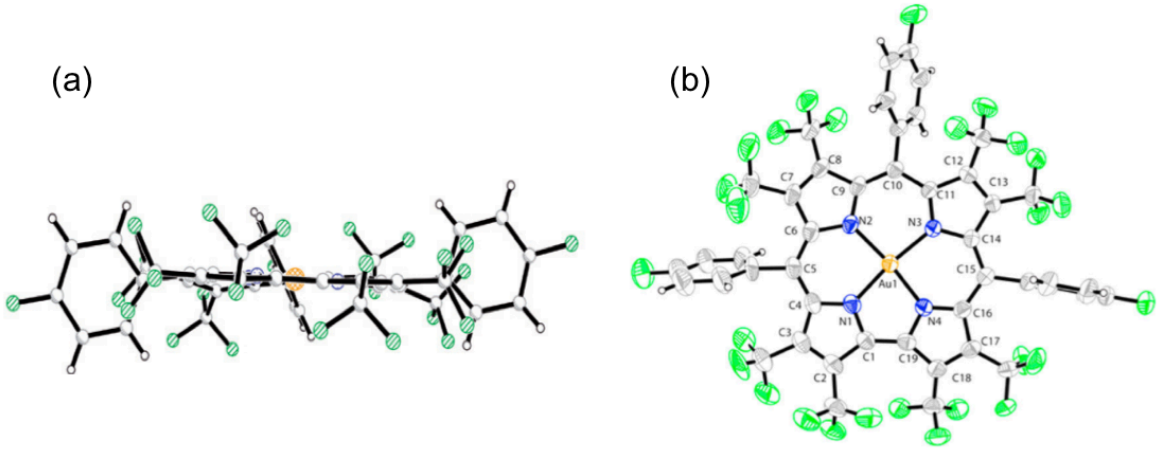

Fig. 2.17 X-ray structure of Au[$(CF_3)_8$T*p*FPC]: (a) side view (b) top view. Reproduced with permission from ref 166.

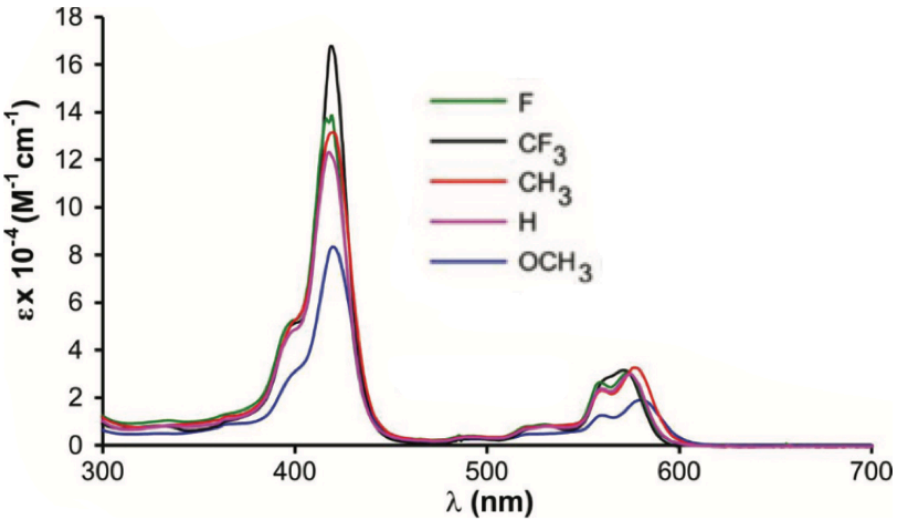

Fig. 2.18 UV-vis spectra of Au[T*p*XPC] as a function of X. Reproduced with permission from ref 151.

2.3.7 Conclusion

Since the original discoveries involving dithiolene complexes, the subject of ligand noninnocence has engaged inorganic and bioinorganic chemists for more than five decades. Although the discussion above focuses largely on electronic-structural aspects, it is worth emphasizing that noninnocent ligands are of great importance in catalytic transformations, especially for transition metal-mediated group transfer reactions. As discussed in section 2.3, research carried out in the Ghosh group including my own research has led to the identification of several metallocorrole families as paradigmatic noninnocent systems. Nearly a half-dozen tools have been

routinely used to characterize the phenomenon in metallocorroles, of which the use of optical spectroscopy is arguably the most convenient and striking. In this thesis, I have used all these tools to identify noninnocent corrole ligands in μ-oxo-diiron corroles (section 4.6.1, paper A) and Co-PPh_3 corroles (section 5.5.1, paper C). I have also used these tools to reexamine the known noninnocent families of FeCl and MnCl triarylcorroles (section 4.6.2; paper B and section 3.6, respectively). Using the same approach, I have also identified four classes of innocent metallocorroles, namely, FePh corroles (section 4.6.2, paper B), MnPh corroles (section 3.6), Rh-PPh_3 corroles (section 5.5.1, paper C), and Co-bispyridine corroles (section 5.5.2).

Chapter 3 – Manganese Corroles

3.1 Introduction

Manganese corroles are among the most intensively investigated 3d metallocorroles and their electronic properties, catalytic behavior, and biological applications have been summarized in a recent review.[168] For Mn corroles reported to date, the oxidation state of the Mn center ranges from +3 to +6. The present chapter focuses on the structural and electronic properties of the three classes of Mn corroles, namely the Mn(III) corroles, MnCl corroles, and Mn-aryl (MnPh) corroles, and concludes with a brief discussion of their fascinating electrochemical behavior.

3.2 Manganese(III) Corroles

Early reports of the synthesis of Mn-corroles involved *in situ* metal-coordination and subsequent cyclization of (a) 1,19-dideoxybiladiene-ac[48b] or (b) 2,2'-bisdipyrrins.[169] In both approaches, an Mn(II) ion serves as a template for the ring closure of the corresponding tetrapyrrolic precursor of corrole. In recent years, Mn(III) corroles have been conveniently prepared in high yields via metalation of the corresponding free-base corroles with a manganese salt such as $Mn(OAc)_2.4H_2O$ in refluxing DMF.[170] Manganese insertion can also be achieved in other solvents like methanol and pyridine.[171-173] Typically, the final product is the four-coordinate neutral Mn(III) corrole. These complexes, especially the more electron-rich ones, tend to undergo aerial oxidation, especially in solution. The electron-deficient complex Mn[TPFPC], however, is reasonably air-stable.[170] Mn(III) corroles serve as convenient starting materials for the synthesis of a variety of higher-valent Mn corrole derivatives, as depicted in Fig. 3.1.

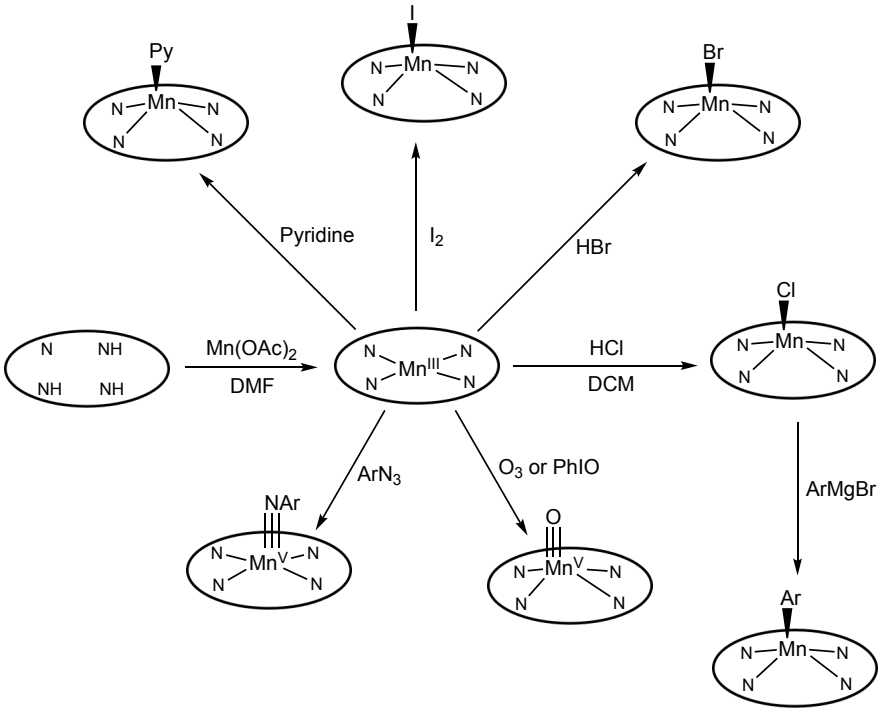

Fig. 3.1 Schematic representation of synthetic transformations of Mn corroles.

The crystal structures of Mn(III) corroles exhibit average Mn-N distances ~1.9 Å, suggesting an optimum steric match between the metal and the macrocyclic ligand. Unsurprisingly, the Mn atom is slightly displaced from corrole N_4 plane in five-coordinate Mn-corroles with an axial ligand such as pyridine, methanol, etc., whereas four-coordinate Mn(III) corroles are generally planar.[172,174-176]

Magnetic susceptibility measurements on Mn(III) corroles indicate a high-spin S = 2 metal center. Consistent with their paramagnetism, the ^{1}H NMR spectra exhibit broad signals with a wide range of chemical shifts. Most Mn(III) corroles are EPR-silent at room temperature. Instead, high-frequency and -field EPR (HFEPR) studies are performed to identify the spin state of manganese corroles. Bendix *et al*. reported the first HFEPR studies on a five-coordinate Mn corrole, Mn[TPFPC](OPPh$_3$), at two different frequencies and temperatures and assigned an S = 2 spin state for the Mn(III) complex.[175] Further HFEPR investigations were carried out by Krzystek *et al*. on the four-coordinate complex Mn[Et$_2$Me$_6$C], who also found an S = 2 state for the compound in the solid state.[177] Interestingly, Licoccia *et al*. have reported that the pyridine adduct of an Mn octaalkylcorrole, Mn[Me$_2$Et$_6$C](py), exhibits a six-line EPR spectrum centered around g = 2, when measured in pyridine at T = 100 K.[178] Temperature variation of the solution magnetic moment of Mn[Me$_2$Et$_6$C](py) was

thought to be indicative of antiferromagnetic coupling between an intermediate-spin Mn(II) (S = 3/2) ion and a corrole radical (S = 1/2) resulting in an overall S_{total} = 1 state. A similar observation was also noted by Kadish and co-workers for Mn[OEC](py), where the authors postulated a temperature dependent high- to low-spin conversion of the Mn(III) center due to the binding of a second pyridine ligand at low temperature.[174] However, according to Krzystek *et al.*, the Mn[Et_2Me_6C] complex exhibits an S = 2 Mn(III) HFEPR spectrum even in frozen pyridine solution, with the occurrence of a temperature-assisted valence isomerization from Mn^{III}−$Corr^{3-}$ at low temperature to Mn^{II}−$Corr^{\bullet 2-}$ at higher temperatures.[177]

Manganese corroles such as Mn[OEC] and Mn[OMC] exhibit characteristic UV-vis spectra in noncoordinating solvents such as DCM, which generally consist of a Soret band around 390 nm and a broad Q band around 600 nm. In coordinating solvents such as pyridine, the corresponding pentacoordinate complex Mn[OEC](py) forms in solution, which is reflected by an increase in intensity of a band around 480 nm.[174,178] Manganese *meso*-triarylcorroles, on the other hand, exhibit a split Soret band in DCM, with two peaks of almost equal intensity – one around 400 nm and another around 430-440 nm. When measured in pyridine, the band around 440 nm, increases in intensity along with a concomitant intensification of bands around 500 nm and 560-650 nm (see Fig. 3.2). These spectral changes are indicative of the formation of the five-coordinate, mono-pyridine adduct of the Mn corrole.[173,179,180] β-Octahalogenation significantly affects the UV-vis spectra of Mn(III) corroles, as evidenced by the significant redshift of both the Soret and Q bands for Mn(III) β-octabromocorroles.[176,234]

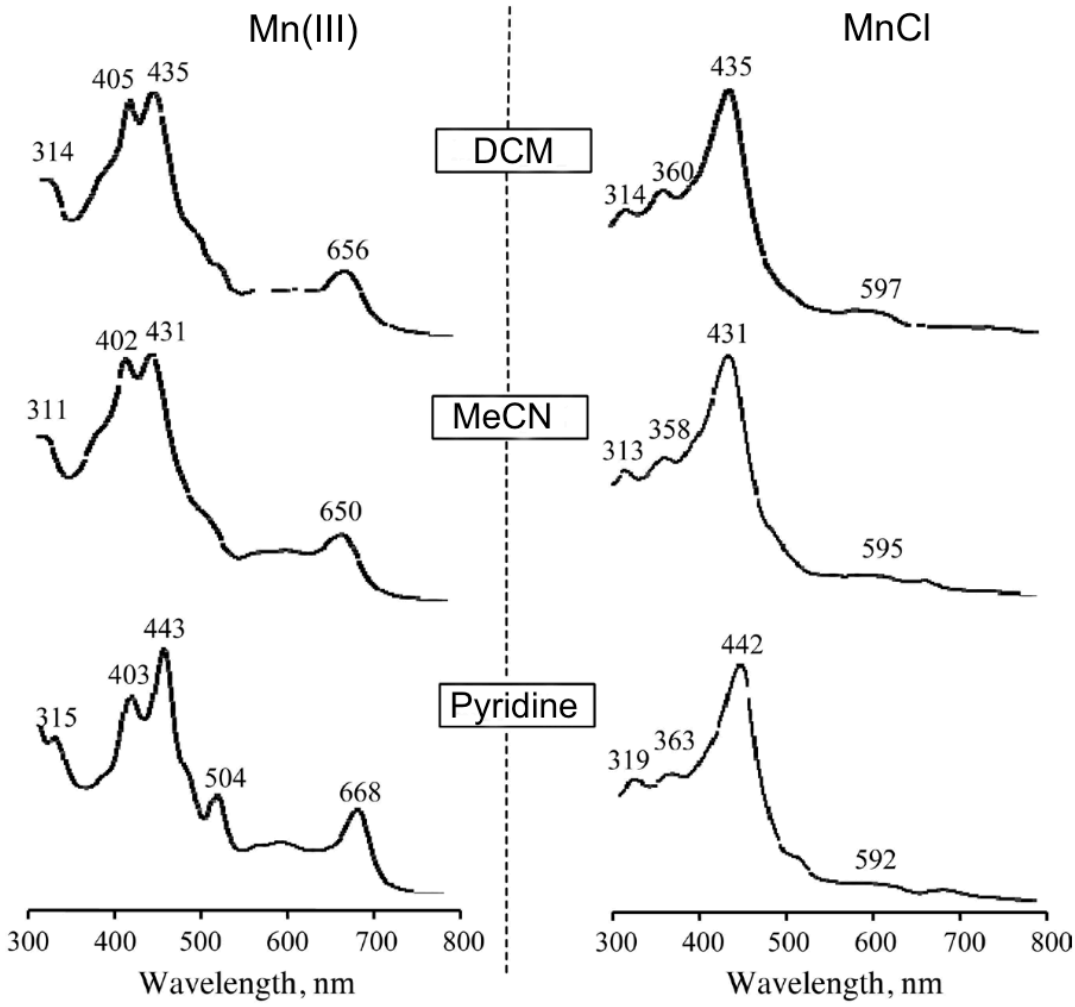

Fig. 3.2 UV-vis spectra of Mn corroles (neutral form) in different solvents, containing 0.1 M TBAP. Reproduced with permission from ref 134 (the original figure is from ref 179).

3.3 Chloromanganse Corroles

Chloromanganese corroles can be readily obtained by treatment of Mn(III) corrole solution with tris(4-bromophenyl)aminium hexachloroantimonate[181] or, more conveniently, with aqueous HCl under aerobic conditions.[179] MnCl corroles undergo ligand exchange reaction to afford pseudohalogeno derivatives, as reported by Bröring *et al*., who managed to synthesize a Mn-NCS corrole, $Mn[Et_8(pMeP)_2(H)C](NCS)$, by treating a MnCl corrole with KSCN at room temperature.[182]

X-ray structures of MnCl corroles reveal a square-pyramidal metal center, $Mn-N_4$ displacements of ~0.43 Å, and a mildly domed macrocycle (Fig. 3.3). The average $Mn-N_{corrole}$ bond distance is ~1.93 Å and the Mn-Cl distance (avg) is ~2.3 Å, which is

~0.05 Å shorter than that in Mn^{III}-Cl porphyrins.[174,183] Interestingly, an iodomanganese corrole, $Mn[Et_8(Ph)_2(H)C](I)$, was found to exhibit a smaller Mn-N_4 displacement (~0.38 Å) relative to a MnCl corrole.[184] The EPR spectrum of MnCl corroles (centered around g = 4) and the temperature-invariant nature of magnetic moment both suggest a Mn(IV) (S = 3/2) oxidation state for MnCl corroles.[174] UV-vis spectra of Mn[TPFPC](X) (X = Cl, Br) complexes also consist of relatively sharp, unsplit Soret bands (λ_{max} = 414 & 416 nm), which may again be viewed as suggestive of a Mn(IV) center.[181]

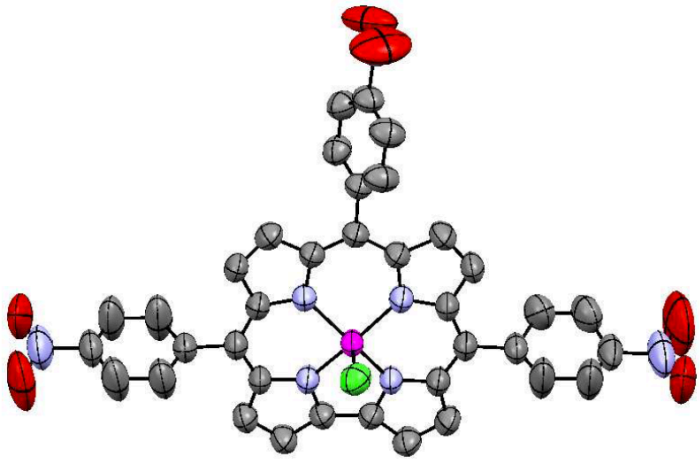

Fig. 3.3 X-ray structure of Mn[T*p*NO_2PC]Cl. Reproduced with permission from ref 183.

Ghosh and co-workers, however, have suggested a different electronic description for MnCl corroles, in light of UV-Vis spectroscopy and DFT calculations.[185,186] Thus, the Soret maxima of Mn[T*p*XPC]Cl derivatives undergo distinct redshifts with increasing electron-donating character of the *para* substituent X, which is suggestive of a Mn^{III}–corrole$^{\bullet 2-}$ description. In addition, DFT spin density profiles also indicate that MnCl corroles are described as a Mn(III) center (S = 2) antiferromagnetically coupled to a corrole a_{2u} radical (S = 1/2). The antiferromagnetic coupling involves a metal(d_z^2)-corrole(a_{2u}) overlap, which is facilitated by the out-of-plane displacement of the Mn atom from the N_4 plane.[185] Finally, the first oxidation and first reduction potential of Mn[T*p*XPC]Cl complexes are found to be almost similar to those of analogous chloroiron corroles, suggesting a similar electronic structure for all these complexes.[185] Based on these spectroscopic results, a noninnocent Mn^{III}–corrole$^{\bullet 2-}$ description suits best for MnCl corroles.

3.4 Manganese-Aryl Corroles

Manganese-aryl corroles can be obtained by the reaction of MnX corroles (X = Cl, Br) with an excess of arylmagnesium bromide (ArMgX) reagent. Although Grignard reagents are generally used,[174] a preformed mixture of equimolar *n*-BuLi and 1,4-$C_6H_4X_2$ (X = Br, I) can also be used for aryl functionalization.[187]

The molecular structure of Mn-aryl corroles exhibit significant differences relative to MnCl corroles. Thus, X-ray structural analysis reveals that the square-pyramidal complex Mn[OEC]Ph has a flattened macrocycle and a nearly in-plane manganese ion.[174] The average Mn-$N_{corrole}$ distance in the Mn-aryl corrole is shorter relative to MnCl corroles (~1.89 Å vs. ~1.93 Å). Also, the Mn-N_4 displacement in Mn-aryl corrole is lower than that in MnCl corroles (~ 0.244-0.286 Å vs. ~ 0.43 Å). Another interesting feature of the crystal structure of Mn[Et_6Me_2C](*p*-C_6H_4Br) is that the complex forms π-stacked dimers with an Mn…Mn distance separation of about 5 Å (Fig. 3.4).[187]

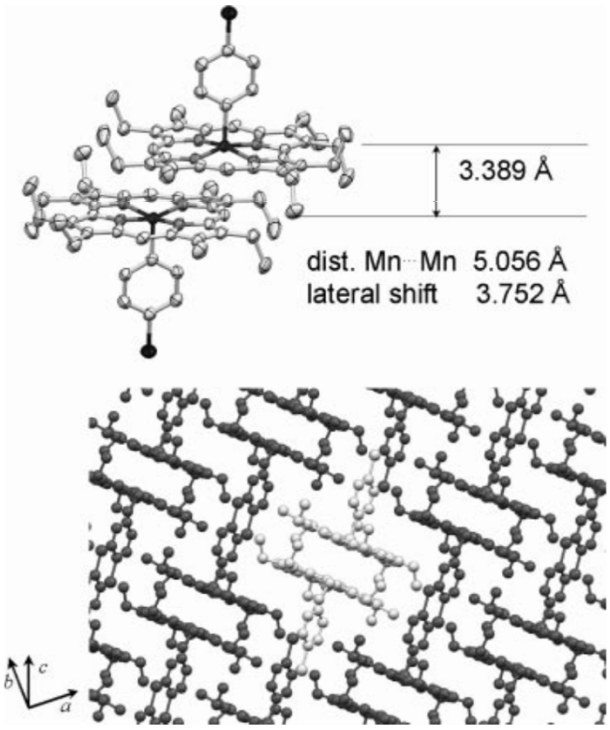

Fig. 3.4 π-Stacked dimers of Mn[Et_6Me_2](*p*-C_6H_4Br). Reproduced with permission from ref 187.

The UV-vis spectra of Mn-aryl corroles exhibit a characteristic single Soret band around 376 nm and broad Q bands between 520-620 nm. As for MnCl corroles, magnetic susceptibility measurements of Mn[OEC]Ph indicated a nearly temperature-independent magnetic moment (μ_{eff} = 3.56 μ_B), consistent with an S = 3/2 Mn(IV) center.[174] Indeed, the DFT spin density profile of Mn[TPC]Ph reveals a much smaller minority spin population on the corrole relative to Mn[TPC]Cl, consistent with a relatively innocent corrole in the former complex.[134] The lower Mn-N_4 displacement of Mn-aryl corroles relative to MnCl corroles can thus be understood in terms of a lesser degree of Mn(d_z^2)−corrole(a_{2u}) orbital interaction (which is necessary for Mn^{III}−corrole$^{\bullet 2-}$ antiferromagnetic coupling) in the former complex.

3.5 Electrochemistry of Mn(III), MnCl, and Mn-aryl Corroles

Manganese corroles exhibit a rich electrochemistry in non-aqueous media, which has been studied extensively.[189] The Mn[OEC] complex exhibits a reversible one-electron reduction ($E_{1/2}$ = −1.58 V) and two reversible, well-defined one-electron oxidations ($E_{1/2}$ = 0.36 and 0.93 V respectively) in PhCN. Based on its EPR spectrum (a six-line hyperfine splitting centered at g = 3.8 due to ^{55}Mn), the singly oxidized product is assigned as a $\{Mn^{IV}[OEC]\}^+$ species.[188,189] In PhCN, the one-electron reductions of Mn[OEC] and Mn[OEC](py) occur at quite highly negative potentials ($E_{1/2}$ = −1.58 V and E_{pc} = −1.66 V for Mn[OEC] and Mn[OEC](py), respectively). These values are substantially more negative than those for metal-centered reduction of Fe^{III}[OEC](py) ($E_{1/2}$ = −1.04 V in DCM) but are similar to those for ring-centered reduction of As^{III}[OEC] and Sb^{III}[OEC] ($E_{1/2}$ = −1.67 V and −1.66 V, respectively, in PhCN).[189] These results suggest that a Mn(III) corrole π-anion radical is formed after one-electron reduction, instead of a Mn(II) species.[189] Similar ligand-based reduction was also observed for the Mn[T*p*NO_2PC](py) complex, where the EPR spectrum after the first reduction at − 1.46 V did not show any signal attributable to a Mn(II) species.[173]

The first reversible reduction of Mn[OEC]Cl occurs at $E_{1/2}$ = −0.01 V in PhCN while the second reduction is irreversible and appears at almost the same value as the first reduction of Mn^{III}[OEC] ($E_{1/2}$ = −1.68 V); the latter suggests the formation of an Mn(III) corrole π-anion radical. Also, the UV-vis spectra obtained after the first and second electroreduction of Mn[OEC]Cl are similar to the spectra of neutral and one-

electron reduced Mn^{III}[OEC], respectively.[174] The nature of the one-electron oxidized MnCl corrole $\{Mn[OEC]Cl\}^+$, however, is a matter of debate. Although Kadish and co-workers assigned it as a Mn^{IV}−π-cation radical, DFT calculations suggest a doubly oxidized corrole formulation, i.e. Mn^{III}Cl−corrole$^-$.[134]

Kadish and co-workers have reported a detailed electrochemical investigation of the Mn[T*p*XPC] and Mn[T*p*XPC]Cl (X = F, Cl, H, Me) series of complexes.[179] Interestingly, the first oxidation of Mn[T*p*XPC] in DCM was found to be split into two wavelets, where the current was smaller for the first process than for the second (see Fig 3.5). The authors assigned the split oxidation to two different oxidation products, the naked cation $\{Mn[Cor]\}^+$ and the tight–ion-pair Mn[Cor](ClO_4), where ClO_4^- is derived from the supporting electrolyte. The potentials for the first reversible reduction of the Mn[T*p*XPC]Cl derivatives were found to be virtually identical to the first oxidation potentials of Mn[T*p*XPC] derivatives. Interestingly, the product formed after first reduction of Mn[T*p*XPC]Cl is a $\{Mn[Cor]Cl\}^-$ anion, with an axially bound chloride ion. Thin-layer UV−vis spectroelectrochemical studies showed that the spectra generated after controlled-potential one-electron reduction of Mn[T*p*XPC]Cl differ significantly from the spectra of neutral Mn^{III}[T*p*XPC], but are remarkably similar to the spectra generated upon addition of TBACl to Mn^{III}[T*p*XPC]. Thus, the one-electron reduced products of Mn[T*p*XPC]Cl derivatives were clearly identified as $\{Mn[Cor]Cl\}^-$.[179] The second reduction potential of Mn[T*p*XPC]Cl was found to be almost similar to the first reduction potential of Mn^{III}[T*p*XPC], indicating fast dissociation of Cl^- from the $\{Mn[TpXPC]Cl\}^-$ anions prior to further reduction ($E_{1/2}$ = −1.33 to −1.40 V in PhCN). The final products obtained after second reduction of Mn[Cor]Cl (or after the first reduction of Mn^{III}[Cor]) were found to exhibit a strongly redshifted Soret band at around 480 nm and a sharp, strong Q band around 660 nm) were assigned as Mn(II) species. With pyridine as solvent, the first reduction of Mn[Cor]Cl initially yields a $\{Mn[Cor]Cl\}^-$ anion, whose chloride axial ligand is replaced by a pyridine molecule to afford neutral Mn^{III}[Cor](py) species as the first reduced product. Again, the second reduction potentials of Mn[T*p*XPC]Cl complexes were found to be identical to the first reduction potentials of Mn[T*p*XPC] in pyridine ($E_{1/2}$ = −1.30 to −1.37 V), indicating formation of a Mn^{III} corrole π-anion radical (after the second reduction) in both cases.[179]

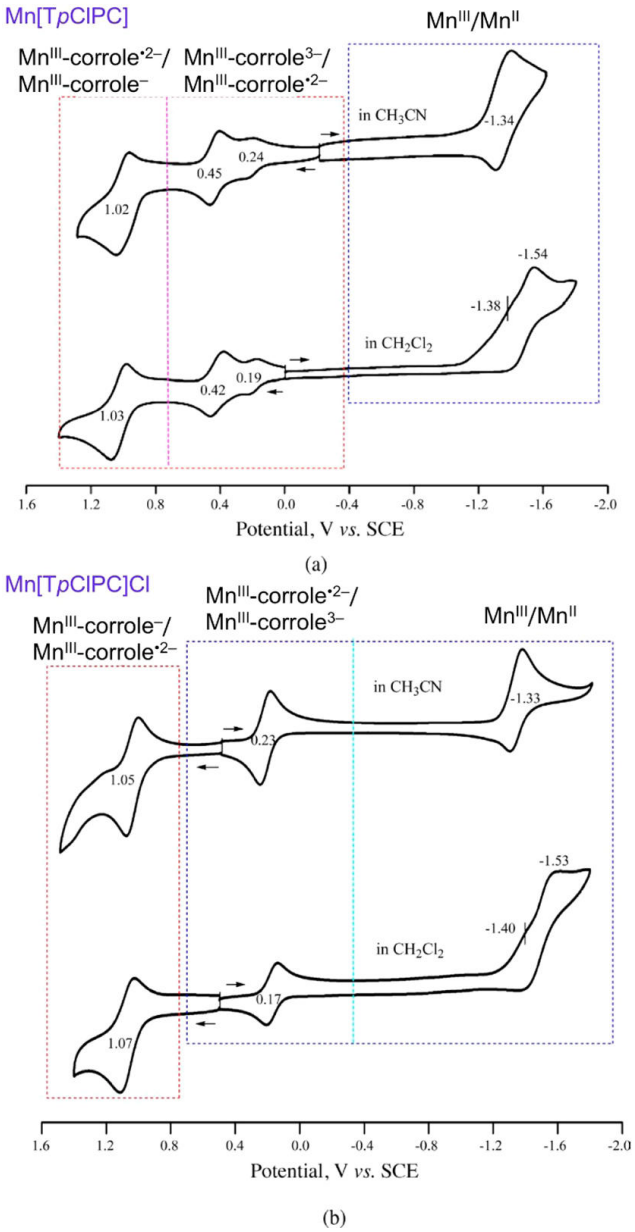

Fig. 3.5 Cyclic voltammograms of Mn(III) and MnCl corroles in DCM and MeCN containing 0.1 M TBAP. Reproduced with permission from ref 134 (the original figure is from ref 179).

The first reduction of Mn[OEC]Ph complex was found to be irreversible in PhCN (E_{pc} = –1.15 V).[174] Spectroelectrochemical studies (Fig. 3.6) revealed that the singly reduced species exhibit UV-vis spectra almost identical to the neutral, unreduced Mn[OEC] complex under the same solution condition, indicating that the reduction involves cleavage of metal-phenyl bond. The second reduction was found to be reversible ($E_{1/2}$ = –1.89 V) and is believed to be macrocycle-centered, based on the UV-vis spectrum obtained after thin-layer controlled-potential reduction of the

complex. Finally, one-electron oxidized Mn[OEC](Ph) corrole was assigned as an Mn^{IV}-corrole$^{\bullet 2-}$ species.[174]

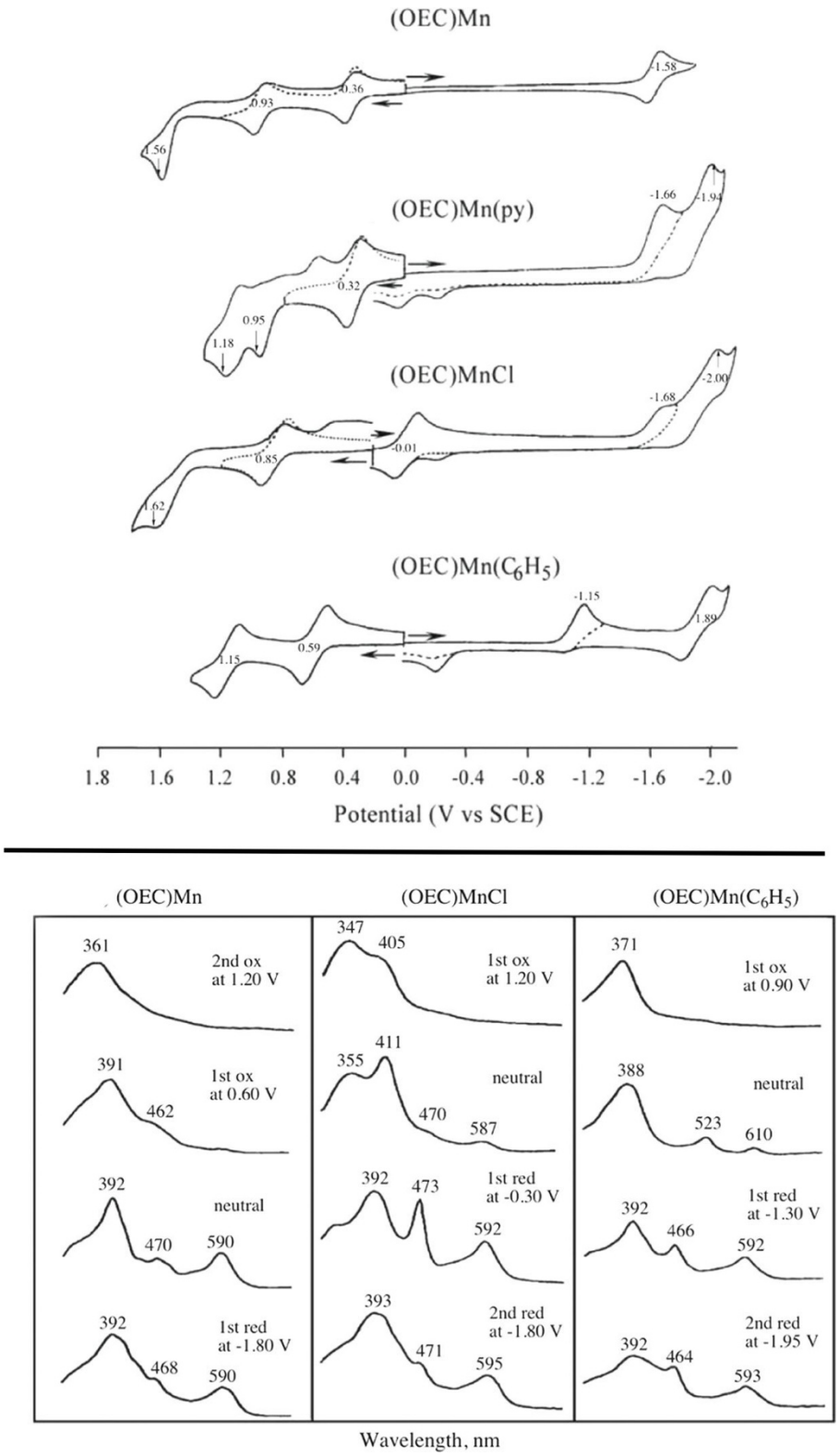

Fig. 3.6 Cyclic voltammograms (top) and electronic absorption spectra of neutral, reduced and oxidized species (bottom) of Mn[OEC] in PhCN containing 0.1 M TBAP. Reproduced with permission from ref 134 (original figure is from ref 174).

3.6 New Results on Ligand Noninnocence in MnCl and MnPh Corroles

In this section, I have summarized my own investigations of the question of ligand noninnocence in MnCl and MnPh corroles. Earlier work in our laboratory revealed a systematic redshift of the Soret maxima of Mn[T*p*XPC]Cl derivatives along the series X = CF_3 → H → Me.[185] As discussed in section 3.3, the MnCl corroles were accordingly thought to be best described as Mn^{III}–corrole$^{\bullet 2-}$ complexes. On the other hand, no such spectral comparisons have been reported for the Mn[T*p*XPC]Ph series, which, at the beginning of my project, had not been synthesized. I have therefore synthesized this series (X = CF_3, H, Me, OMe) as well as the new compound Mn[T*p*OMePC]Cl as well as the known compounds Mn[T*p*XPC]Cl (X = CF_3, H).

(a) Synthesis. The Mn[T*p*XPC]Cl corroles (X = CF_3, H, Me, OMe) were synthesized following a previously reported procedure.[179] Interaction of the corresponding free-base corroles with Mn(II) acetate in DMF at 165-170°C for approximately 45 min followed by column chromatography on silica gel with *n*-haxane/ethyl acetate as eluent afforded the pure Mn(III) corroles. The Mn corroles thus synthesized were then subjected to aerial oxidation in the presence of 10% aq. HCl, whereupon they oxidized to MnCl corroles. Silica gel column chromatography with DCM and DCM/MeOH as eluent afforded the pure Mn[T*p*XPC]Cl corroles. The new complex Mn[T*p*OMePC]Cl was obtained as a dark brown solid (dark brownish red in DCM solution) in approximately 39% yield (relative to H_3[T*p*OMePC]).

Arylation of the MnCl corroles was performed according to a published protocol.[174] The Mn[T*p*XPC]Cl complexes were dissolved in anhydrous DCM and treated with an excess (6 equiv) of phenylmagnesium bromide (3.0 M in Et_2O) under an inert atmosphere, whereupon Mn[T*p*XPC]Ph corroles formed via ligand exchange. The optimum reaction time was found to be about 7-8 min; longer reaction times resulted in drastic reductions of yield. The MnPh products were obtained in 33-42% yield after aerobic work-up. The Mn-Ph corroles are moderately stable as dry solids and can be stored in a freezer at low temperature. In solution under aerobic conditions, they decompose fairly quickly, via cleavage of the Mn-Ph bond, as shown by ESI-MS. The decomposition of Mn-Ph corroles is also visible to the naked eye as the dark reddish-brown solution turns yellowish-green within 1-2 hours under aerobic condition. Accordingly, accurate elemental analyses of the Mn-Ph corroles could not

be accomplished. For both the MnCl and MnPh complexes, the purity of the freshly prepared samples was judged primarily via ESI-MS.

(b) Optical Spectroscopy. The UV-vis spectra of the Mn[T*p*XPC]Cl series indicate a large redshift of the Soret maxima from X = CF_3 (423 nm) to X = OMe (460 nm) (see Fig. 3.7 and Table 3.1). The new complex Mn[T*p*OMePC]Cl exhibits an interesting split Soret band with absorptions of almost equal intensity at 394 and 460 nm. The substituent-sensitive Soret feature, along with DFT calculations (mentioned above), strongly suggest a noninnocent Mn^{III}–$corrole^{\bullet 2-}$ electronic description for the Mn[T*p*XPC]Cl complexes.

In contrast, the Soret maxima of the Mn[T*p*XPC]Ph series exhibit much smaller and somewhat erratic variations with respect to *para* substituent X. Although a nominal blue-shift of Soret maxima is observed on going from X = CF_3 (398 nm) to X = OMe (387 nm), the overall Soret envelope does not shift appreciably (Fig. 3.7). This observation appears to be consistent with an innocent Mn^{IV}–$corrole^{3-}$ electronic description for MnPh corroles.

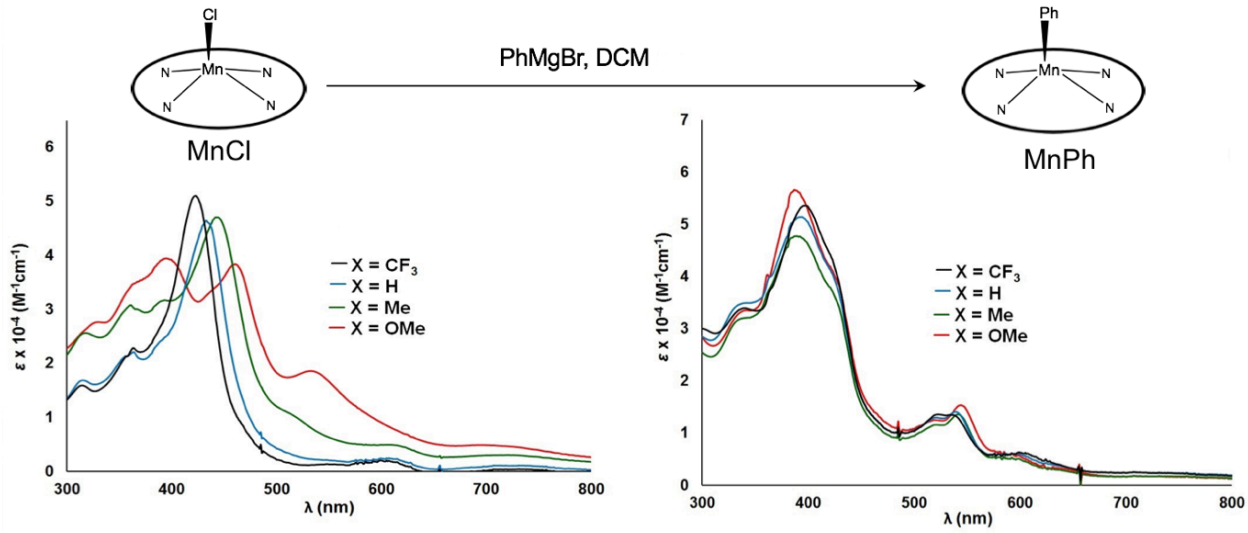

Fig. 3.7 UV-vis spectra of Mn[T*p*XPC]Cl (left) and Mn[T*p*XPC]Ph corroles (right), measured in DCM as a function of X.

Table 3.1 Soret absorption maxima (nm) of Mn corroles in DCM.

	p-substituent			
Series	CF_3	H	Me	OMe
Mn[T*p*XPC]Cl	423	433	442	460
Mn[T*p*XPC]Ph	398	394	389	387

(c) Electrochemistry. The cyclic voltammograms of Mn[T*p*XPC]Cl corroles in DCM exhibit a reversible one-electron reduction at 0.06 V-0.23 V, depending on the electronic nature of the *para* substituent X, which can be assigned as the following redox couple:

$$Mn^{III}(Cl)–corrole^{\bullet 2–} / Mn^{III}(Cl)–corrole^{3–}.$$

On the other hand, one-electron reduction of Mn[T*p*XPC]Ph corroles in DCM is irreversible (Fig. 3.8). The irreversible nature of the process can be explained in terms of reductive cleavage of the axial Mn-phenyl bond. This is in accord with partial radical character of the axial phenyl group, as suggested by DFT calculations. The second reduction is reversible and appears at high negative potential (–1.50 V – – 1.68 V). Also, two reversible oxidations are seen for the Mn-Ph corroles in DCM. The electrochemical HOMO-LUMO gap is observed to be much larger for Mn-Ph corroles (~1.7 V) compare to analogous Mn-Cl corroles (~0.9 V) (see Table 3.2)

Table 3.2 Electrochemical data (V) for Mn corroles.

Series	X	E_{ox2}	E_{ox1}	E_{red1}	$E_{red\text{-}irrev}$	E_{red2}	$E_{HOMO\text{-}LUMO}$
Mn[T*p*XPC]Cl	CF_3		1.17	0.23			0.94
	H		1.05	0.10			0.95
	Me		1.00	0.07			0.93
	OMe		0.93	0.06			0.87
Mn[T*p*XPC]Ph	CF_3	1.27	0.86		-0.90	-1.50	1.76
	H	1.13	0.77		-0.95	-1.68	1.72
	Me	1.06	0.73		-0.97	-1.66	1.70
	OMe	0.98	0.70		-0.99	-1.64	1.69

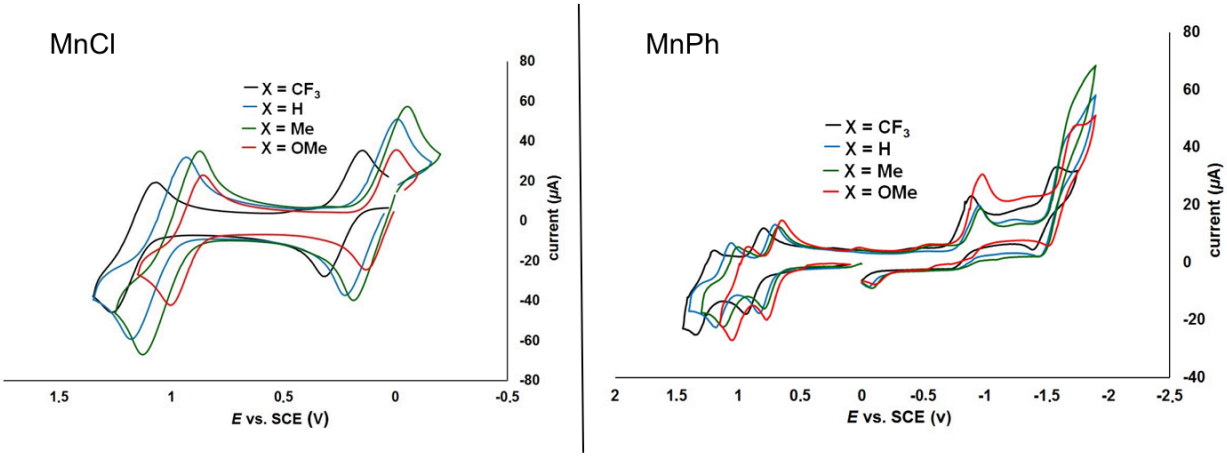

Fig. 3.8 Cyclic voltammograms of Mn[T*p*XPC]Cl (left) and Mn[T*p*XPC]Ph (right), measured in DCM containing 0.1 M TBAP (scan rate: 0.1 V/s).

(d) X-ray crystallography. I obtained a single-crystal X-ray structure for Mn[T*p*OMePC]Ph via vapor diffusion of MeOH into a concentrated $CHCl_3$ solution, the first Mn-σ-aryl structure with *meso*-triarylcorrole ligand. The complex was found to crystallize as a face-to-face stacked dimer (two units together in one unit cell). The average Mn-N distance for Mn[T*p*OMePC]Ph is ~1.9 Å, with the Mn…Mn distance being ~5.2 Å and a lower Mn-N_4 displacement (~0.28 Å).

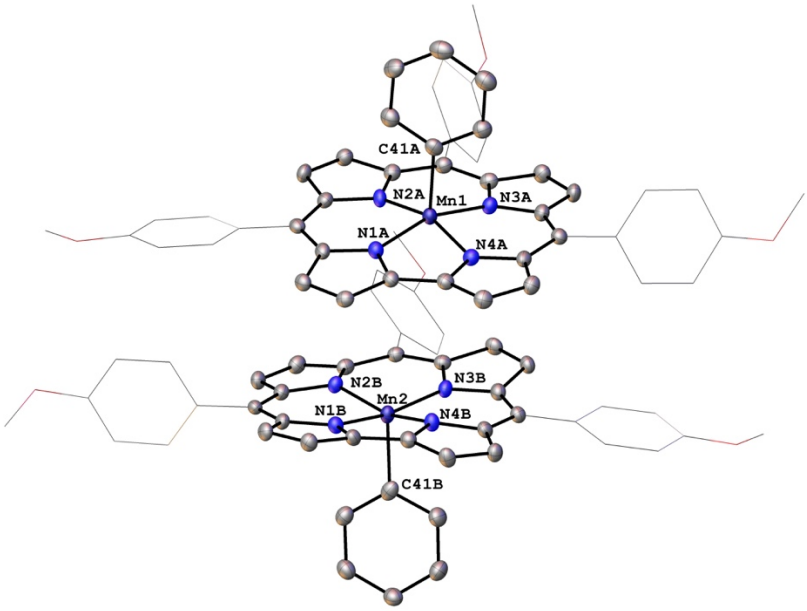

Fig. 3.9 X-ray structure of Mn[T*p*OMePC]Ph (π-stacked dimer).

(e) DFT calculations. DFT calculations on Mn[Cor]Ph indicated an *S* = 3/2 Mn(IV) center coordinated to an essentially innocent corrole^{3-} ligand (Fig. 3.10).[134]

However, the spin density profile of Mn[Cor]Ph reveals a large negative spin population on the *ipso* carbon of the σ-aryl group, which is suggestive of radical character of the axial phenyl group. Thus Mn-aryl corroles can be described as a resonance hybrid:

$$Mn^{IV} - Ar \leftrightarrow Mn^{III} - Ar^{\bullet}.$$

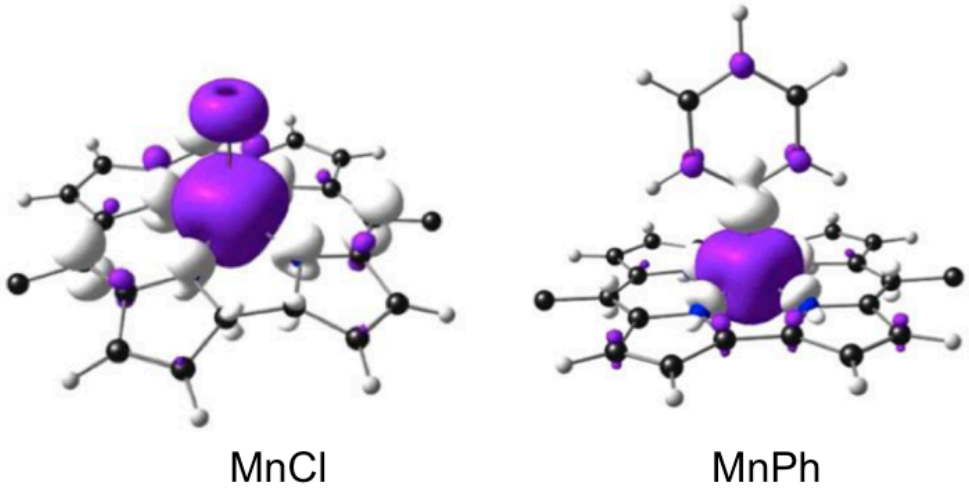

Fig. 3.10 DFT spin density profile of Mn[TPC] derivatives. Reproduced with permission from ref 134.

My contribution to the above work consisted of the syntheses and characterization (UV-Vis spectroscopy, MS, and electrochemistry) of the Mn[T*p*XPC]Cl and Mn[T*p*XPC]Ph derivatives and also obtaining an X-ray single crystals for Mn[T*p*OMePC]Ph, which was solved at the Advanced Light Source, Lawrence Berkeley National Laboratory. The DFT calculations were carried out by our collaborator Prof. Jeanet Conradie. The work on manganese corroles has not yet been written in manuscript form; accordingly an experimental section is provided below.

(f) Experimental section

Materials. All reagents and solvents were used as purchased unless otherwise noted. CHROMASOLV® HPLC-grade *n*-hexane and DCM were used as solvents for column chromatography. Silica gel 150 (35-70 *μ*m particle size, Davisil) was used as the stationary phase for flash chromatography and silica gel 60 preparative thin-layer chromatographic (PLC) plates (20 x 20 cm, 0.5 mm thick, Merck) were used for final purification of the products. Phenylmagnesium bromide

(3.0 M in diethyl ether) obtained from Sigma-Aldrich, and $Mn(OAc)_2.4H_2O$, obtained from Merck, were both used as received. Anhydrous DCM for electrochemistry was prepared by distillation after pre-drying with CaH_2 and stored over 3 Å molecular sieves. The free-base corroles H_3[T*p*XPC] (X = CF_3, H, Me, OMe) were synthesized as previously reported.[65]

Instrumentation. Ultraviolet-visible spectra were recorded on an Agilent Cary 8454 UV-Visible spectrophotometer in DCM. Cyclic voltammetry experiments were performed with an EG&G Princeton Applied Research Model 263A potentiostat equipped with a three-electrode system consisting of a glassy carbon working electrode, a platinum wire counterelectrode, and a saturated calomel reference electrode (SCE). Tetrakis(*n*-butyl)ammonium perchlorate (Sigma-Aldrich, TBAP), recrystallized three times from absolute ethanol, vacuum-dried at 40°C for two days, and kept in a desiccator for further drying for at least two weeks, was used as the supporting electrolyte. The reference electrode was separated from bulk solution by a fritted-glass bridge filled with the solvent/supporting electrolyte mixture. All potentials were referenced to the SCE. A scan rate of 100 mV/s was used. The anhydrous DCM solutions were purged with argon for at least 5 min prior to electrochemical measurements and an argon blanket was maintained over the solutions during the measurements. High-resolution electrospray ionization (HR-ESI) mass spectra were recorded on an LTQ Orbitrap XL spectrometer.

Synthesis of MnCl corrole complexes. A detailed procedure is described below for the synthesis of Mn[T*p*OMePC]Cl. A similar procedure was also followed for synthesis of the other Mn complexes, except for details of the chromatographic purifications, which are specified separately.

Synthesis of Mn[T*p*OMePC]Cl. A 100-mL two-necked round-bottomed flask equipped with a magnetic stir-bar was charged with free-base tris(4-methoxyphenyl)corrole (0.1 g, 0.16 mmol) and DMF (40 mL) as solvent. To the solution was added 10 equiv $Mn(OAc)_2$•$4H_2O$ (0.392 g, 1.6 mmol) and argon was bubbled through the solution for 5 min. The reaction flask was then fitted with a reflux condenser and heated on an oil bath at 165-170°C with stirring for approximately 45 min. Completion of the reaction was confirmed by UV-vis spectroscopy and mass spectrometry. Upon cooling, the solution was rotary evaporated to dryness to yield a dark brownish-green residue. The residue was

redissolved in a minimum volume of 1:1 DCM/ethyl acetate and was chromatographed on a silica gel column (8-10 cm in height) with 1:1 *n*-hexane/ethyl acetate as eluent. The front-running green band and the second, reddish-brown band were collected and combined; these contained the initially formed Mn(III) corrole (as confirmed by ESI-MS).

The combined fraction was rotary evaporated to dryness and the residue was redissolved in DCM (25 mL). The DCM solution of the Mn(III) corrole was treated with 10% aqueous HCl (3 x 25 ml), washed twice with distilled water, dried over anhydrous Na_2SO_4, and filtered, and the filtrate was rotary evaporated under vacuum to yield a dark reddish-brown residue. The residue was redissolved in a minimum volume of DCM and chromatographed on a silica gel column (10 cm in height) with DCM and subsequently with 1:0.01 DCM/methanol as eluent. The reddish-brown band was collected and identified as pure Mn[T*p*OMePC]Cl (0.044g, 0.062 mmol, 39% yield relative to free-base H_3[T*p*OMePC]. UV-vis (CH_2Cl_2) λ_{max} [nm, ε x 10^{-4} ($M^{-1}cm^{-1}$)]: 330 (2.77), 394 (3.95), 460 (3.84), 533 (1.86). HRMS (major isotopomer) $[M]^-$: 703.1314 (expt), 703.1314 (calc).

Synthesis of Mn[T*p*MePC]Cl. Silica gel column chromatography with DCM and subsequently with 1:0.005 DCM/methanol as eluent afforded the pure product (0.061g, 0.09 mmol, 53% relative to H_3[T*p*OMePC]). UV-vis (CH_2Cl_2) λ_{max} [nm, ε x 10^{-4} ($M^{-1}cm^{-1}$)]: 318 (2.56), 361 (3.08), 442 (4.71). HRMS (major isotopomer) $[M]^-$: 655.1467 (expt), 655.1467 (calc).

Synthesis of Mn[TPC]Cl. Silica gel column chromatography with DCM and subsequently with 1:0.005 DCM/methanol (200 mL) as eluent afforded the pure product (0.053g, 0.086 mmol, 45% relative to H_3[TPC]). UV-vis (CH_2Cl_2) λ_{max} [nm, ε x 10^{-4} ($M^{-1}cm^{-1}$)]: 315 (1.69), 363 (2.21), 433 (4.64). HRMS (major isotopomer) $[M]^-$: 613.1000 (expt), 613.0997 (calc).

Synthesis of Mn[T*p*CF_3PC]Cl. Silica gel column chromatography with DCM (3 x 500 mL) and subsequently with 1:0.005 DCM/methanol (100 mL) as eluent afforded the pure product (0.062g, 0.076 mmol, 54% relative to H_3[T*p*CF_3PC]). UV-vis (CH_2Cl_2) λ_{max} [nm, ε x 10^{-4} ($M^{-1}cm^{-1}$)]: 314 (1.59), 363 (2.29), 423 (5.10). HRMS (major isotopomer) $[M]^-$: 817.0612 (expt), 817. 0619 (calc).

Synthesis of Mn-phenyl corroles. A detailed procedure is described below for the synthesis of Mn[T*p*OMePC]Ph. A similar procedure was also followed for

synthesis of the other Mn complexes, except for details of the chromatographic purifications, which are specified separately.

Synthesis of Mn[T*p*OMePC]Ph. A 50-mL round-bottom flask equipped with a magnetic stir-bar was charged with Mn[TpOMePC]Cl (0.04g, 0.057 mmol). Anhydrous DCM (15 mL) was added with a syringe under argon and the mixture was stirred under argon for 5 min. Phenylmagnesium bromide (114 μL, 6 equiv) was then added with a syringe, and the mixture was stirred under argon for 7-8 min. The solution was then quenched with an excess of distilled water and extracted with DCM. The organic fraction was dried with anhydrous $MgSO_4$ and filtered, and the filtrate was dried on a rotary evaporator under vacuum. The dark brown residue obtained was redissolved in a minimum volume of DCM and chromatographed on a silica gel column with 1:1 *n*-hexane/DCM as eluent. The product eluted as an intense dark red band, which was collected and evaporated to dryness. Final purification was carried out with PLC using 1:2 *n*-hexane/DCM as eluent. The frontrunning red band contained pure Mn[T*p*OMePC]Ph (0.014g, 33%). UV-vis (CH_2Cl_2) λ_{max} [nm, ε x 10^{-4} ($M^{-1}cm^{-1}$)]: 341 (3.35), 387 (5.67), 429(sh) (3.8), 519 (1.26), 544 (1.54). HRMS (major isotopomer) $[M]^+$: 745.2009 (expt), 745.2006 (calc).

Needle-shaped X-ray quality crystals were obtained by slow diffusion of MeOH vapor into a concentrated $CHCl_3$ solution of the complex over one week.

Synthesis of Mn[T*p*MePC]Ph: Silica gel column chromatography with 3:1 *n*-hexane/DCM followed by PLC with 3:2 *n*-hexane/DCM as eluent afforded pure Mn[T*p*MePC]Ph (0.0156 g, 37%). UV-vis (CH_2Cl_2) λ_{max} [nm, ε x 10^{-4} ($M^{-1}cm^{-1}$)]: 341 (3.21), 389 (4.8), 521 (1.16), 542 (1.36). HRMS (major isotopomer) $[M]^+$: 697.2150 (expt), 697.2158 (calc).

Synthesis of Mn[TPC]Ph: Silica gel column chromatography with 3:1 *n*-hexane/DCM followed by PLC with 2:1 *n*-hexane/DCM as eluent afforded pure Mn[TPC]Ph (0.018g, 42%). UV-vis (CH_2Cl_2) λ_{max} [nm, ε x 10^{-4} ($M^{-1}cm^{-1}$)]: 341 (3.5), 394 (5.15), 521 (1.3), 539 (1.4). HRMS (major isotopomer) $[M]^+$: 655.1690 (expt), 655.1689 (calc).

Synthesis of Mn[T*p*CF_3PC]Ph: Silica gel column chromatography with 4:1 *n*-hexane/DCM followed by PLC with 3:1 *n*-hexane/DCM as eluent afforded pure Mn[T*p*CF_3PC]Ph (0.016 g, 38%). UV-vis (CH_2Cl_2) λ_{max} [nm, ε x 10^{-4} ($M^{-1}cm^{-1}$)]: 340 (3.4), 398 (5.36), 523 (1.36), 535 (1.35). HRMS (major isotopomer) $[M]^+$: 859.1317 (expt), 859.1311 (calc).

Chapter 4 – Iron Corroles

4.1 Introduction

Iron corroles are notable for their rich electronic-structural features and their application as catalysts for several important transformations. In this chapter, key Fe-corrole derivatives relevant to this thesis, including Fe(III), FeCl, Fe-aryl and $Fe_2(\mu\text{-O})$ corroles, are discussed, with emphasis on their structural and electronic properties.

4.2 Iron(III) Corroles

Iron(III) corroles are formed upon initial iron insertion into free base corroles, but they are readily oxidized during aerobic work-up. Vogel *et al*. experienced formation of μ-oxo diiron corroles due to aerial oxidation of the corresponding Fe(III) corroles and observed that such oxidation could be prevented by treating the Fe(III) corroles with pyridine prior to admission of air.[190] The complex formed under the latter conditions was a five-coordinate mono-pyridine adduct, Fe[OEC](py), as revealed by its X-ray crystal structure. Magnetic susceptibility measurements of the complex indicated an S = 3/2 state, whereas the Mössbauer isomer shift was suggestive of a Fe(IV) center.

Gross *et al*. showed that oxidation of Fe(III) corroles could be prevented when diethyl ether is used as solvent. Using diethyl ether as solvent and eluent, the Fe^{III}[TPFPC] complex could be isolated as an air-stable bisetherate, $Fe[TPFPC](OEt_2)_2$.[191] The bisetherate complex can serve as a convenient precursor for a variety of other Fe corroles, as illustrated below in Figure 4.1.

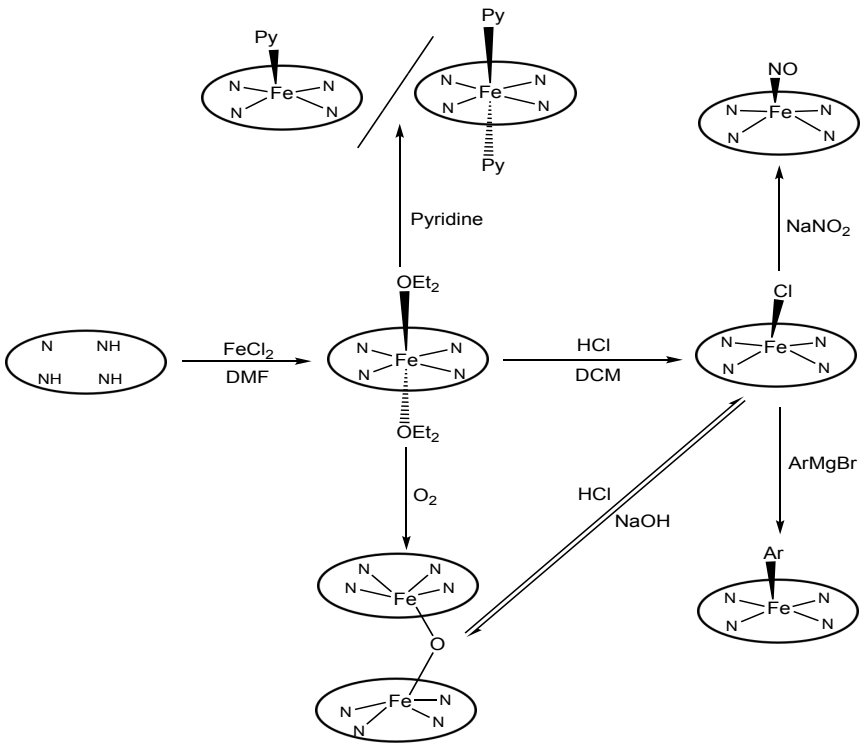

Fig. 4.1 Synthetic transformations of Fe corroles.

Recrystallization of Fe[TPFPC]$(OEt_2)_2$ from a solvent mixture containing pyridine afforded the corresponding bispyridine-ligated iron(III) corrole, Fe[TPFPC]$(py)_2$.[191] The X-ray structures of both Fe[TPFPC]$(py)_2$[191] and Fe[OEC](py)[190] reveal a planar corrole ring and short Fe−$N_{corrole}$ distances (1.89 ± 0.025 Å). However, Fe[OEC](py) exhibits slightly a significant Fe-N_4 displacement (0.273 Å), as well as a longer Fe-N_{py} bond distance (2.188 Å), relative to Fe[TPFPC]$(py)_2$. A recent X-ray structure of an Fe-bispyridine octabromocorrole, Fe[Br_8TDCPC]$(py)_2$, exhibits structural parameters similar to Fe[TPFPC]$(py)_2$, i.e. a planar corrole with Fe-$N_{corrole}$ averaging 1.90 Å and an Fe-N_{py} distance of 2.02 Å, as well as coplanar alignment of the axial pyridines along the C_5−C_{15} axis of the corrole ring (Fig. 4.2).[87b]

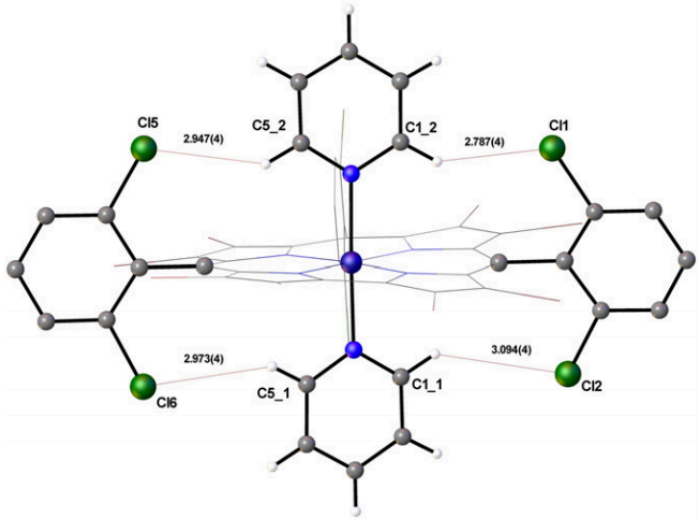

Fig. 4.2 X-ray structure of Fe[Br_8TDCPC]$(py)_2$. Reproduced with permission from ref 87b.

The β-pyrrolic protons of Fe(III) corroles exhibit interesting ^{1}H NMR chemical shifts that are indicative of their spin states and can be interpreted by analogy with Fe(III) porphyrins. As observed for the Fe(III) porphyrins, these protons appear at very low fields for high-spin (S = 5/2) state, at very high fields for low-spin (S = 1/2) state, and at moderately high to moderately low fields for intermediate-spin (S = 3/2) state.[192] For the Fe[TPFPC]$(OEt_2)_2$ complex, two β-protons resonances appear at high field(δ = −60.0, −126.0 ppm), while the other two resonances appear at low field (δ = 19.7, 13.4 ppm), which is indicative of an intermediate-spin (S = 3/2) Fe(III) complex (Fig. 4.3).[191] In contrast, all four β-proton resonances for Fe[TPFPC]$(py)_2$ appear at high field (δ = 3.2, −61.1, −65.8, −134.6 ppm), suggesting a low spin (S = 1/2) Fe(III) state (Fig. 4.4).[193] The EPR spectra of these two complexes also agree with these spin-state assignments. Thus, the EPR spectrum of Fe[TPFPC]$(py)_2$ exhibits a typical pattern for low-spin S = 1/2 species, centered around g = 2. On the other hand, Fe[TPFPC]$(OEt_2)_2$ exhibits a broad g = 3.8 feature, consistent with an S = 3/2 state. Moreover, the S = 3/2 spin state for Fe[TPFPC]$(OEt_2)_2$ could also be confirmed by magnetic susceptibility measurements.[193]

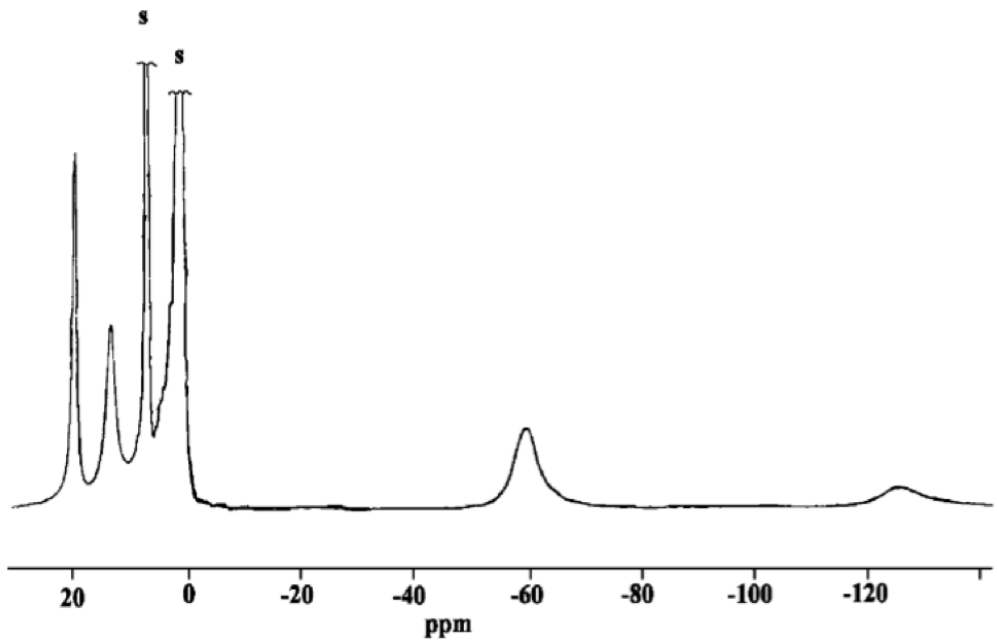

Fig. 4.3 ^{1}H NMR spectrum of Fe[TPFPC]$(Et_2O)_2$. Reproduced with permission from ref 193.

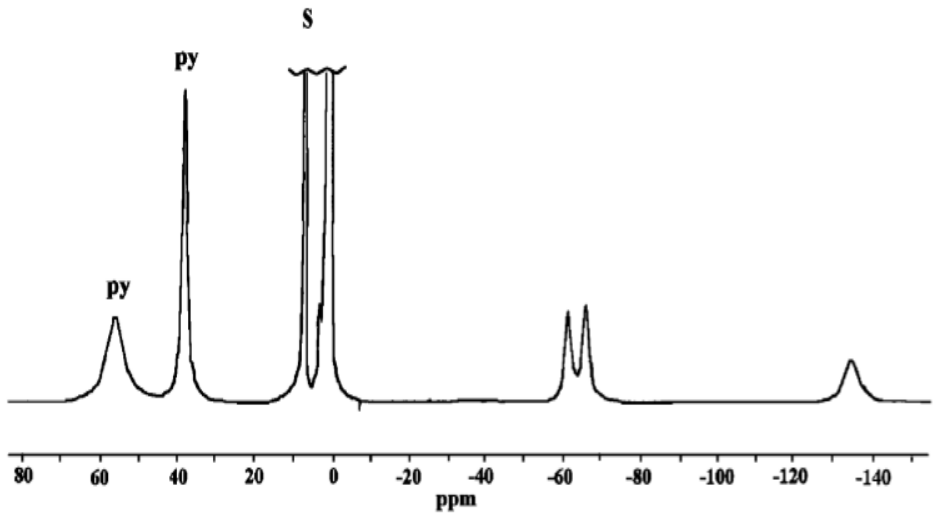

Fig. 4.4 ^{1}H NMR spectrum of Fe[TPFPC]$(py)_2$. Reproduced with permission from ref 193.

4.3 Chloroiron Corroles

Vogel *et al*. reported the first FeCl corrole in their seminal work on iron corroles, where the initially formed μ-oxo diiron corroles (obtained via the reaction of free-base H_3[OEC] with $Fe_2(CO)_9$) afforded Fe[OEC]Cl upon treatment with 1 M HCl.[190] The ^{1}H NMR spectrum of Fe[OEC]Cl revealed its paramagnetic character, with extreme downfield chemical shifts observed for the *meso*-protons {δ: 177 (br, 2H, 5,15-H) and 189 (br, 1H, 10-H)}. Based on the results from magnetic

susceptibility (μ_{eff} = 2.97) and Mössbauer spectroscopic studies, the authors suggested a formally Fe(IV) center with an S = 1 ground state for Fe[OEC]Cl. Subsequently, the Fe(IV) formulation[195,196] was questioned and the current electronic structural picture is that of a noninnocent metalloradical, Fe^{III}–$corrole^{\bullet 2-}$.

A consideration of ^{1}H NMR chemical shifts led Walker *et al*. to propose that FeCl corroles are intermediate-spin Fe(III) centers (S = 3/2) antiferromagnetically coupled to $corrole^{\bullet 2-}$ radicals,[125] and not Fe(IV) complexes. As for Fe[OEC]Cl, these authors observed extremely large downfield shifts of *meso*-H resonances for Fe[OMC]Cl and Fe[Me_2Et_6C]Cl (δ: ~172-189 ppm) (Fig. 4.5). It may be recalled that for the analogous porphyrin complex Fe[OEP]Cl (S = 5/2), the *meso*-H resonance exhibits a considerable upfield shift (δ: –56 ppm). The strikingly divergent *meso*-^{1}H shifts of Fe[OEC]Cl and Fe[OEP]Cl suggested *meso* spin populations of opposite signs for the two compounds. Moreover, the large positive chemical shifts of the *meso*-H's of FeCl corroles could only indicate large negative π-spin densities at the meso positions, which would be antiferromagnetically coupled to the unpaired electrons on the Fe.[197] The FeCl corroles were found to be EPR silent while magnetic susceptibility measurements (μ ~3.0 μ_B) indicated an overall S = 1 state.[198]

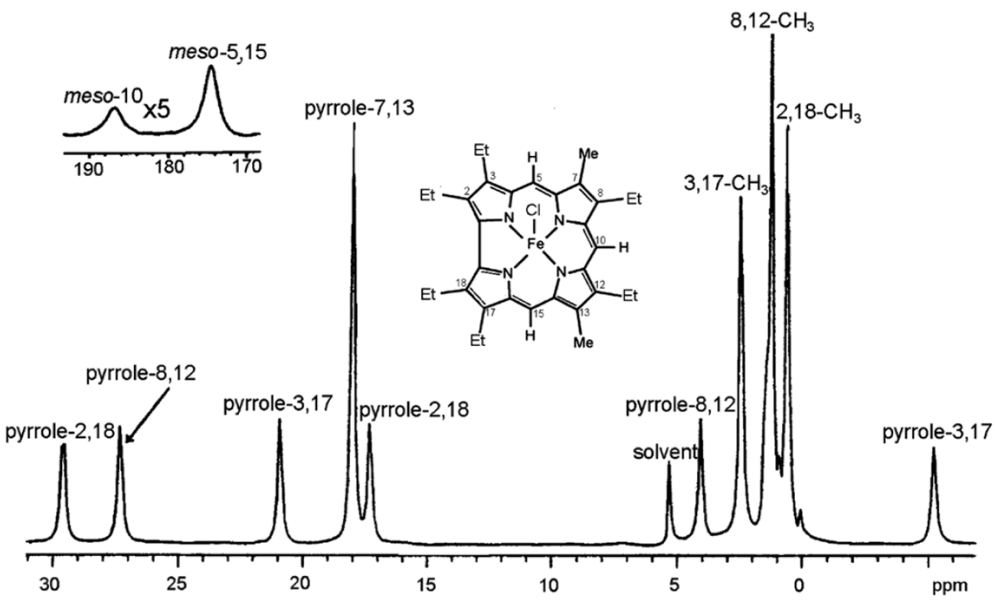

Fig. 4.5 ^{1}H NMR spectrum of Fe[Me_2Et_6C]Cl. Reproduced with permission from ref 197.

Walker and co-workers further investigated the ^{1}H NMR paramagnetic shifts for several Fe[T*p*XPC]Cl derivatives and found a notable pattern for the *meso*-phenyl

proton resonances.[199] Thus, the ^{1}H NMR spectrum of Fe[TPC]Cl exhibits positive (i.e., downfield) chemical shifts for the *ortho*-H and *para*-H and a negative shift for *meta*-H (i.e., upfield) of *meso*-phenyl rings (Fig. 4.6). This leads to the negative chemical shift differences (δ_m - δ_o) and (δ_m - δ_p), which are characteristic of negative spin densities at the *meso*-carbons, as for FeCl octaalkylcorroles.

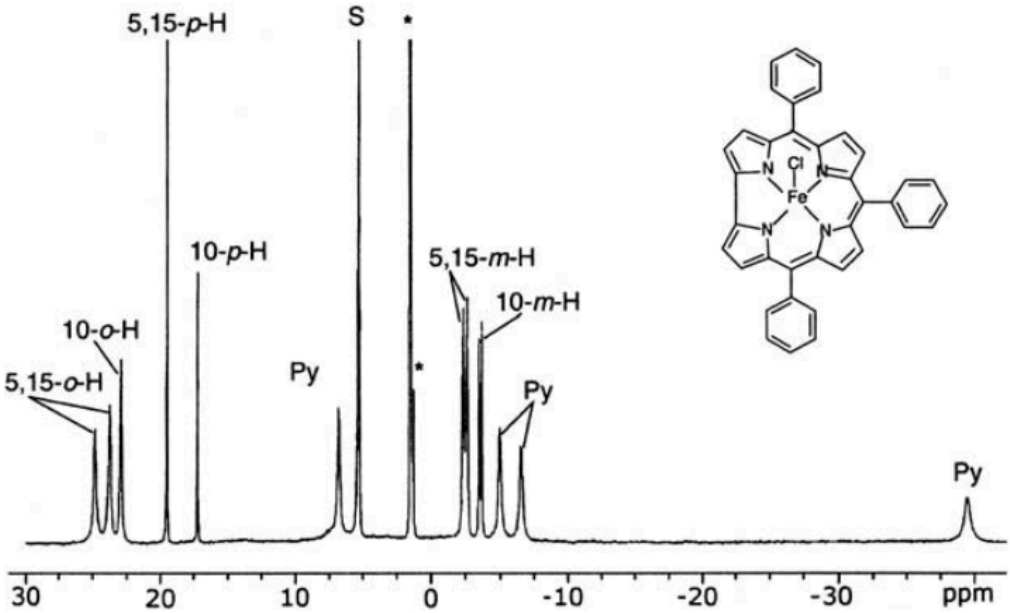

Fig. 4.6 ^{1}H NMR spectrum of Fe[TPC]Cl. Reproduced with permissions from ref 199.

^{13}C NMR paramagnetic shifts for FeCl corroles were also found to be useful for mapping the spin density around the macrocycle.[200] The *meso*-carbon spin densities of Fe[TPC]Cl and the undecasubstituted complex Fe[Me$_8$TPC]Cl could be predicted by estimating the ^{13}C chemical shift differences for *meso*-phenyl carbons. As expected, the δ_m–δ_p value indicated a negative spin density at the *meso* positions of Fe[TPC]Cl. Surprisingly, the shift difference the δ_m–δ_p value for the *meso*-phenyl carbons of Fe[Me$_8$TPC]Cl was opposite in sign relative to Fe[TPC]Cl, suggesting significant *positive* spin density at the *meso*-carbons of Fe[Me$_8$TPC]Cl. This was explained in terms of an intermediate spin (S = 3/2) Fe(III) center, ferromagnetically coupled to a corrole$^{\bullet 2-}$ radical to give an overall S = 2 state for Fe[Me$_8$TPC]Cl. A solution magnetic moment of μ_{eff} = 4.7 ±0.5 μ_B also supported this conclusion. The crystal structure of Fe[Me$_8$TPC]Cl also shows a smaller out-of-plane displacement of Fe of 0.387 Å from the mean corrole plane, qualitatively consistent with ferromagnetic coupling between Fe(III) and the corrole radical.[200]

^{19}F NMR spectroscopy also proved useful for mapping the spin density profile of fluorinated FeCl corroles.The Walker group found out that, for Fe[TPFPC]Cl, all the aryl fluorines exhibit negative paramagnetic shifts with respect to the diamagnetic free base (with the highest shift exhibited by the *ortho*-F's at about –32.3 ppm).[201] Although the authors were not able to dissect the ^{19}F paramagnetic shifts into contact and dipolar contributions, they proposed that the sign of the large paramagnetic shift of the *ortho*-F's must be related to the sign of the spin density at the *meso*-carbons.

Ghosh and co-workers studied several Fe[T*p*XPC]Cl corroles by means of DFT calculations, electronic absorption, NMR, and resonance Raman spectroscopy,[185] and confirmed the Fe^{III}–corrole$^{\bullet 2-}$ description proposed by Walker *et al*. DFT calculations showed negative spin populations at *meso*-carbons and corrole nitrogens (Fig. 4.7).[121,202] The calculations clearly indicated a $d_{xy}^2 d_{xz}^1 d_{yz}^1 d_{z2}^1$ configuration for the S = 3/2 Fe(III) center and assigned the negative spin density to a corrole b_1 radical (using C_{2v} notation), where the b_1 HOMO qualitatively resembles the porphyrin a_{2u} HOMO in shape.[202] The calculations furthermore showed that the antiferromagnetic coupling between the Fe and the corrole radical is mediated by an Fe(d_{z2})-corrole(b_1) orbital interaction, facilitated by the significant out-of-plane displacement of the Fe atom (~0.4 Å) from the N_4 plane.[185]

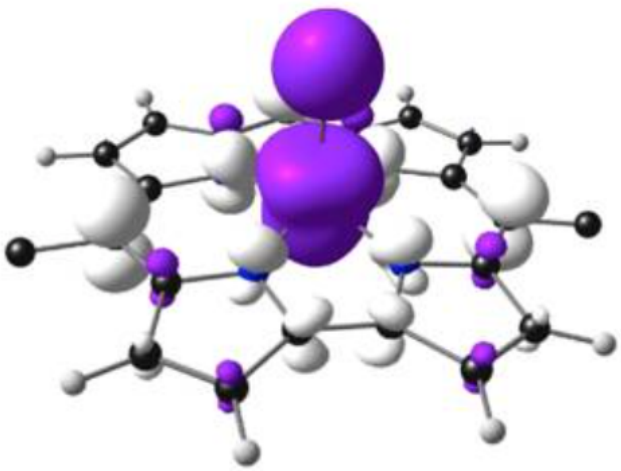

Fig. 4.7 DFT spin-density plot of Fe[TPC]Cl. Reproduced with permissions from ref 134.

A study β-octafluorinated Fe[F_8T*p*XPC]Cl complexes also indicated an alternating pattern of ^{1}H paramagnetic shifts for the *meso*-phenyl protons, similar to Fe[TPC]Cl but ~20% lower in magnitude, again indicating a substantial negative π-

spin density at *meso*-carbons.[75b] Also, the ^{19}F paramagnetic shifts in Fe[F_8T*p*XPC]Cl complexes were also thought to primarily reflect the contact or spin density contribution.

For both the Fe[T*p*XPC]Cl and Fe[F_8T*p*XPC]Cl series, the Soret maxima were found to redshift with increasingly electron-donating character of the *para* substituent X, (Fig. 4.8) consistent with a noninnocent Fe^{III}–corrole$^{\bullet 2-}$ formulation for these complexes.[75b,185]

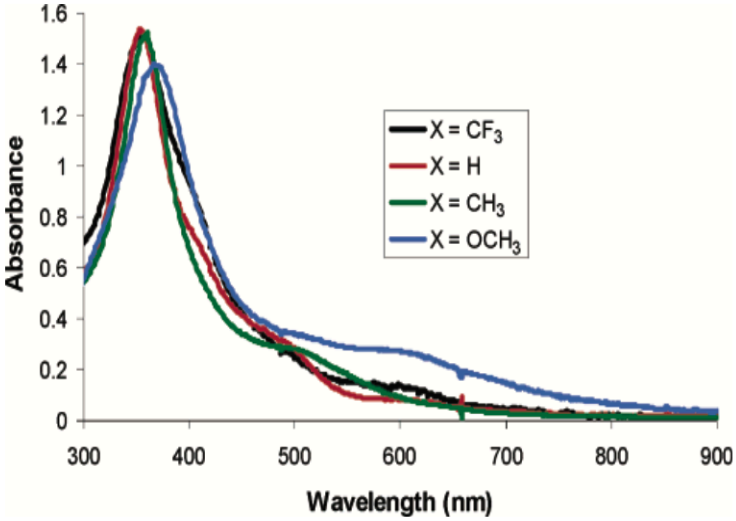

Fig. 4.8 UV-vis spectra of Fe[F_8T*p*XPC]Cl as a functions of X. Reproduced with permissions from ref 75b.

Two additional studies completed the case for the Fe^{III}–corrole$^{\bullet 2-}$ formulation.

The first was a high-level ab initio CASSCF/CASPT2 study by Ghosh, Roos, and coworkers, which confirmed the expected S = 1 Fe^{III}–corrole$^{\bullet 2-}$ ground state with no evidence of a true Fe(IV) state within 1.5 eV of the ground state.[203]

The second study, by Gross, Neese, and co-workers, consisted of Mössbauer spectroscopy, temperature- and field-dependent magnetization measurements, and DFT calculations, which also confirmed a Fe^{III}(S = 3/2)−corrole$^{\bullet 2-}$ description for Fe[TPFPC]Cl.[204]

4.4 Iron-Aryl Corroles

In their original study of Fe corroles, Vogel et al. synthesized air-stable Fe[OEC]Ph by reacting Fe[OEC]Cl with excess phenylmagnesium bromide.[190] The X-ray structure of Fe[OEC]Ph reveals a much smaller Fe-N_4 displacement compared to Fe[OEC]Cl (0.27 Å *vs*. 0.42 Å). The Fe[OEC]Ph complex exhibits ^{1}H paramagnetic shifts with moderately downfield *meso*-H resonances (δ: 54.5 and 49.3 ppm) and upfield axial phenyl-H resonances (maximum $\delta = -153.6$ ppm for *o*-H). Magnetic susceptibility measurement and Mössbauer spectroscopy suggested an $S = 1$ Fe(IV) state for the complex.[190] Walker et al. also proposed a similar description for Fe[Me_2Et_6C]Ph, based on temperature-dependent magnetic susceptibility measurements and the low isomer shift ($\delta = -0.10$ mm/s) in field-dependent Mössbauer spectroscopic studies.[198] The ^{1}H NMR spectrum of Fe[Me_2Et_6C]Ph also revealed positive chemical shifts for *meso*-H resonances ($\delta = 53.4$ and 49.4 ppm) and negative chemical shifts for the axial phenyl-H's (maximum value of $\delta = -148$ ppm for *o*-H and minimum value of $\delta = -3.7$ ppm for *m*-H), analogous to Fe[OEC]Ph.

DFT calculations suggested only small negative spin densities at the *meso*-carbons but the net spin density on the macrocycle was practically zero, thus indicating a Fe^{IV}–corrole^{3-} electronic description.[198] Further, the calculated contact shifts of axial-phenyl protons have alternating signs, consistent with π-spin delocalization from the Fe to phenyl ligand. Apparently, the strongly basic character of phenyl carbanion helps stabilize the Fe(IV) state via a strong σ-donor interaction, as reflected in the short Fe-Ph bond distance (1.98 Å).

A recent study of Fe[T*p*MePC]Ph revealed small isotropic shift for the *meso*-aryl protons but larger isotropic shifts are observed for the β-pyrrolic protons (Fig. 4.9).[205] Extreme upfield resonances of *ortho* and *para*-protons of the axial phenyl ligand were also observed for Fe[T*p*MePC]Ph, apparently reflecting the combined effects of substantial paramagnetic shifts and shielding by the corrole macrocycle.[205]

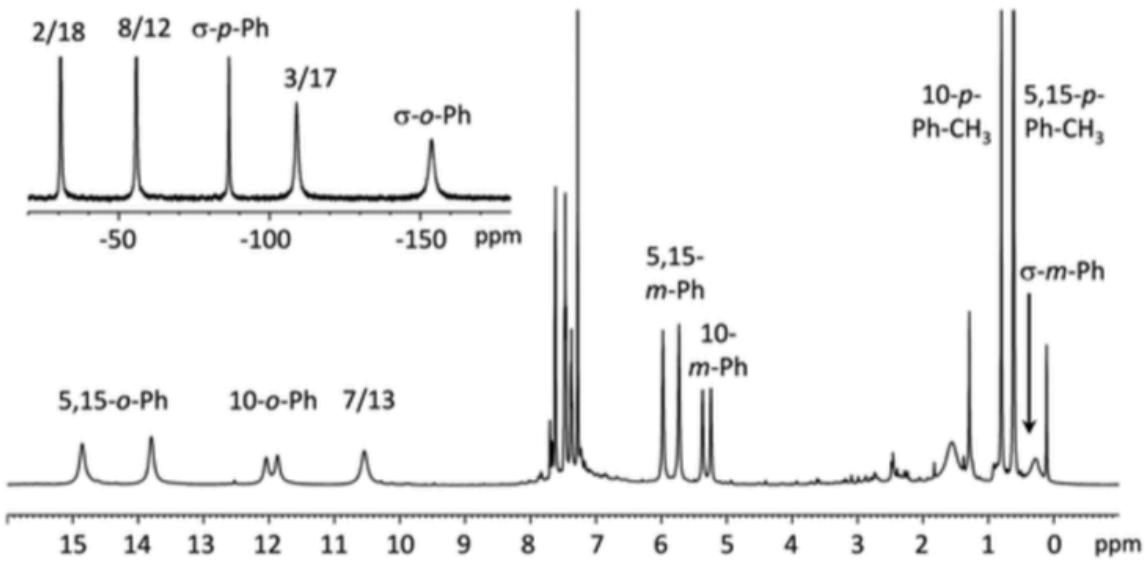

Fig. 4.9 ^{1}H NMR spectrum of Fe[T*p*MePC]Ph. Reproduced with permission from ref 205.

Finally, UV-vis substituent effects, XANES measurements, and DFT calculations indicated that the corrole ligand in FePh corroles is essentially innocent (see paper B).

4.5 μ-Oxo Diiron Corroles

Vogel *et al*. reported the first μ-oxo-diiron corrole, $\{Fe[OEC]\}_2O$, which formed via spontaneous aerial oxidation of an Fe^{III} precursor during workup.[190] X-ray crystallography confirmed the molecular stoichiometry, i.e., two Fe-corrole units connected through a μ-oxo bridge. The ^{1}H NMR spectrum showed that the complex is diamagnetic and Mössbauer spectral parameters suggested a low-spin Fe(IV) description, similar to heme protein Compound I and II intermediates. An analogous compound $\{Fe[TPFPC]\}_2O$ was subsequently obtained by Gross *et al*. during recrystallization of the monomeric precursor $Fe^{III}[TPFPC](OEt_2)_2$ from aerobic mixtures of acetonitrile and *n*-heptane.[191] Alternatively, μ-oxo diiron complexes can also be synthesized by washing Fe^{III}-diethyletherate[206] or FeCl corroles (paper A) with aqueous NaOH. Gross *et al*. reported four sets of sharp *ortho*-F resonances in the ^{19}F NMR spectra of the diamagnetic $\{Fe[TPFPC]\}_2O$. The crystal structure reveals a smaller Fe-O-Fe angle compared to the previously reported$\{Fe[OEC]\}_2O$ complex (158° *vs*. 170°), which the authors attributed to steric repulsion between the

C_6F_5 groups of the adjacent corrole units.[191] Paolesse and co-workers also reported a crystal structure of a β-dinitro-substituted $Fe_2(\mu\text{-O})$ corrole (Fig. 4.10), which was also obtained accidentally during their attempt to crystallize the corresponding FeNO corrole.[207] The μ-oxo derivative of Fe tris(4-pyridyl)corroles[208] and xanthene-modified Fe corroles[209] have also been synthesized.

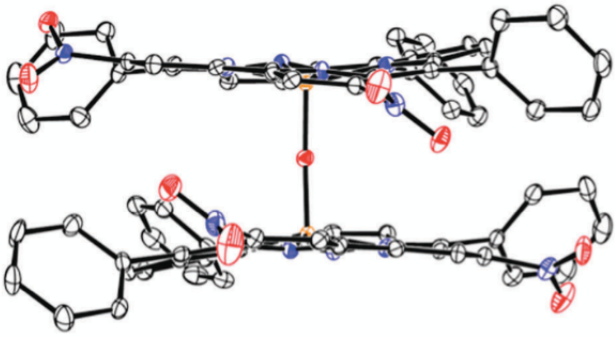

Fig. 4.10 X-ray structure of $\{Fe[3,17\text{-}(NO_2)_2TPC]\}_2O$. Reproduced with permission from ref 207.

μ-Oxo diiron corroles have also been observed as side products of Fe(III)-corrole catalyzed decomposition of H_2O_2[210] and of chemical oxidation of Fe^{III}[TPFPC] by iodobenzene diacetate in the absence of any substrate.[211] The Fe-O-Fe bond has also been found to be photochemically cleaved by visible light to generate a putative $Fe^{V}O$ intermediate that can oxidize hydrocarbons effectively.[212]

Ghosh and co-workers have reported a comparative study of $\{Fe[T\textit{p}XPC]\}_2O$ derivatives, where they observed lower oxidation potentials of μ-oxo dimers compared with analogous FeCl corroles.[185] The authors interpreted this observation in terms of ligand-centered oxidation.

Recently, as part of my own studies, the iron centers in μ-oxo diiron corroles have been described as intermediate-spin Fe(III) coupled to corrole$^{\bullet 2-}$ radicals (see Paper A).

4.6.1 Introduction to Paper A: Wolves in Sheep's Clothing: μ-Oxo-Diiron Corroles Revisited

Since their discovery by Vogel in 1994,[190] μ-oxo diiron corroles were long thought of as comprising two low-spin Fe(IV) centers (S = 1) that are antiferromagnetically coupled to each other. Earlier work in our laboratory revealed a modest redshift of Soret maxima in the optical spectra of $\{Fe[Tp XPC]\}_2O$ derivatives across the series X = $CF_3 \rightarrow H \rightarrow Me$.[185] The fourth member of this series, the $\{Fe[TpOMePC]\}_2O$ complex had not been reported before. Accordingly, I synthesized $\{Fe[TpOMePC]\}_2O$ and reexamined the complex along with the three other previously reported $\{Fe[TpXPC]\}_2O$ derivatives.

The $\{Fe[TpXPC]\}_2O$ derivatives were synthesized via a modified procedure relative to the one reported earlier.[185,190] First, the Fe[T*p*XPC]Cl derivatives were according to a literature procedure.[191] The $\{Fe[TpXPC]\}_2O$ complexes were then prepared by treating the Fe[T*p*XPC]Cl complexes with aq. NaOH (2M) under aerobic conditions. Attempts were made to directly oxidize the Fe(III)-bisetherate corroles by treating with aq. NaOH under aerobic conditions, but this procedure led to incomplete reaction. ESI-MS showed the expected product along with monomeric products in substantial amounts. In contrast, the new procedure with FeCl corroles as starting materials led to $Fe_2(\mu\text{-}O)$-corroles in nearly quantitative yields (>90%). The newly synthesized $\{Fe[TpOMePC]\}_2O$ could be obtained in 92% yield after chromatographic purification.

As solids, the $\{Fe[TpXPC]\}_2O$ complexes are air-stable. In solution, however, they tend to degrade over time under aerobic conditions. The Fe-O-Fe linkage is light-sensitive and it also cleaves in the presence of traces of acid in solution. Even the presence of slightly acidic methanol leads to cleavage of the Fe-O-Fe linkage in the course of an ESI-MS experiment. Flushing the mass spectrometer with pure DCM several times before injecting the sample solution (also made in DCM) helps retain the dimeric form as the main species.

Overall, however, the $Fe_2(\mu\text{-}O)$ corroles are stable enough for storage as solids as well as for manipulations such as column chromatography or crystallization under normal conditions. Such stability stands in sharp contrast the instability of Fe(IV)-oxo porphyrin intermediates, which generally can only be observed in solution at low temperatures.

The optical spectra of three known {Fe[T*p*XPC]}$_2$O corroles were reexamined along with that of the newly synthesized {Fe[T*p*OMePC]}$_2$O complex. The moderate redshift of the Soret maxima from X = CF_3 (383 nm) to H (386 nm) to Me (389 nm) was reestablished. Interestingly, the new complex {Fe[T*p*OMePC]}$_2$O was found to exhibit a strongly perturbed spectrum with a blue-shifted Soret band (375 nm) and a prominent shoulder around 410 nm. This higher wavelength shoulder is believed to be a plausible candidate for the LL'CT transition characteristic of a noninnocent metallocorrole. These observations served as a preliminary indication of a different oxidation than simple Fe(IV) for the {Fe[T*p*XPC]}$_2$O complexes.

Broken-symmetry DFT calculations on {Fe[TPC]}$_2$O carried out by my colleague Dr. Hugo Vazquez-Lima showed that the overall S = 0 ground state may be viewed as the following spin-coupled assembly of S = 3/2 Fe(III) and corrole$^{\bullet 2-}$ radical fragments:

$$\text{corrole}^{\bullet 2-}(\downarrow)-\text{Fe}^{\text{III}}(\uparrow\uparrow\uparrow)-\text{Fe}^{\text{III}}(\downarrow\downarrow\downarrow) - \text{corrole}^{\bullet 2-}(\uparrow)$$

Moreover, both the optimized geometry of {Fe[TPC]}$_2$O and the published X-ray structure of {Fe[TPFPC]}$_2$O show bond length alternations in and adjacent to the bipyrrole part of the corrole macrocycle, which are also indicative of corrole radical character.

The Fe-O-Fe asymmetric stretch of the complexes was identified with IR spectroscopy and ^{18}O labeling. All four {Fe[T*p*XPC]}$_2$^{18}O complexes were synthesized by treating the corresponding FeCl corroles with 2 M Na^{18}OH in $H_2{}^{18}O$,[i] which was generated by a reported procedure.[248] Complete exclusion of ambient O_2 and moisture were mandatory for these experiments, which were therefore carefully conducted with Schlenck techniques. The ^{16}O/^{18}O stretching frequencies for the {Fe[T*p*XPC]}$_2$O complexes were found to be as follows, as a function of X: CF_3 (821/792 cm^{-1}), H (829/791 cm^{-1}), Me (832/795 cm^{-1}), and OMe (820/790 cm^{-1}). For {Fe[TPC]}$_2$O, both the ^{16}O and ^{18}O frequencies were found to be in excellent accord with corresponding DFT values, indicating the essential correctness of the electronic-structural description afforded by DFT.

[i] A solution of Na^{18}OH was prepared by dropwise addition of $H_2{}^{18}O$ to NaH. This solution was combined with a DCM solution of an FeCl corrole. These manipulations were all carried out under argon and the dark brown ^{18}O-labeled μ-oxo dimer was also stored under argon.

The ^{1}H NMR spectrum of the new compound {Fe[T*p*OMePC]}$_2$O was difficult to assign at room temperature because of several overlapping signals. Lowering the temperature appeared to result in sharper and better separated peaks and a well-resolved spectrum was obtained at −15 °C. Further lowering of temperature again led to merging of the β-H and aryl-H peaks and, at −60°C, only a broad and unresolved signal was obtained.

My contributions to this paper consisted of the syntheses, the ^{18}O labeling studies, and all spectroscopic characterization (UV-vis, IR, NMR). The computational studies were carried out by my colleague Dr. Hugo Vazquez-Lima.

4.6.2 Introduction to Paper B: Ligand Noninnocence in Iron Corroles: Insights from Optical and X-ray Absorption Spectroscopies and Electrochemical Redox Potentials

A study of Fe-aryl corroles was undertaken to test the validity of the substituent effect criterion for Fe-aryl corroles. For Fe[T*p*XPC]Cl, we already know that the Soret maximum redshifts with increasing electron-donating character of the *para* substituent X. In this project, I synthesized two series of Fe-aryl corroles, Fe[T*p*XPC]Ph and Fe[T*p*XPC]Tol (Tol = 4-methylphenyl), to examine the influence of X on their spectroscopic and electrochemical properties with a few to gaining insight into the question of ligand noninnocence. Existing studies[190,205] already suggested that these complexes are essentially low-spin (S = 1) Fe(IV) species. The hypothesis thus was that the Soret maxima the Fe-aryl series should not redshift as a function of X, which indeed turned out to be the case, providing powerful support for the validity of the substituent effect criterion to families of complexes.

The Fe-aryl corroles were synthesized by treating the corresponding FeCl corroles in anhydrous DCM with arylmagnesium bromide, ArMgX (Ar = Ph, 4-MePh), under an inert atmosphere. As solids, the complexes are moderately stable. In solution, however, the Fe-aryl bond was seen to undergo cleavage over time under aerobic conditions. However, the Fe[T*p*XPC]Ph and Fe[T*p*XPC]Tol corroles are more stable than the analogous Mn[T*p*XPC]Ph complexes and reasonably satisfactory elemental analyses could be obtained for the Fe complexes.

As part of this study, the FeCl complex Fe[T*p*OMePC]Cl was synthesized for the first time. The complex exhibits a highly perturbed UV-vis spectrum with a split Soret band. We proposed that the higher-wavelength Soret peak at 426 nm is

attributable to an LL'CT (aryl-to-corrole charge transfer) transition. With this assumption, the Soret maxima for the Fe[T*p*XPC]Cl series was found to redshift with increasingly electron-donating X, as expected for their noninnocent character. As mentioned, the Fe-aryl corroles did not show such substituent sensitivity.

The ^{1}H NMR spectra of Fe[T*p*XPC]Ar derivatives provided clear evidence of their paramagnetic character. However, the corrole paramagnetic shifts were found to be much smaller than those observed for the Fe[T*p*XPC]Cl series, consistent with a relatively innocent macrocycle in the case of the Fe-aryl complexes. DFT spin density profiles also supported the conclusion of a low-spin Fe(IV) center with an essentially $d_{xy}^2 d_{xz}^1 d_{yz}^1$ electronic configuration and a relatively innocent corrole in Fe[TPC]Ph.

The Fe[T*p*XPC]Ar derivatives were subjected to cyclic voltammetry measurements. In the interest of a complete comparative study, the analogous FeCl, FeNO, and $Fe_2(\mu\text{-O})$ corroles were also reexamined with cyclic voltammetry. The Fe[T*p*XPC]Ar corroles all exhibit two reversible oxidations and two reversible reductions in DCM. In general, the oxidation potentials are similar across the different Fe corrole families. However, the FeAr corroles are reduced at somewhat more negative potentials than analogous FeCl corroles, but at almost similar potentials as analogous FeNO corroles. The overall picture that emerged is that the first one-electron oxidation and reduction potentials as well as the electrochemical HOMO-LUMO gaps (~1.0-1.2 V) of the innocent Fe-aryl corroles are qualitatively similar to those of analogous noninnocent FeCl, $Fe_2(\mu\text{-O})$, and FeNO corroles. In other words, redox potentials in and of themselves do not appear to provide a clear indication of the innocence or noninnocence of the corrole ligand in Fe corroles.

Finally, four iron corroles, Fe[TPC]Cl, Fe[TPC]NO, Fe[TPC]Ph, and $\{Fe[TPC]\}_2O$, were investigated with K-edge X-ray absorption spectroscopy.[194] The integrated pre-edge (1s→3d) intensity of Fe[TPC]Ph was found to be approximately 2.5 times those for Fe[TPC]Cl or Fe[TPC]NO. Considering similar coordination geometries of these complexes, the dramatically higher pre-edge intensity of Fe[TPC]Ph indicates greater number of 3d holes relative to the other complexes and is thus consistent with a high-valent Fe(IV) electronic configuration.

My contributions to this paper consisted of the synthesis of all the complexes studied as well as their characterization by means of UV-vis, ^{1}H NMR, MS, and

electrochemistry. The XAS measurements and associated theoretical calculations were carried out by our collaborator Dr. Ritimukta Sarangi at the Stanford Synchrotron Radiation Lightsource.

Chapter 5 – Cobalt and Rhodium Corroles

5.1 Introduction

Cobalt insertion in corroles dates back the very first report of corrole synthesis by Johnson and Kay in 1965.[45b] Between 1970-1995, several Co corroles were obtained through the metal-assisted cyclization of a linear tetrapyrrolic precursor of the corrole.[47,49] More recently, Co corroles have been studied as effective catalysts in the oxygen reduction reaction (ORR)[221b,233,239] and in the hydrogen evolution reaction (HER).[231,236] In this chapter, the electronic structures and spectroscopic properties of cobalt corroles with a single triphenylphosphine (PPh_3) ligand and one or two pyridine $(py)_2$ ligands are discussed with emphasis on the possibility of a noninnocent corrole macrocycle. For comparison, I also present an analogous discussion of Rh-PPh_3 corroles.

5.2 Cobalt-Triphenylphosphine Corroles

In the early days of corrole chemistry, Co-PPh_3 corroles were obtained directly as the result of Co-templated corrole synthesis.[49,213] At present, Co-PPh_3 corroles are most conveniently synthesized by reacting an alcoholic solution of the corresponding free-base corroles with cobalt(II) acetate in presence of an excess of (PPh_3) ligand (see Fig. 5.1), whereupon air-stable Co-PPh_3 corroles are obtained in high yield after work-up.[56,195,220,221a] The presence of PPh_3 ligand in the reaction mixture from the very beginning of the synthesis is crucial. In the absence of a suitable coordinating ligand (or solvent), four-coordinate cobalt corroles are unstable and tend to dimerize oxidatively. Gross *et al*. showed that, when PPh_3 is added after cobalt insertion into H_3[TPFPC], a C3(β)-C3'(β) linked dimeric Co corrole by-product is obtained, whose amount on how late the PPh_3 is added after the metalation.[214] However, for Co 5,15-dimesityl-10-pyrimidinylcorroles, addition of PPh_3 even 24 hours after cobalt insertion doesn't affect its stability. Here the unusual stability of the four-coordinate cobalt corrole (without any axial PPh_3 ligand) was attributed to the presence of bulky mesityl groups at the 5,15-positions, which presumably hinders dimerization via β-β' coupling.[76b]

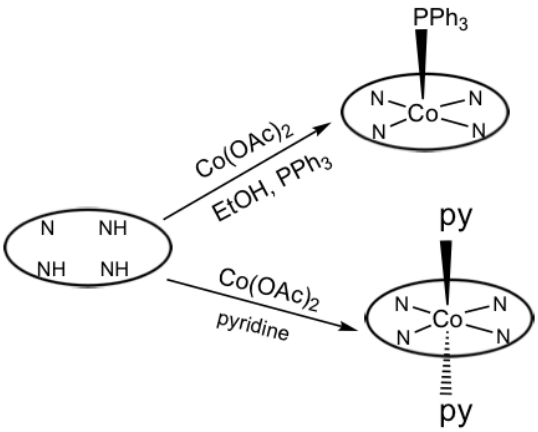

Fig. 5.1 Synthesis of Co corrole complexes.

The X-ray structures of several *meso*-triarylcorroles reveal an essentially planar corrole geometry with short equatorial Co-N distances (Co-N_{avg} ≈1.88 Å) and modest Co-N_4 displacements (~0.27 Å), indicating an optimum fit of the Co ion with the corrole ligand (Fig. 5.2).[56,215,217] The Co-P bond distance for all complexes is found to be approximately 2.21 Å. The planarity of the corrole macrocycle is maintained even in the presence of considerable steric hindrance, e.g. as a result of multiple bromine,[57] aryl,[84a] alkyl,[49a] and perfluoroalkyl[216] groups. The planar macrocyclic core also appears to be responsible for the strong supramolecular complexation of a Co-PPh_3 corrole with fullerenes, both in the solid state and in solution.[218]

Co-PPh_3 corroles are diamagnetic species, as reflected in their ^{1}H NMR spectra, which show well-resolved signals for both the *meso*-aryl and β-pyrrolic protons.[214,219] The *ortho*, *meta*, and *para*-protons of axial PPh_3 group (4-7 ppm) are strongly shielded by the diamagnetic ring current of the corrole.

The UV-visible spectra of Co[T*p*XPC](PPh_3) complexes in non-coordinating solvents such as DCM consist of an intense Soret band around 372-400 nm and a prominent Q band around 560 nm.[221a] However, certain Co corroles such as Co[TPFPC](PPh_3) exhibit a split Soret band, reflecting the essentially composite nature of the Soret manifold.[214,215b]

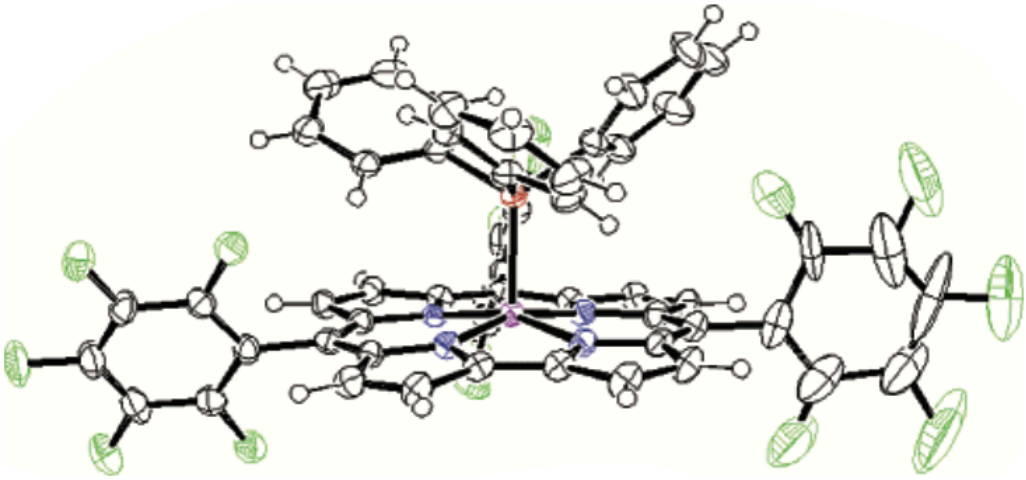

Fig. 5.2 X-ray structure of Co[TPFPC](PPh_3). Reproduced with permission from ref 215.

Co-PPh_3 corroles exhibit rich electrochemical properties, as established in a detailed study of Co[T*p*XPC](PPh_3) derivatives by Kadish *et al.*[221] In noncoordinating solvents such as DCM, Co-PPh_3 corroles generally undergo two reductions and up to three oxidations (Fig. 5.3). The first reduction process is irreversible, which may be explained by rapid dissociation of the axial PPh_3 from the $\{Co^{II}[Cor](PPh_3)\}^-$ anion. A similar conclusion was also reached in an earlier electrochemical study of Co[Me_8T*p*XPC](PPh_3) complexes by the same group.[222] Thus, the EPR spectrum of Co[Me_8TPC](PPh_3) after bulk electroreduction at −1.3 V, exhibited partially resolved hyperfine splitting due to ^{59}Co, but no additional hyperfine splitting due to ^{31}P. This suggests dissociation of PPh_3 after the first one-electron reduction; moreover, the *g* and A^{Co} values were supportive of a Co(II) formulation.

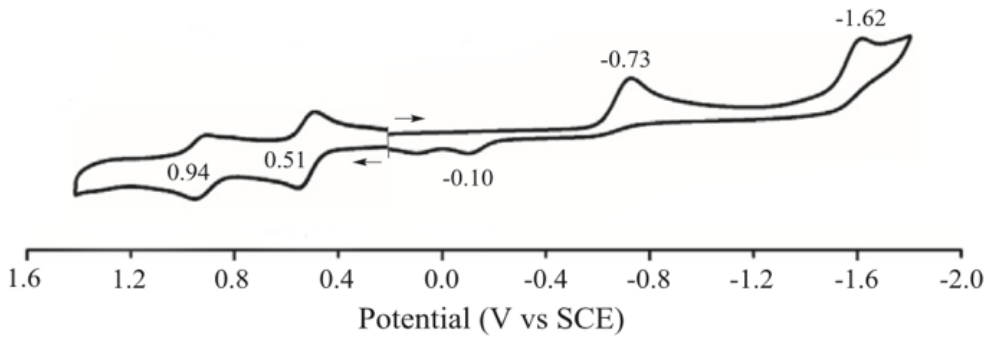

Fig. 5.3 Cyclic voltammogram of Co[TPC](PPh_3) in DCM containing 0.1 M TBAP. Reproduced with permissions from ref 219.

The $\{Co^{II}[Cor]\}^{-}$ species is further reduced to the Co(I) form at more negative potentials. Interestingly, this second reduction (Co^{II}/Co^{I}) occurs reversibly in DMF, but is irreversible in DCM. The irreversible reduction in DCM is thought to reflect the formation of a σ-bonded Co(III)-alkyl intermediate from the reaction of the $\{Co^{I}[Cor]\}^{2-}$ species with a DCM solvent molecule.[221a] A similar irreversible second reduction is also observed for several Co-PPh_3 triarylcorroles in DMF in the presence of lindane/γ-hexachlorocyclohexane (1.0 eq.), again presumably reflecting the formation of Co(III)-alkyl intermediate.[223] When the electrochemical measurement is done under a CO_2 atmosphere, the $\{Co^{I}[Cor]\}^{2-}$ species is also found to react with CO_2, as evidenced by an increase in the current of the second reduction wave.[224]

Electrogenerated Co corrole species have been further characterized with thin-layer UV–visible spectroelectrochemistry. The first electroreduction of cobalt corroles is generally accompanied by a modest decrease in intensity of the Soret and Q bands, with concomitant appearance of a new Soret band redshifted by 20-30 nm. For example, Co[TPC](PPh_3) upon controlled-potential reduction at −1.20 V exhibits a significantly redshifted Soret band (which has shifted 387 nm to 421 nm) and a weak Q band (575 nm, Fig. 5.4).[219] Similar spectral changes were also observed for both electro- and chemical reduction of Co[Me_8TPC](PPh_3).[222] These spectral changes were ascribed to an essentially metal-centered $Co^{III}\rightarrow Co^{II}$ reduction process. Further reduction of $\{Co^{II}[TPC]\}^{-}$ at –1.80 V results in the appearance of a sharp Soret band at 415 nm.[219] This spectral change was also interpreted as another metal-centered reduction process ($Co^{II}\rightarrow Co^{I}$) leading to an $S = 0$ $\{Co^{I}[TPC]\}^{-}$ anion.[219]

The spectral changes accompanying successive one-electron oxidations of Co-PPh_3 corroles, carried out at controlled potentials in DCM, are accompanied by a weakening of the Soret and Q bands.[221a,225] According to Gray *et al*., one-electron oxidation of Co[TPFPC](PPh_3) by tris(4-bromophenyl)aminium hexachloroantimonate also results in the weakening of both the Soret and Q bands and the appearance of a broad absorption band at 690 nm.[245] These processes have been assigned to corrole-centered oxidations.

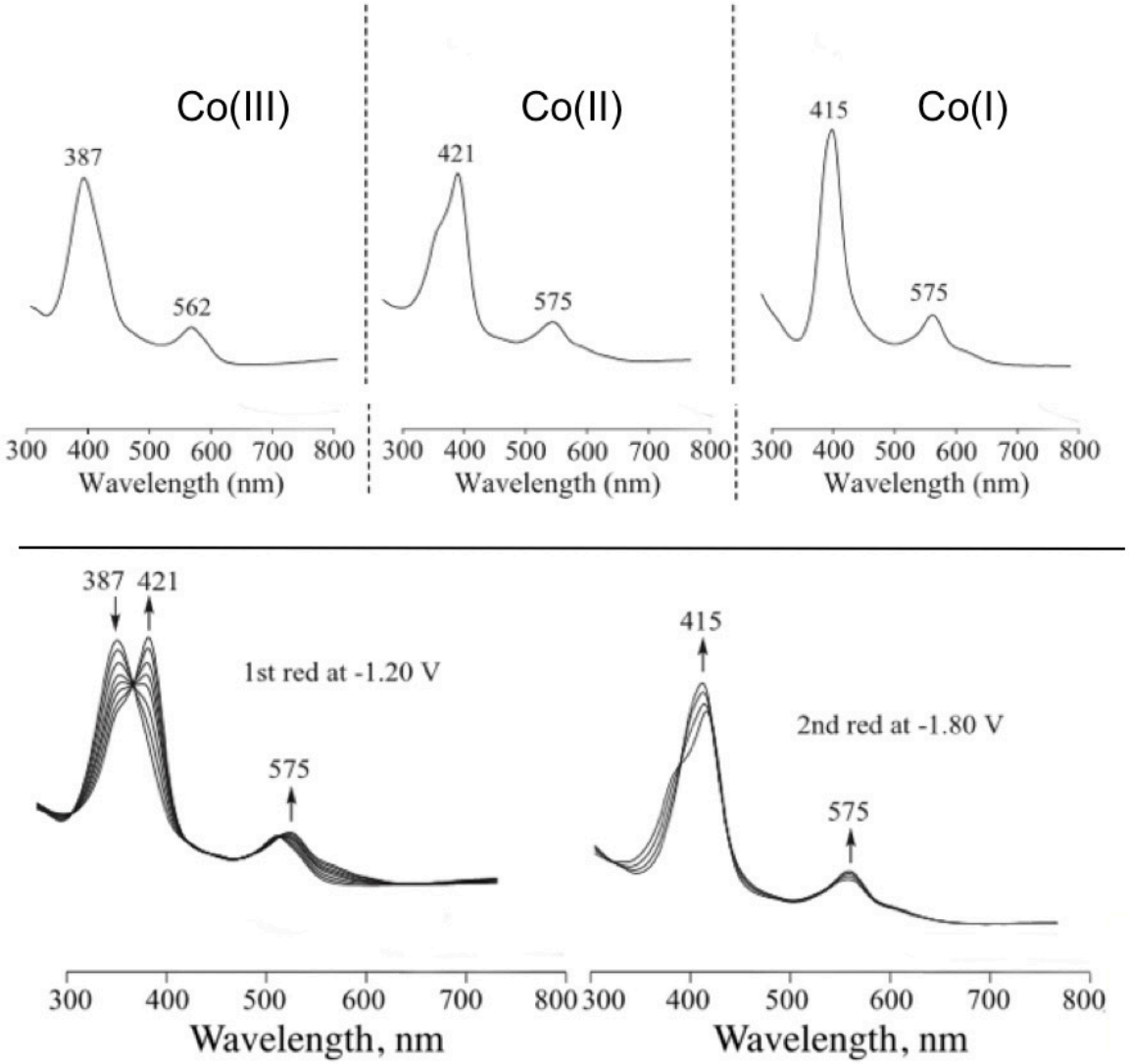

Fig. 5.4 UV−vis spectra of the Co(III), Co(II), and Co(I) states (top) and spectral changes of Co[TPC](PPh_3) upon electroreduction (bottom) in DCM containing 0.1 M TBAP. Reproduced with permission from ref 219.

5.3 Cobalt-Bispyridine Corroles

Cobalt-bispyridine corroles can be readily synthesized by metalation of free-base corroles in pyridine (see Fig. 5.1).[214] The X-ray structures of Co-bispyridine corroles indicate an essentially planar macrocycle, where the two axial pyridine molecules exist in a nearly mutually coplanar orientation (Fig. 5.5).[231] The short Co–$N_{corrole}$ bond distances (~ 1.89 Å), slightly longer Co–$N_{pyridine}$ bond distances (~ 1.99 Å), and a perfectly in-plane cobalt atom all indicate a low-spin Co(III) state.[214,226-228] Substitution of the β-positions by chlorine atoms does not induce any distortion from planarity, as evidenced by the perfectly planar structure of Co[Cl_8TPFPC]$(py)_2$.[229] As

expected for a low-spin Co(III) state, the diamagnetic Co[TPFPC](py)$_2$ complex was found to exhibit sharp resonances for both β-pyrrole protons and the pyridine protons.[214]

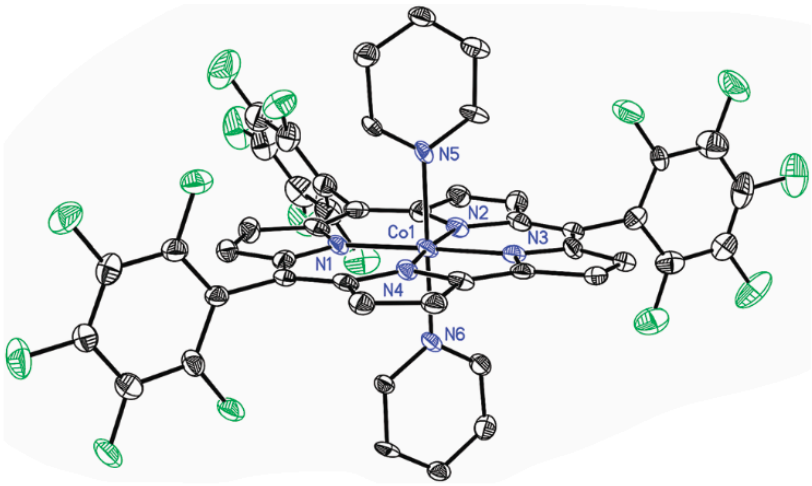

Fig. 5.5 X-ray structure of Co[TPFPC](py)$_2$. Reproduced with permission from ref 231.

The UV-vis spectra of Co-bispyridine complexes differ markedly in the presence and absence of pyridine. Thus, Co[TPFPC](py)$_2$ complex in pure DCM exhibits a split Soret band (380 nm and 440 nm). Gradual addition of pyridine to the DCM solution decreases the intensity of the 380-nm band while intensifying the 440-nm band. A single Soret band at 440 nm and two intense Q bands around 580 nm and 600 nm are observed in presence of substantial amounts of pyridine in the DCM solution as well as in neat pyridine (Fig. 5.6). [214,245] Further dilution of the sample using only DCM, results in re-appearance of the band around 380 nm (see Fig. 5.7). Based on these observation, Gross *et al*. pointed out that in dilute solutions in noncoordinating solvents such as DCM, the Co-bispyridine corrole undergoes dissociation of one axial pyridine ligand to form the pentacoordinate monopyridine complex.[214] The pentacoordinate form (Soret λ_{max} 380 nm) exists in equilibrium with the corresponding six-coordinate bispyridine form (Soret λ_{max} 440 nm) in solution and, with higher pyridine concentrations, the bispyridine form prevails. A recent MCD and TDDFT study also suggests dissociation of one axial pyridine from the bispyridine form.[230]

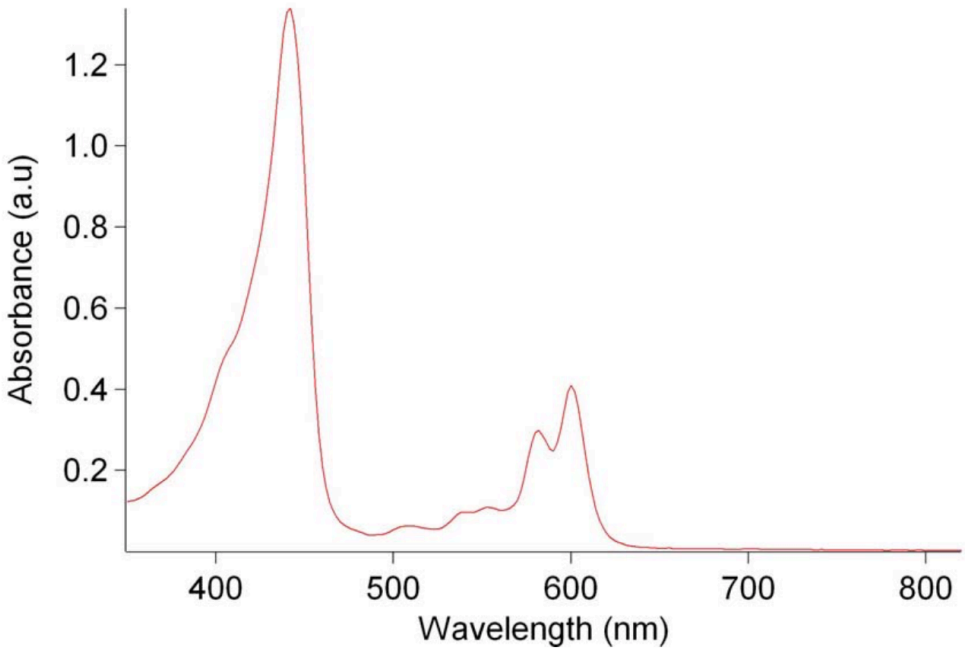

Fig. 5.6 UV-vis spectrum of Co[TPFPC]$(py)_2$ in DCM containing 5% pyridine. Reproduced with permission from ref 245.

The lability of the axial pyridine ligands can be further demonstrated by adding excess PPh_3 to a DCM solution of Co-bispyridine corroles, which leads to the formation of pentacoordinate Co-PPh_3. The bispyridine adduct can be regenerated by adding an excess of pyridine to the same solution.[245] These substitution reactions can be conveniently monitored by means of UV-vis spectroscopy (Fig. 5.7). Gross *et al*. have estimated that the dissociation constant of six-coordinate Co[TPFPC]$(py)_2$ is quite low (3.3×10^{-5} M) in DCM.[214]

In their attempt to isolate the mono-pyridine form Co[TPFPC](py) via column-chromatography with *n*-hexane/DCM followed by crystallization, Gross *et al*. actually obtained a dimeric Co-bispyridine corrole, with a direct C3(β)-C3'(β') link between two corrole units. The dimerization is believed to occur when the monopyridine form is left in solution for crystallization, presumably as a result of corrole radical character in such a species.[214] Therefore, the presence of an excess of pyridine is necessary during workup for obtaining the bispyridine form. The monopyridine form Co[TPFPC](py), however, is believed to be the actual species adsorbed on the surface of multi-walled carbon nanotube (MWNT), during application of the corrole-MWNT assembly for oxygen reduction in acidic media.[232]

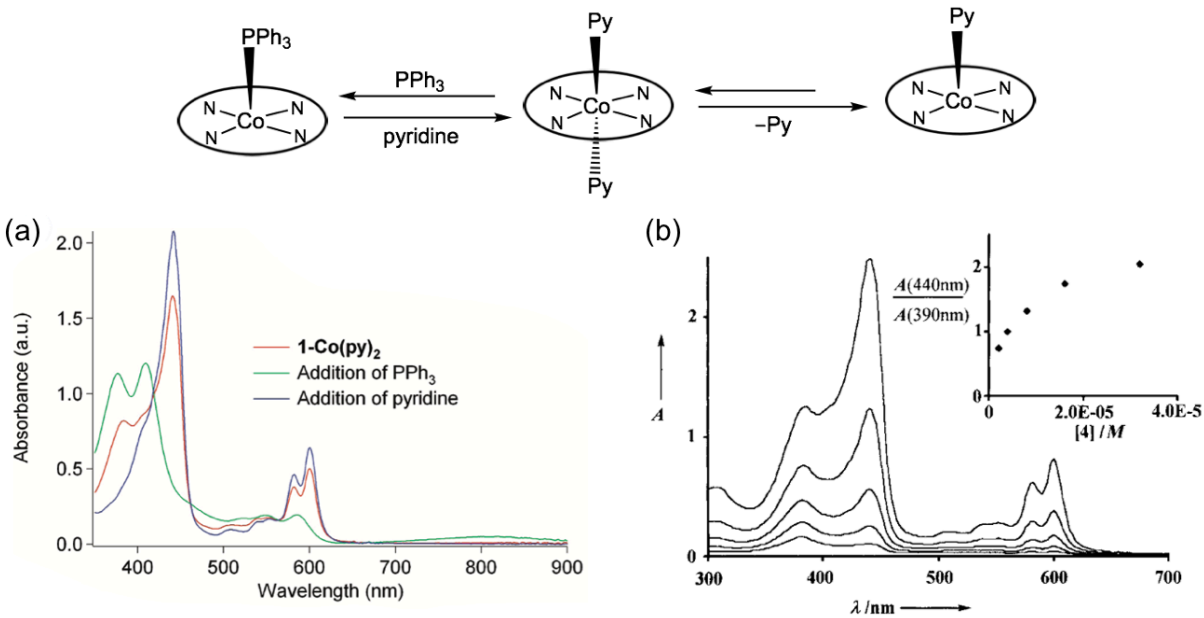

Fig. 5.7 Transformations of a Co-bispyridine corrole via ligand dissociation and substitution. Also shown are UV-vis spectral changes accompanying (a) gradual addition of PPh_3 into a DCM solution of Co[TPFPC]$(py)_2$ (left) and (b) dilution in a noncoordinating solvent DCM (right). Adapted with permissions from ref 245 and ref 214 respectively.

The cyclic voltammogram of Co[TPFPC]$(py)_2$ in acetonitrile consists of two oxidations and two reductions. The first reduction is irreversible and shifts from –0.2 V to –0.7 V, when pyridine (0.5 M) is present externally in the electrochemical system.[214] The irreversibility of the reduction wave results from the dissociation of pyridine upon one-electron reduction. The second reduction process is reversible and appears at an almost similar potential to that of the second reduction of Co[TPFPC](PPh_3). This observation suggests the formation of similar square-planar, tetracoordinate $\{Co^{I}[Cor]\}^{2-}$ species in both cases. One-electron oxidation of Co[TPFPC]$(py)_2$ corrole is thought to be essentially ligand centered, based on the EPR spectra (a single g = 2.008 feature) of the oxidized species.[245]

Cobalt β-halogenocorroles exhibit a variety of interesting physical and electronic properties. Gross *et al*. have synthesized the paramagnetic square-planar complex Co[Br_8TPFPC] by metal insertion into the corresponding free-base β-octabromocorrole.[234] The ^{19}F NMR spectrum of this complex in a noncoordinating solvent such as DCM or benzene exhibits opposite isotropic shifts of the C-10 C_6F_5 resonances relative to the C-5 and C-15 C_6F_5 resonances, which were interpreted in

terms of an intermediate-spin Co(III) center.[234] Addition of pyridine to this species affords the corresponding bispyridine complex, $Co[Br_8TPFPC](py)_2$, which is diamagnetic. The electron-withdrawing bromine atoms induce a strong positive shift of both the first and second reduction potentials, relative to the analogous nonbrominated complex (e.g. 0.36 V *vs.* –0.2 V for first reduction), indicating that the octabrominated complex is much easier to reduce.

The diamagnetic Co β-octachlorocorrole $Co[Cl_8TPFPC](py)_2$ on the other hand was obtained by direct chlorination of the corresponding nonchlorinated cobalt corrole $Co[TPFPC](py)_2$ with chlorine gas, followed by quenching with $NaBH_4$ and pyridine.[229] Gradual addition of TFA to a benzene solution of $Co[Cl_8TPFPC](py)_2$ resulted in a blueshift of the Soret band from 444 nm to 410 nm as well as large paramagnetic shifts in the ^{19}F NMR spectrum. These changes were interpreted in terms of TFA-induced dissociation of the axial pyridines leading to the formation of the intermediate-spin four-coordinate Co(III) complex $Co[Cl_8TPFPC]$.

A comparative study of β-octahalogenated series $Co[X_8TPFPC](py)_2$ (X = F, Cl, Br) showed that the first reduction is irreversible in all cases (because of lability of axial pyridine) and appears at practically a constant potential of 0.36 V.[235] However, prior removal of pyridines by TFA makes the first reduction reversible (see Fig. 5.8). The second reduction is reversible for all the complexes even in the absence of TFA, further supporting the dissociation of axial pyridines after the first one-electron reduction. Unsurprisingly, all the halogenated complexes are reduced at much less negative potentials than their nonhalogenated counterparts.

Dey and co-workers have demonstrated that the second electroreduction product of $Co[F_8TPFPC](py)_2$ complex, i.e., the corresponding $\{Co^{I}[Cor]\}^{2-}$ species, acts as a highly efficient catalyst for hydrogen gas evolution by proton reduction.[236] The putative protonated intermediate, $\{Co[Cor](H)\}^{-}$, however, has not been detected, presumably because it undergoes very fast protonolysis to generate $\{Co^{II}[Cor]\}^{-}$ and H_2. DFT calculations and ^{19}F NMR spectroscopy indicated a diamagnetic Co(I) description for the $\{Co^{I}[Cor]\}^{2-}$ species.[235] In a recent study by Dey and co-workers, the low-spin Co(II) species originated obtained by one-electron reduction of $Co[Cl_8TPFPC]$ was found to bind dioxygen. EPR and IR spectra and DFT calculations indicated a $Co^{III}–O_2^{\bullet 2-}$ description for the resulting adduct.[237]

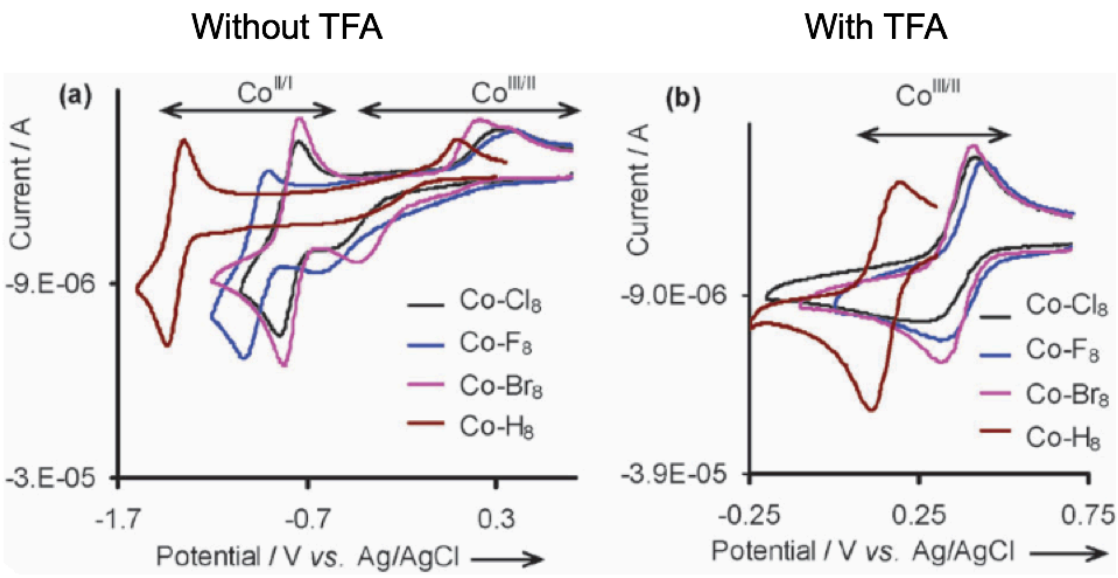

Fig. 5.8 Cyclic voltammograms of $Co[Y_8TPFPC](py)_2$ (Y = H, Cl, F, Br) in MeCN containing 0.1 M TBAP, with and without added TFA. Reproduced with permission from ref 235.

β-Alkyl and/or aryl-substituted cobalt corroles have been extensively studied by Kadish *et al*. with respect to their electrochemical properties and pyridine binding. The bispyridine adduct of a nonasubstituted Co corrole, $Co[Me_4Ph_5](py)_2$, was also structurally characterized.[238] Gradual addition of pyridine to a DCM solution of $Co[Me_4Ph_5]$ resulted in a redshift of the Soret band from 398 nm to 433 nm, with the appearance of a new intense band at ~600 nm; these changes were ascribed to stepwise formation the mono- and bispyridine adducts (Fig. 5.9). The pyridine binding constants for the stepwise formation of the mono- and bispyridine complexes were found to be log K_1 = 4.9 and log K_2 = 2.1. respectively.

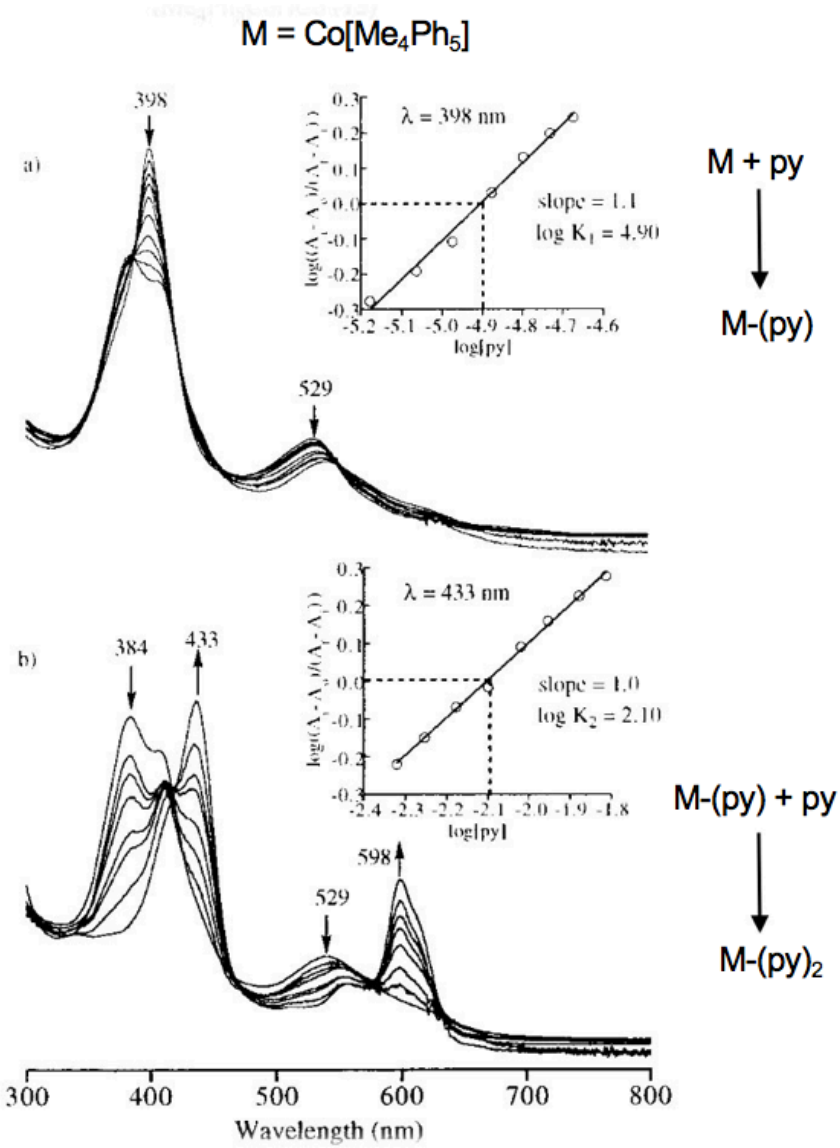

Fig. 5.9 UV-vis spectral changes of Co[Me_4Ph_5] in DCM upon titration with pyridine. Reproduced with permission from ref 238.

The first one-electron reduction of Co[Me_4Ph_5] at –0.15 V was found to be reversible in DCM. In pyridine, the first reduction shifted to a much more negative potential (–0.72 V) and also became irreversible (see Fig. 5.11). The irreversible nature of the reduction could be attributed to dissociation of a pyridine molecule from the bisligated form prior to the first reduction. A spectroelectrochemial study of the Co[Me_4Ph_5]$(py)_2$ in pyridine revealed that the characteristic 'marker band' at 598 nm of the neutral, bispyridine form disappeared completely upon first electroreduction leading to the Co(II) oxidation state (Fig. 5.10).[238]

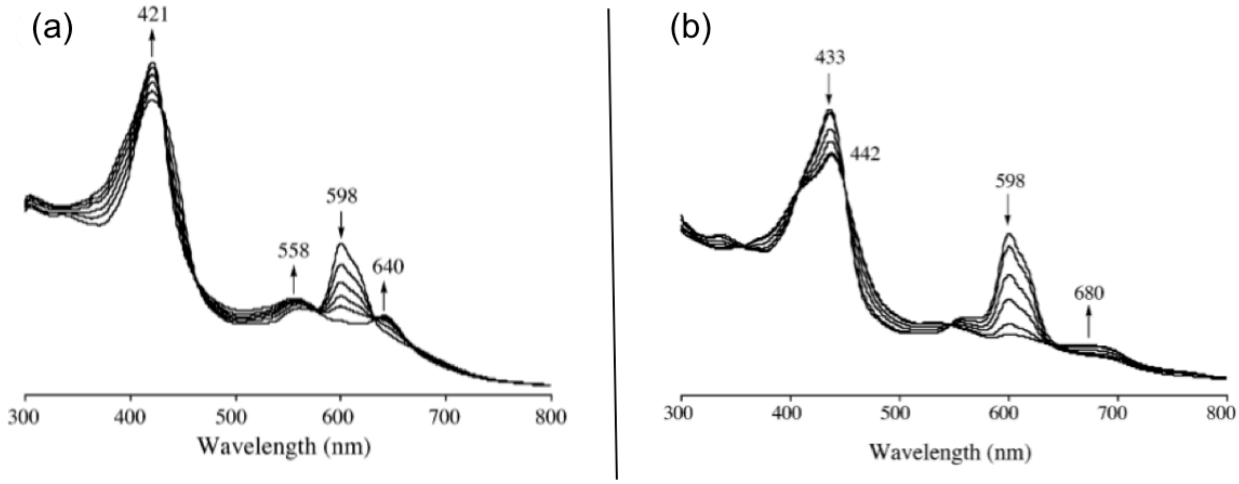

Fig. 5.10 UV-vis spectral changes of $Co[Me_4Ph_5]$ during (a) electroreduction and (b) electrooxidation in pyridine containing 0.2 M TBAP. Reproduced with permission from ref 238.

On the other hand, a total of four oxidation processes were observed in the cyclic voltammogram of $Co[Me_4Ph_5]$ in DCM (Fig. 5.11).[238] The first one-electron oxidation process appeared to be split into two processes occurring at different potentials, with the corresponding peak currents approximately half as large as that observed for the first reduction ($Co^{III} \rightarrow Co^{II}$) process. This intriguing observation was attributed to dimer formation during electrooxidation. The formation of 'half-oxidized' corrole dimers depends on the nature of the solvent and of the peripheral substituents. Interestingly, in neat pyridine, such dimerization did not occur, presumably due to the formation of bispyridine adducts, which preclude π-stacking. Also, the first oxidation in pyridine was found to yield a corrole π-cation radical that retained both its axial pyridines, i.e., a $\{Co[Cor^{\bullet}](py)_2\}^+$ species.

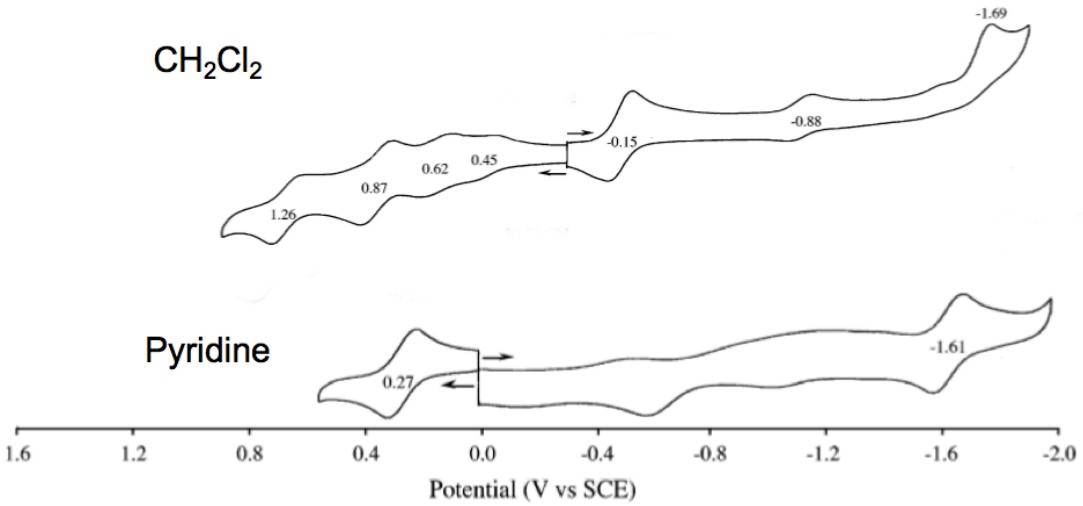

Fig. 5.11 Cyclic voltammograms of Co[Me_4Ph_5] in DCM and pyridine containing 0.1 M TBAP. Reproduced with permission from ref 238.

Finally, a most interesting property of four-coordinate Co corroles such as Co[Me_4Ph_5] is their ability to bind one molecule of CO.[238a] Guilard and coworkers have exploited this property to design CO sensors based on Co corroles.[240,241] DFT calculations have also suggested the potential application of Co corroles for HNO sensing, a possibility that still has to be experimentally realized.[242]

5.4 Rhodium Corroles

Early reports on rhodium corroles included the reaction of [$Rh(CO)_2Cl]_2$ with octaalkylcorroles or N-alkyl corroles, which afforded an Rh(I) corrole after metalation.[243] The first Rh(III) corrole was synthesized by Boschi *et al*., who obtained Rh[OMC](PPh_3) by treating octamethylbiladiene with hydrated $RhCl_3$ in the presence of PPh_3.[48a] Alternatively, a six-coordinate Rh(III) complex Rh[OMC](CO)(PPh_3) was formed when [$Rh(CO)_2Cl]_2$ was used as the metal source. The triphenylarsine-ligated complex Rh[OMC]($AsPh_3$) was also synthesized in an analogous manner and structurally characterized by the same group.[48b]

Subsequently, Gross *et al*. reported the synthesis of Rh[TPFPC](PPh_3)[195] and Rh[TDCPC](PPh_3)[244] via metalation of the corresponding free-base corroles with [$Rh(CO)_2Cl]_2$ in presence of PPh_3. A similar methodology was also used for synthesizing a tricyclohexylphosphine adduct of Rh[TPFPC].[191]

The UV-vis spectra of Rh-PPh_3 corroles exhibit a Soret band around 430 nm and Q band around 560 nm. The diamagnetic complexes exhibit ^{1}H NMR spectra that are qualitatively similar to those of Co-PPh_3 corroles. The X-ray structure of Rh[TPFPC](PPh_3) exhibits a slightly domed macrocycle and a moderate Rh−N_4 displacements of ~0.27 Å (Fig. 5.12).[195] The average M−$N_{corrole}$ distances in Rh-PPh_3 corroles (~1.968 Å) are significantly longer than those in analogous Co-PPh_3 corroles, as expected for the larger ionic radius of the 4d metal.

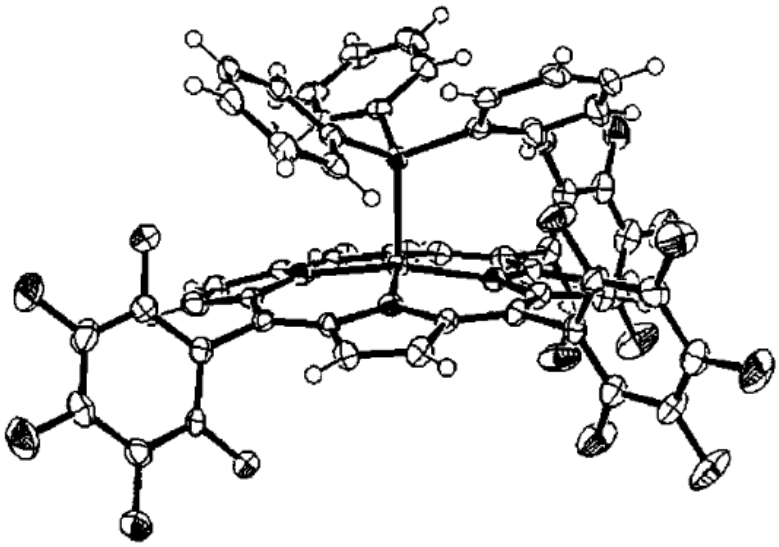

Fig. 5.12 X-ray structure of Rh[TPFPC](PPh_3). Reproduced with permission from ref 195.

Interestingly, addition of pyridine to a DCM solution of Rh-PPh_3 corroles results in the formation of the six-coordinate complex Rh[Cor](PPh_3)(py) via ligand addition.[244] This reactivity may be sharply contrasted from that of Co-PPh_3 corroles, where only ligand substitution takes place, leading to the Co-bispyridine adducts.[214,245] Addition of pyridine into the coordination sphere of the Rh atom is accompanied by a redshift of Soret band by ~20 nm and the appearance of new Q bands at 595-610 nm, as well as visible change in color from wine-red to intense green.[244] The X-ray structure of Rh[TPFPC](PPh_3)(py) revealed a near-planar macrocycle with a smaller Rh−N_4 displacement (~ 0.1 Å) relative to the pentacoordinate Rh[TPFPC](PPh_3) corrole.[244] A similar ligand addition is also observed upon the addition of excess PPh_3 into a solution of Rh[TPFPC](PPh_3), as suggested by changes in visible spectra (see Fig. 5.13).[245]

Gray and coworkers performed one-electron oxidation of Rh[TPFPC](PPh_3) with *t*-4bpa, which resulted in sharp reductions in the intensity of the Soret and Q bands, along with formation of a new, broad band around 710 nm, suggesting corrole-centered oxidation (Fig. 5.13).[245] For six-coordinate Rh[TPFPC]$(py)_2$, one-electron oxidation was also found to be essentially corrole-centered, based on a sharp g = 2.003 EPR signal.[245] Extensive DFT calculations by these researchers also confirmed corrole-centered oxidation for these complexes.[246]

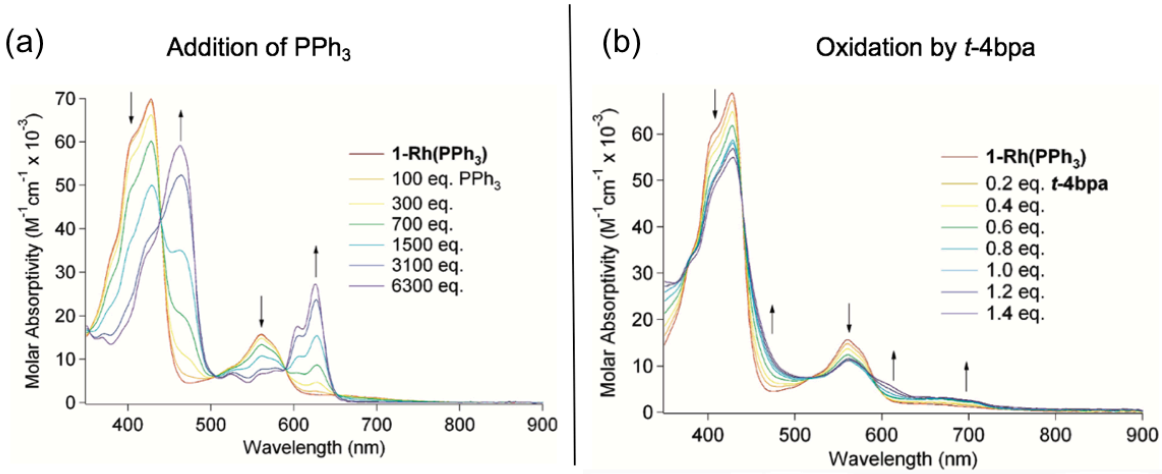

Fig. 5.13 UV-vis spectral changes of Rh[TPFPC](PPh_3) upon (a) addition of excess PPh_3 (left) and (b) oxidation by *t*-4bpa in DCM (right). Reproduced with permission from ref 245.

The cyclic voltammogram of Rh[OMC](PPh_3) consists of three reversible oxidations and one irreversible reduction in PhCN (Fig. 5.14).[247] The oxidations are believed to be macrocycle-centered. Addition of excess PPh_3 to the system results in formation of $\{Rh[OMC](PPh_3)_2\}^+$ after first oxidation. One-electron reduction was found to be irreversible, presumably reflecting the loss of the axial PPh_3 ligand and leading ultimately to a $\{Rh^{II}[OMC]\}^-$ species, which parallels the electroreduction behavior of Co-PPh_3 corroles. In an interesting twist, the singly reduced $\{Rh^{II}[OMC]\}^-$ species was found to undergo rapid dimerization, after electrogeneration. The dimerization could be slowed down or prevented by performing the experiment at low temperature (THF, –70°C) or in presence of excess PPh_3 in PhCN.[247] Thus, on applying high scan rates in the presence of an excess PPh_3 in PhCN, $\{Rh^{I}[OMC](PPh_3)\}^{2-}$ was found to form via stepwise two-electron reduction of the neutral complex; the dianion subsequently was found to lose PPh_3 to yield the bare

$\{Rh^{I}[OMC]\}^{2-}$ dianion. This Rh(I) corrole dianion could then be reoxidized to the original charge-neutral Rh(III) species via two one-electron oxidations.

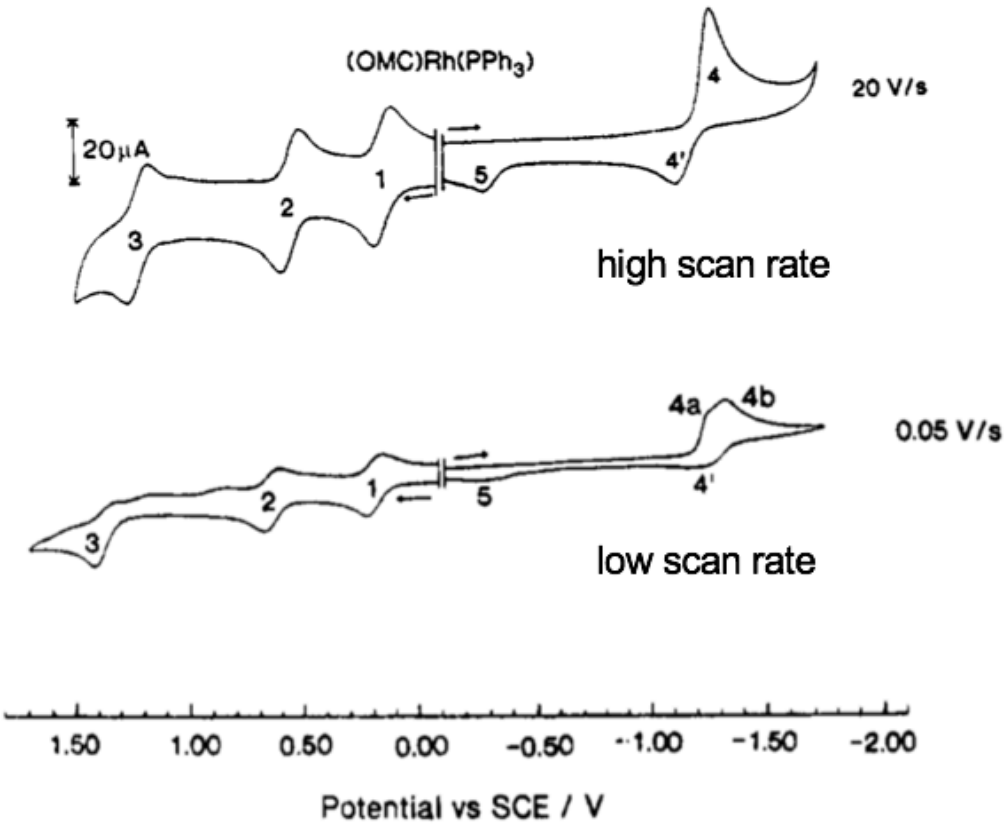

Fig. 5.14 Cyclic voltammograms of Rh[OMC](PPh_3) in PhCN containing 0.1 M TBAP at two different scan rates. Reproduced with permission from ref 247.

5.5.1 Introduction to paper C: Cobalt- and Rhodium-Corrole-Triphenylphosphine Complexes Revisited: The Question of a Noninnocent Corrole

Cobalt-PPh_3 corroles have long been thought of as classic low-spin Co(III) complexes. A multitechnique investigation, including UV-Vis spectroscopy, electrochemistry, XAS and XES analyses, and DFT calculations, however, suggests that Co-PPh_3 corroles are noninnocent with partial Co^{II}-corrole$^{\bullet 2-}$ character. In contrast, no evidence of ligand noninnocence was found for Rh-PPh_3 corroles.

A total of nine Co[Y_8T*p*XPC](PPh_3) corroles (X = NO_2, CF_3, H, Me, OMe; and Y = H, Br) and four Rh[T*p*XPC](PPh_3) corroles (X = CF_3, H, Me, OMe) were synthesized for this study. Unlike in previous studies, THF was chosen as the solvent for Co insertion into free-base corroles, which was carried out at 45-50°C in the

presence of excess PPh_3 and NaOAc. The choice of THF ensured good solubility of all free-base corroles in the reaction medium. The complexes were generally purifiied by column chromatography on silica gel with *n*-hexane/DCM as eluent.

The synthesis of Rh[T*p*XPC](PPh_3) complexes was initially attempted with $[Rh(cod)_2Cl]_2$ as the metal source (5 equiv) in refluxing THF under argon in the presence of excess PPh_3 (5 equiv) and dry K_2CO_3, a procedure akin to the synthesis of Ir-PPh_3 corroles.[245] Except for X = CF_3, this method failed miserably for all the other free-base H_3[T*p*XPC] ligands. A new procedure, where smaller amounts of the metal source $[Rh(cod)_2Cl]_2$ (1.5 equiv) and PPh_3 (1 equiv) were used in 2:1 DCM/EtOH (2:1), led to good yields (48-54%) of Rh[T*p*XPC](PPh_3) derivatives along with simpler purification. The Rh-PPh_3 corroles are stable as solid and also in solution for reasonable time periods, allowing for satisfactory elemental analyses.

The UV-vis spectra of Co[T*p*XPC](PPh_3) corroles were found to exhibit substantial redshifts of the Soret maxima along the series: $NO_2 \rightarrow CF_3 \rightarrow H \rightarrow Me \rightarrow OMe$, i.e., with increasing electron-donating character of the *para*-substituent X. This observation provided the first indication that Co[T*p*XPC](PPh_3) corroles may be significantly noninnocent, i.e., with significant Co^{II}-corrole$^{\bullet 2-}$ character. In contrast, the Soret maxima of Rh[T*p*XPC](PPh_3) derivatives were found not to shift as a function of *para*-substituent X, implying an essentially innocent Rh^{III}-corrole^{3-} system.

DFT calculations carried out by our collaborator Prof. Jeanet Conradie yielded a broken-symmetry spin density profile for Co[TPC](PPh_3) that matched a Co^{II}-corrole$^{\bullet 2-}$ description as well as a small singlet-triplet enery gap (0.15 eV). The broken-symmentry optimized geometry of Co[TPC](PPh_3) also showed small skeletal bond length alternations in the bipyrrole half of the corrole, further suggesting corrole$^{\bullet 2-}$ radical character in the complex. Analogous calculations on Rh[TPC](PPh_3) yielded neither a broken-symmetry solution nor the characteritic bond length alternations; the calculated singlet-triplet enery gap was also much larger than for the Co complex, all of which was consistent with an innocent Rh^{III}–corrole^{3-} electronic description for the Rh complex.

The electrochemistry of Co-PPh_3 corroles has been described at some length earlier in this chapter. Both the Co- and Rh-PPh_3 complexes studied in this work exhibited irreversible one-electron reductions, reflecting reductive cleavage of the PPh_3 ligand. An interesting difference between the two metals is that the Rh-PPh_3 corroles undergo reduction at considerably more negative potential (~400 mV) than

the analogous Co-PPh_3 corroles. This can be attributed to the greater stability of the Rh(III) states relative to the Co(III) or Co^{II}-corrole$^{\bullet 2-}$ state.

The Co[Br_8T*p*CF_3PC](PPh_3) complex proved amenable to single crystal X-ray structure determination. The structure revealed a mildly saddled corrole macrocycle, which is quite unusual for metallocorroles other than Cu corroles. X-ray structures were also obtained for two Rh-PPh_3 corroles, Rh[TPC](PPh_3) and Rh[T*p*OMePC](PPh_3), both of which exhibited domed corrole macrocycles. The M-$N_{corrole}$, M-P, and M-N_4 distances of these complexes were all found to be in good accord with literature values.

Finally, four complexes – Co[TPP], Co[TPP](py)Cl, Co[TPC](PPh_3) and Co[TPC]$(py)_2$, (TPP = tetraphenylporphyrin, py = pyridine) – were examined by X-ray absorption spectroscopy (XAS). The XAS data showed that the K-rising-edge energy of Co[TPC](PPh_3), which corresponds to a 1s→4p transition, is significantly lower than that of the genuine Co(III) complex Co[TPP](py)Cl. This suggests a relatively low positive charge on the Co ion in Co[TPC](PPh_3), consistent with partial Co^{II}-corrole$^{\bullet 2-}$ character.

My contribution to this paper consisted of all syntheses and characterization of the complexes by means of UV-vis, MS, and ^{1}H NMR spectroscopies as well as electrochemistry of the nine Co-PPh_3 corroles and the four Rh-PPh_3 corroles. The X-ray absorption spectroscopic measurements were carried out by our collaborator Dr. Ritimukta Sarangi at the Stanford Synchrotron Radiation Lightsource. The three X-ray structures were solved at the Advanced Light Source, Lawrence Berkeley National Laboratory. The DFT calculations were carried out by Professors Jeanet Conradie and Abhik Ghosh.

5.5.2 Introduction to paper D: Electronic Structure of Cobalt-Corrole-Pyridine Complexes: Noninnocent Five-coordinate Co(II) Corrole-Radical States

After discovering clear evidence of noninnocent character in Co-PPh_3 corroles, I wished to investigate whether Co corrole pyridine adducts might also exhibit indications of ligand noninnocence. Toward this end, I synthesized Co[T*p*XPC]$(py)_2$ and Co[Br_8T*p*XPC]$(py)_2$ derivatives and characterized them by UV-vis spectroscopy and ^{1}H NMR spectroscopies and electrochemistry. As described below, substituent effects in the *meso*-T*p*XPC series (X = CF_3, H, Me, OMe) series of complexes provided unique insight into the question of ligand noninnocence in the Co-pyridine

adducts.

The Co[T*p*XPC]$(py)_2$ and Co[Br_8T*p*XPC]$(py)_2$ complexes could all be synthesized by reacting the corresponding free-base corroles with Co(II) acetate in pyridine at 100°C for approximately 30 minutes. For stability, the Co[T*p*XPC]$(py)_2$ derivatives were found to require a small amount of pyridine (~1-2% v/v) in the eluent mixture (DCM/hexane) during column chromatography. In the absence of pyridine, the complexes degraded severely in contact with the silica. The Co[Br_8T*p*XPC]$(py)_2$ complexes on the other hand proved to be more stable towards silica and could be chromatographed with *n*-hexane/DCM as eluent without any added pyridine. For long-term stability in solution, however, a small amount of added pyridine was still necessary. Thus, attempted crystallization of Co[Br_8T*p*XPC]$(py)_2$ from $CHCl_3$/MeOH led to a poor quality structure (not shown) of a six-coordinate cobalt isocorrole with a pyridine and a chloride as the axial ligands. X-ray quality crystals of Co[T*p*MePC]$(py)_2$ and Co[Br_8T*p*MePC]$(py)_2$ were successfully obtained in the presence of a small amount of pyridine in the solvent mixture.

In noncoordinating solvent like DCM, $CHCl_3$, etc. in absence of any added pyridine, Co-bispyridine corroles dissolve to yield yellow to brown solutions, where the main species are thought to be the five-coordinate monopyridine adducts. The Soret maxima of these solutions were found to redshift strongly from X = CF_3 to electron donating X = OMe, much as was observed for the Co[T*p*XPC](PPh_3) series, suggesting a noninnocent Co^{II}-corrole$^{\bullet 2-}$ electronic description for the Co[Cor](py) species. Upon addition of pyridine, these solutions turn bright green, where the main species are thought to be the six-coordinate bispyridine adducts. The Soret maxima of these solutions proved insensitive to the nature of the substituent X, suggesting an innocent Co^{III}–corrole^{3-} description for the Co[Cor]$(py)_2$ forms. Unsurprisingly, solutions Co[Cor]$(py)_2$ in noncoordinating solvents such as DCM exhibit different electrochemical behavior in the absence and presence of pyridine.

The ^{1}H NMR spectra of the Co[T*p*XPC]$(py)_2$ complexes in relatively polar NMR solvents such as $CDCl_3$, CD_2Cl_2, CD_3CN, etc. consist of weak, broad, and unresolved signals. This behavior can be related to the rapid dissociation and reassociation of the axial pyridines of Co[T*p*XPC]$(py)_2$ on the NMR time scale. In benzene-d_6, however, sharp and well resolved signals for aryl-H's and β-H's could be observed, consistent with diamagnetic bispyridine adducts. The axial pyridines of Co[T*p*XPC]$(py)_2$ were found to resonate in a high-field region (2:4:4 ratio), reflecting

the diamagnetic current of the corrole ring.

Single crystal X-ray structures were obtained for two complexes, Co[T*p*MePC](py)$_2$ and Co[Br$_8$T*p*MePC](py)$_2$. The former was found to exhibit a planar corrole ligand, whereas the latter complex exhibited a mildly ruffled macrocycle, an unusual deformation for corroles.

Finally, broken-symmetry DFT calculations strongly support a Co^{II}-corrole$^{\bullet 2-}$ formulation for the ground states of five-coordinate Co[Cor](py) complexes. The calculations further indicate that these species are open-shell singlets with antiferromagnetic coupling between the Co(d_{z2}) electron and a corrole a_{2u} radical.

My contributions to this paper consisted of all the syntheses and characterization of the complexes with UV-vis, NMR, MS and electrochemistry. The two X-ray structures were solved at the Advanced Light Source, Lawrence Berkeley National Laboratory. The DFT calculations were carried out by Professors Jeanet Conradie and Abhik Ghosh.

Conclusion

Half a century after the concept was first introduced, the phenomenon of ligand noninnocence continues to captivate chemists. In this thesis, I have examined the phenomenon, as it applies to first-row transition metal corroles, in particular Mn, Fe, and Co corroles. I identified multiple families of metallocorroles as noninnocent, which until now had not been recognized as such. I also studied in greater depth metallocorroles that have been recognized as noninnocent by others. The principal achievements of this work can be summarized as follows:

I synthesized several series of Mn, Fe, and Co corroles with different axial ligands. In many cases, I developed new synthetic protocols. Out of the 50 or so compounds examined in this thesis, 30 are new compounds. A total of six crystal structures were obtained in the course of this work.

I have investigated the role of substituent effects on the Soret maxima of metallocorroles as an indicator of a noninnocent corrole ligand. As a result of my work, this 'optical probe' of ligand noninnocence has been placed on a much firmer footing. Indeed, I used the optical probe to identify $Fe_2(\mu\text{-}O)$ and Co-PPh_3 corroles as substantially noninnocent systems. Given that these complexes are diamagnetic and do not offer convenient NMR and EPR handles, the availability of a simple optical probe of ligand noninnocence is quite valuable for these compounds. I also applied the optical probe for the first time to Mn-aryl and Fe-aryl corroles, for which the corrole emerged as an innocent ligand.

Obviously, optical spectroscopy was far from a standalone tool in my research; a wide variety of other techniques including NMR and EPR spectroscopies, electrochemistry, X-ray crystallography and DFT calculations were routinely used and they led to a deeper appreciation of the many possible manifestations of the phenomenon of ligand noninnocence. To give a couple of examples, ^{1}H NMR spectroscopy provided a detailed experimental probe of the spin density profiles of Fe corroles and X-ray crystallographic studies demonstrated characteristic skeletal bond length alternations in a noninnocent corrole ligand.

I examined the influence of pyridine binding on the innocence or otherwise of the corrole macrocycle in cobalt corroles. Again, the optical probe proved useful. The key conclusion is that whereas Co-bispyridine complexes are innocent Co(III)

species, the corresponding monopyridine adducts are noninnocent with a Co^{II}-corrole$^{\bullet 2-}$ ground state as well as other low-energy open-shell excited states.

Last, through a collaboration with the Stanford Synchrotron Radiation Lightsource (SSRL), I began to explore the use of X-ray absorption spectroscopy and related techniques to shed light on the issue of ligand noninnocence in metallocorroles. Although I have not been able to participate in a hands-on manner in the experimental work, the findings on my complexes have provided some of the first high-quality XAS data on metallocorroles and important electronic-structural insights especially in the case of Fe corroles. The current renaissance of X-ray science, including the emergence of new third- and fourth-generation light sources as well as new X-ray spectroscopic methods, promise a major new approach to electronic-structural studies of transition metal complexes – if I have the opportunity, I hope to pursue this fascinating area as a PhD scientist.

References

1. (a) A. Shelnutt, J.; Song, X.-Z.; Ma, J.-G.; Jia, S.-L.; Jentzen, W.; J. Medforth, C.; J. Medforth, C. Nonplanar Porphyrins and their Significance in Proteins. *Chem. Soc. Rev.* **1998**, *27*, 31-42. (b) Jentzen, W.; Song, X.-Z.; Shelnutt, J. A. Structural Characterization of Synthetic and Protein-Bound Porphyrins in Terms of the Lowest-Frequency Normal Coordinates of the Macrocycle. *J. Phys. Chem. B* **1997**, *101*, 1684-1699.
2. Harada, R.; Matsuda, Y.; Ōkawa, H.; Miyamoto, R.; Yamauchi, S.; Kojima, T. Synthesis and Characterization of Chromium(III) Octaphenylporphyrin Complexes with Various Axial Ligands: An Insight into Porphyrin Distortion. *Inorg. Chim. Acta* **2005**, *358*, 2489-2500.
3. Y. Nelson, N.; J. Medforth, C.; J. Nurco, D.; M. Smith, K.; Jia, S.-L.; A. Shelnutt, J. Synthesis and Unusual Properties of the First 2,3,7,8,12,13,17,18-octabromo-5,10,15,20-tetraalkylporphyrin. *Chem. Commun.* **1999**, 2071-2072.
4. Senge, M. O.; Renner, M. W.; Kallisch, W. W.; Fajer, J. Molecular Structure of (5,10,15,20-tetrabutyl-2,3,7,8,12,13,17,18-octaethylporphyrinato)nickel(II)-Correlation of Nonplanarity with Frontier Orbital Shifts. *J. Chem. Soc., Dalton Trans.* **2000**, 381-385.
5. Birnbaum, E. R.; Hodge, J. A.; Grinstaff, M. W.; Schaefer, W. P.; Henling, L.; Labinger, J. A.; Bercaw, J. E.; Gray, H. B. ^{19}F NMR Spectra and Structures of Halogenated Porphyrins. *Inorg. Chem.* **1995**, *34*, 3625-3632.
6. Thomassen, I. K.; Vazquez-Lima, H.; Gagnon, K. J.; Ghosh, A. Octaiodoporphyrin. *Inorg. Chem.* **2015**, *54*, 11493-11497.
7. Senge, M. O. Prevention of Out-of-Plane Macrocycle Distortion by Thallium in the Sterically Strained 2,3,7,8,12,13,17,18-octaethyl-5,10,15,20-Tetranitroporphyrin. *J. Chem. Soc., Dalton Trans.* **1993**, 3539-3549.
8. Barkigia, K. M.; Fajer, J.; Adler, A. D.; Williams, G. J. B. Crystal and Molecular Structure of (5,10,15,20-tetra-N-propylporphinato)lead(II): a "Roof" Porphyrin. *Inorg. Chem.* **1980**, *19*, 2057-2061.
9. Nurco, D. J.; Medforth, C. J.; Forsyth, T. P.; Olmstead, M. M.; Smith, K. M. Conformational Flexibility in Dodecasubstituted Porphyrins. *J. Am. Chem. Soc.* **1996**, *118*, 10918-10919.
10. Paolesse, R.; Marini, A.; Nardis, S.; Froiio, A.; Mandoj, F.; Nurco, D. J.; Prodi, L.; Montalti, M.; Smith, K. M. Novel Routes to Substituted 5,10,15-Triarylcorroles. *J. Porphyrins Phthalocyanines* **2003**, *07*, 25-36.
11. Ding, T.; Harvey, J. D.; Ziegler, C. J. N-H Tautomerization in Triaryl Corroles. *J. Porphyrins Phthalocyanines* **2005**, *09*, 22-27.
12. Capar, J.; Conradie, J.; Beavers, C. M.; Ghosh, A. Molecular Structures of Free-Base Corroles: Nonplanarity, Chirality, and Enantiomerization. *J. Phys. Chem. A* **2015**, *119*, 3452-3457.
13. Palmer, J. H.; Day, M. W.; Wilson, A. D.; Henling, L. M.; Gross, Z.; Gray, H. B. Iridium Corroles. *J. Am. Chem. Soc.* **2008**, *130*, 7786-7787.
14. Thomas, K. E.; Alemayehu, A. B.; Conradie, J.; Beavers, C. M.; Ghosh, A. The Structural Chemistry of Metallocorroles: Combined X-ray Crystallography and Quantum Chemistry Studies Afford Unique Insights. *Acc. Chem. Res.* **2012**, *45*, 1203-1214.
15. Luobeznova, I.; Raizman, M.; Goldberg, I.; Gross, Z. Synthesis and Full Characterization of Molybdenum and Antimony Corroles and Utilization of the Latter

Complexes as Very Efficient Catalysts for Highly Selective Aerobic Oxygenation Reactions. *Inorg. Chem.* **2006**, *45*, 386-394
16. Reith, L. M.; Stiftinger, M.; Monkowius, U.; Knör, G.; Schoefberger, W. Synthesis and Characterization of a Stable Bismuth(III) A_3-Corrole. *Inorg. Chem.* **2011**, *50*, 6788-6797.
17. Eikey, R. A.; Khan, S. I.; Abu-Omar, M. M. The Elusive Terminal Imido of Manganese(V). *Angew. Chem. Int. Ed.* **2002**, *41*, 3591-3595
18. (a) Pomarico, G.; Tortora, L.; Fronczek, F. R.; Smith, K. M.; Paolesse, R. Selective Nitration and Bromination of Surprisingly Ruffled Phosphorus Corroles. *J. Inorg. Biochem.* **2016**, *158*, 17-23. (b) Gao, D.; Azarias, C.; D'Aléo, A.; Giorgi, M.; Siri, O.; Balaban, T. S.; Jacquemin, D.; Canard, G. Synthesis and Characterization of Ruffled Phosphorus *meso*-Ester Corroles. *Eur. J. Inorg. Chem.* **2017**, *2017*, 780-788.
19. (a) Gouterman, M.; Wagnière, G. H.; Snyder, L. C. Spectra of porphyrins. *J. Mol. Spectroscopy* **1963**, *11*, 108-127. (b) Gouterman, M.: 1 - Optical Spectra and Electronic Structure of Porphyrins and Related Rings A2 - DOLPHIN, DAVID. In *The Porphyrins*; Academic Press, 1978; pp 1-165.
20. Namuangruk, S.; Sirithip, K.; Rattanatwan, R.; Keawin, T.; Kungwan, N.; Sudyodsuk, T.; Promarak, V.; Surakhot, Y.; Jungsuttiwong, S. Theoretical Investigation of the Charge-Transfer Properties in different *meso*-linked Zinc Porphyrins for Highly Efficient Dye-Sensitized Solar Cells. *Dalton Trans.* **2014**, *43*, 9166-9176.
21. Hush, N. S.; Dyke, J. M.; Williams, M. L.; Woolsey, I. S. Electronic Spectra of Metal Corrole Anions. *J. Chem. Soc., Dalton Trans.* **1974**, 395-399.
22. Ghosh, A.; Wondimagegn, T.; Parusel, A. B. J. Electronic Structure of Gallium, Copper, and Nickel Complexes of Corrole. High-Valent Transition Metal Centers versus Noninnocent Ligands. *J. Am. Chem. Soc.* **2000**, *122*, 5100-5104.
23. Fischer, H.; Zeile, K. Synthese des Hämatoporphyrins, Protoporphyrins und Hämins. *Justus Liebigs Annalen der Chem.* **1929**, *468*, 98-116.
24. Rothemund, P. Formation of Porphyrins from Pyrrole and Aldehydes. *J. Am. Chem. Soc.* **1935**, *57*, 2010-2011.
25. Rothemund, P. A New Porphyrin Synthesis. The Synthesis of Porphin. *J. Am. Chem. Soc.* **1936**, *58*, 625-627.
26. Rothemund, P.; Menotti, A. R. Porphyrin Studies. IV.1 The Synthesis of *α,β,γ,δ*-Tetraphenylporphine. *J. Am. Chem. Soc.* **1941**, *63*, 267-270.
27. (a) Aronoff, S.; Calvin, M. The Porphyrin-Like Products of the Reaction of Pyrrole with Benzaldehyde. *J. Org. Chem.* **1943**, *08*, 205-223. (b) Ball, R. H.; Dorough, G. D.; Calvin, M. A Further Study of the Porphine-like Products of the Reaction of Benzaldehyde and Pyrrole. *J. Am. Chem. Soc.* **1946**, *68*, 2278-2281
28. Priesthoff, J. H.; Banks, C. V. A New Method of Purifying *α,β,γ,δ*-Tetraphenylporphine. *J. Am. Chem. Soc.* **1954**, *76*, 937-938.
29. Thomas, D. W.; Martell, A. E. Tetraphenylporphine and Some *para*-Substituted Derivatives. *J. Am. Chem. Soc.* **1956**, *78*, 1335-1338.
30. (a) Corwin, A. H.; Sydow, V. L. New Methods for Porphyrin Synthesis. *J. Am. Chem. Soc.* **1953**, *75*, 4484-4486. (b) Krol, S. Notes- A New Synthesis of Porphin. *J. of Org. Chem.* **1959**, *24*, 2065-2067
31. Adler, A. D.; Longo, F. R.; Shergalis, W. Mechanistic Investigations of Porphyrin Syntheses. I. Preliminary Studies on *ms*-Tetraphenylporphin. *J. Am. Chem. Soc.* **1964**, *86*, 3145-3149.
32. Adler, A. D.; Sklar, L.; Longo, F. R.; Finarelli, J. D.; Finarelli, M. G. A Mechanistic Study of the Synthesis of *meso*-Tetraphenylporphin. *J. Heterocyclic Chem.* **1968**, *5*, 669-678.

33. Adler, A. D.; Longo, F. R.; Finarelli, J. D.; Goldmacher, J.; Assour, J.; Korsakoff, L. A Simplified Synthesis for *meso*-Tetraphenylporphine. *J. Org. Chem.* **1967**, *32*, 476-476.
34. (a) Barnett, G. H.; Hudson, M. F.; Smith, K. M. *meso*-Tetraphenylporphyrin Purification. *Tetrahedron Lett.* **1973**, *14*, 2887-2888. (b) Rousseau, K.; Dolphin, D. A Purification of *meso*-Tetraphenylporphyrin. *Tetrahedron Lett.* **1974**, *15*, 4251-4254. (c) Barnett, G. H.; Hudson, M. F.; Smith, K. M. Concerning *meso*-Tetraphenylporphyrin Purification. *J. Chem. Soc., Perkin Trans. 1* **1975**, 1401-1403.
35. Lindsey, J. S.; Hsu, H. C.; Schreiman, I. C. Synthesis of Tetraphenylporphyrins under Very Mild Conditions. *Tetrahedron Lett.* **1986**, *27*, 4969-4970.
36. Mauzerall, D. The Thermodynamic Stability of Porphyrinogens. *J. Am. Chem. Soc.* **1960**, *82*, 2601-2605.
37. Lindsey, J. S.; Schreiman, I. C.; Hsu, H. C.; Kearney, P. C.; Marguerettaz, A. M. Rothemund and Adler-Longo Reactions Revisited: Synthesis of Tetraphenylporphyrins under Equilibrium Conditions. *J. Org. Chem.* **1987**, *52*, 827-836.
38. Wagner, R. W.; Lawrence, D. S.; Lindsey, J. S. An Improved Synthesis of Tetramesitylporphyrin. *Tetrahedron Lett.* **1987**, *28*, 3069-3070
39. Lindsey, J. S.; Wagner, R. W. Investigation of the Synthesis of *ortho*-Substituted Tetraphenylporphyrins. *J. Org. Chem.* **1989**, *54*, 828-836.
40. Lindsey, J. S.; MacCrum, K. A.; Tyhonas, J. S.; Chuang, Y. Y. Investigation of a Synthesis of *meso*-Porphyrins Employing High Concentration Conditions and an Electron Transport Chain for Aerobic Oxidation. *J. Org. Chem.* **1994**, *59*, 579-587.
41. Li, F.; Kexin, Y.; Tyhonas, J. S.; MacCrum, K. A.; Lindsey, J. S. Beneficial Effects of Salts on an Acid-Catalyzed Condensation Leading to Porphyrin Formation. *Tetrahedron* **1997**, *53*, 12339-12360.
42. Geier, G. R.; Lindsey, J. S. Effects of Diverse Acid Catalysts on the Reaction Course in the Two-Step One-Flask Synthesis of *meso*-Tetraphenylporphyrin. *J. Porphyrins Phthalocyanines* **2002**, *06*, 159-185.
43. (a) Geier Iii, G. R.; Lindsey, J. S. Investigation of porphyrin-forming reactions. Part 1. Pyrrole + Aldehyde Oligomerization in Two-Step, One-Flask Syntheses of *meso*-Substituted Porphyrins. *J. Chem. Soc., Perkin Trans. 2,* **2001**, 677-686. (b) Geier Iii, G. R.; Lindsey, J. S. Investigation of Porphyrin-Forming Reactions. Part 2. Examination of the Reaction Course in Two-Step, One-Flask Syntheses of *meso*-Substituted Porphyrins. *J. Chem. Soc., Perkin Trans. 2,* **2001**, 687-700.
44. Orłowski, R.; Gryko, D.; Gryko, D. T. Synthesis of Corroles and Their Heteroanalogs. *Chem. Rev.* **2017**, *117*, 3102-3137
45. (a) Johnson, A. W.; Kay, I. T. *Proc. R. Soc. London, Ser. A* **1965**, *288*, 334. (b) Johnson, A. W.; Kay, I. T. Corroles. Part I. Synthesis. *J. Chem. Soc.* **1965**, *0*, 1620-1629. (c) Harris, R. L. N.; Johnson, A. W.; Kay, I. T. The Synthesis of Porphins and Related Macrocycles. *Q. Rev. Chem. Soc.* **1966**, *20*, 211-244.
46. Dolphin, D.; Johnson, A. W.; Leng, J.; Broek, P. v. d. The Base-Catalysed Cyclisations of 1,19-dideoxybiladienes-ac. *J. Chem. Soc. C* **1966**, *0*, 880-884.
47. Conlon, M.; Johnson, A. W.; Overend, W. R.; Rajapaksa, D.; Elson, C. M. Structure and Reactions of Cobalt Corroles. *J. Chem. Soc., Perkin Trans. 1* **1973**, *0*, 2281-2288.
48. (a) Boschi, T.; Licoccia, S.; Paolesse, R.; Tagliatesta, P. Synthetic Routes to Rhodium(III) Corrolates. *Inorg. Chim. Acta* **1988**, *141*, 169-171. (b) Boschi, T.; Licoccia, S.; Paolesse, R.; Tagliatesta, P.; Tehran, M. A.; Pelizzi, G.; Vitali, F. Synthesis and Characterization of Novel Metal(III) Complexes of Corrole. Crystal and

Molecular Structure of (2,3,7,8,12,13,17,18-octamethylcorrolato)(triphenylarsine) rhodium(III). *J.Chem. Soc., Dalton Trans.* **1990**, *0*, 463-468.

49. (a) Paolesse, R.; Licoccia, S.; Bandoli, G.; Dolmella, A.; Boschi, T. First Direct Synthesis of a Corrole Ring from a Monopyrrolic Precursor. Crystal and Molecular Structure of (Triphenylphosphine)(5,10,15-triphenyl-2,3,7,8,12,13,17,18-octamethylcorrolato)cobalt(III)-Dichloromethane. *Inorg. Chem.* **1994**, *33*, 1171-1176. (b) Paolesse, R.; Tassoni, E.; Licoccia, S.; Paci, M.; Boschi, T. One-pot Synthesis of Corrolates by Cobalt Catalyzed Cyclization of Formylpyrroles. *Inorg. Chim. Acta* **1996**, *241*, 55-60.
50. (a) Broadhurst, M. J.; Grigg, R.; Johnson, A. W. Preparation of some Sulphur-Containing Polypyrrolic Macrocycles. Sulphur Extrusion from a *meso*-Thiaphlorin. *J. Chem. Soc. D. Chem. Commun.* **1970**, 807-809. (b) Broadhurst, M. J.; Grigg, R.; Johnson, A. W. Sulphur Extrusion Reactions Applied to the Synthesis of Corroles and Related Systems. *J. Chem. Soc., Perkin Trans. 1* **1972**, 1124-1135.
51. Kin Tse, M.; Zhang, Z.; Shing Chan, K. Synthesis of an Oxorhenium(V) Corrolate from Porphyrin with Detrifluoromethylation and Ring Contraction. *Chem. Commun.* **1998**, 1199-1200.
52. (a) Pandey, R. K.; Zhou, H.; Gerzevske, K.; Smith, K. M. Stepwise Synthesis of 1,19-dibromo-a,c-biladienes and their Conversion into Biliverdins, Corroles and Azaporphyrins. *J. Chem. Soc., Chem. Commun.* **1992**, 183-185. (b) Pandey, R. K.; Gerzevske, K. R.; Zhou, H.; Smith, K. M. New Syntheses of Biliverdins, Corroles and Azaporphyrins from 1,19-dibromo-ac-biladiene salts. *J. Chem. Soc., Perkin Trans. 1* **1994**, 971-977.
53. Licoccia, S.; Di Vona, M. L.; Paolesse, R. Acid-Catalyzed Cyclization of 1,19-Unsubstituted a,c-Biladienes. *J. Org. Chem.* **1998**, *63*, 3190-3195.
54. Gross, Z.; Galili, N.; Saltsman, I. The First Direct Synthesis of Corroles from Pyrrole *Angew. Chem., Int. Ed.* **1999**, *38*, 1427-1429.
55. Gross, Z.; Galili, N.; Simkhovich, L.; Saltsman, I.; Botoshansky, M.; Bläser, D.; Boese, R.; Goldberg, I. Solvent-Free Condensation of Pyrrole and Pentafluorobenzaldehyde: A Novel Synthetic Pathway to Corrole and Oligopyrromethenes *Org. Lett.* **1999**, *1*, 599-602.
56. Paolesse, R.; Mini, S.; Sagone, F.; Boschi, T.; Jaquinod, L.; J. Nurco, D.; M. Smith, K. 5,10,15-Triphenylcorrole: a Product from a Modified Rothemund Reaction *Chem. Commun.* **1999**, *0*, 1307-1308.
57. Paolesse, R.; Nardis, S.; Sagone, F.; Khoury, R. G. Synthesis and Functionalization of *meso*-Aryl-Substituted Corroles. *J. Org. Chem.* **2001**, *66*, 550-556.
58. Ka, J.-W.; Cho, W.-S.; Lee, C.-H. Expedient Synthesis of Corroles by Oxidant-Mediated, Direct *α-α′* Coupling of Tetrapyrromethanes. *Tetrahedron Lett.* **2000**, *41*, 8121-8125.
59. Asokan, C. V.; Smeets, S.; Dehaen, W. Sterically Encumbered Triarylcorroles from Aryldipyrromethanes and Aromatic Aldehydes. *Tetrahedron Lett.* **2001**, *42*, 4483-4485.
60. Gryko, D. T. A Simple, Rational Synthesis of *meso*-Substituted A_2B-Corroles. *Chem. Commun.* **2000**, 2243-2244.
61. Gryko, D. T.; Jadach, K. A Simple and Versatile One-Pot Synthesis of *meso*-Substituted *trans*-A_2B-Corroles. *J. Org. Chem.* **2001**, *66*, 4267-4275.
62. Gryko, D. T.; Koszarna, B. Refined Methods for the Synthesis of *meso*-Substituted A_3- and *trans*-A_2B-Corroles. *Org. Biomol. Chem.* **2003**, *1*, 350-357.

63. Guilard, R.; Gryko, D. T.; Canard, G.; Barbe, J.-M.; Koszarna, B.; Brandès, S.; Tasior, M. Synthesis of Corroles Bearing up to Three Different Meso Substituents. *Org. Lett.* **2002**, *4*, 4491-4494.
64. Gryko, D. T.; Koszarna, B. Refined Synthesis of *meso*-Substituted *trans*-A_2B-Corroles Bearing Electron-Withdrawing Groups. *Synthesis* **2004**, 2205-2209.
65. Koszarna, B.; Gryko, D. T. Efficient Synthesis of *meso*-Substituted Corroles in a H_2O−MeOH Mixture. *J. Org. Chem.* **2006**, *71*, 3707-3717.
66. V. Král, P.; Dolenský, V., B. *Collection of Czechoslovak Chem. Commun.* **2004**, *69*, 1126.
67. Collman, J. P.; Decréau, R. A. Microwave-Assisted Synthesis of Corroles. *Tetrahedron Lett.* **2003**, *44*, 1207-1210.
68. Kumari, P.; Chauhan, S. M. S. Efficient Synthesis of 5,10,15-triarylcorroles using Amberlyst 15 under Solvent-Free Conditions. *J. Heterocyclic Chem.* **2008**, *45*, 779-783.
69. Zhan, H.-Y.; Liu, H.-Y.; Chen, H.-J.; Jiang, H.-F. Preparation of *meso*-Substituted *trans*-A_2B-corroles in Ionic Liquids. *Tetrahedron Lett.* **2009**, *50*, 2196-2199.
70. Dogutan, D. K.; Stoian, S. A.; McGuire, R.; Schwalbe, M.; Teets, T. S.; Nocera, D. G. Hangman Corroles: Efficient Synthesis and Oxygen Reaction Chemistry. *J. Am. Chem. Soc.* **2011**, *133*, 131-140.
71. (a) Barata, J. F. B.; Santos, C. I. M.; Neves, M. G. P. M. S.; Faustino, M. A. F.; Cavaleiro, J. A. S. Functionalization of Corroles. In *Topics in Heterocyclic Chemistry*; Paolesse, R., Ed.; Springer-Verlag: Berlin, **2014**; Vol. 10, pp 79−141. (b) Lemon, C. M.; Brothers, P. J. The Synthesis, Reactivity, and Peripheral Functionalization of Corroles. *J. Porphyrins Phthalocyanines* **2011**, *15*, 809-834. (c) Barata, J. F. B.; Neves, M. G. P. M. S.; Faustino, M. A. F.; Tomé, A. C.; Cavaleiro, J. A. S. Strategies for Corrole Functionalization. *Chem. Rev.* **2017**, *117*, 3192-3253.
72. Buckley, H. L.; Arnold, J. Recent developments in Out-of-Plane Metallocorrole Chemistry across the Periodic Table. *Dalton Trans.* **2015**, *44*, 30-36.
73. (a) Mandoj, F.; Nardis, S.; Pomarico, G.; Paolesse, R. Demetalation of Corrole Complexes: An Old Dream Turning into Reality. *J. Porphyrins Phthalocyanines* **2008**, *12*, 19-26. (b) Capar, C.; Thomas, K. E.; Ghosh, A. Reductive Demetalation of Copper Corroles: First Simple Route to Free-Base *β*-Octabromocorroles. *J. Porphyrins Phthalocyanines* **2008**, *12*, 964-967.
74. (a) Gross, Z.; Galili, N. N-Substituted Corroles: A Novel Class of Chiral Ligands. *Angew. Chem. Int. Ed.* **1999**, *38*, 2366-2369. (b) Naito, W.; Yasuda, N.; Morimoto, T.; Shigeta, Y.; Takaya, H.; Hisaki, I.; Maeda, H. Doubly N-Methylated Porphyrinoids. *Org. Lett.* **2016**, *18*, 3006-3009.
75. (a) Liu, H.-Y.; Lai, T.-S.; Yeung, L.-L.; Chang, C. K. First Synthesis of Perfluorinated Corrole and Its MnO Complex. *Org. Lett.* **2003**, *5*, 617-620. (b) Steene, E.; Dey, A.; Ghosh, A. *β*-Octafluorocorroles. *J. Am. Chem. Soc.* **2003**, *125*, 16300-16309. (c) Dogutan, D. K.; McGuire, R.; Nocera, D. G. Electocatalytic Water Oxidation by Cobalt(III) Hangman *β*-Octafluoro Corroles. *J. Am. Chem. Soc.* **2011**, *133*, 9178-9180.
76. (a) Ngo, T. H.; Van Rossom, W.; Dehaen, W.; Maes, W. Reductive Demetallation of Cu-Corroles-a New Protective Strategy towards Functional Free-Base Corroles. *Org. Biomol. Chem.* **2009**, *7*, 439-443. (b) Ngo, T. H.; Puntoriero, F.; Nastasi, F.; Robeyns, K.; Van Meervelt, L.; Campagna, S.; Dehaen, W.; Maes, W. Synthetic, Structural, and Photophysical Exploration of *meso*-Pyrimidinyl-Substituted AB_2-Corroles. *Chem. Eur. J.* **2010**, *16*, 5691-5705.
77. Wasbotten, I. H.; Wondimagegn, T.; Ghosh, A. Electronic Absorption, Resonance Raman, and Electrochemical Studies of Planar and Saddled Copper(III) *meso*-

Triarylcorroles. Highly Substituent-Sensitive Soret Bands as a Distinctive Feature of High-Valent Transition Metal Corroles. *J. Am. Chem. Soc.* **2002**, *124*, 8104-8116.
78. Mahammed, A.; Gray, H. B.; Meier-Callahan, A. E.; Gross, Z. Aerobic Oxidations Catalyzed by Chromium Corroles. *J. Am. Chem. Soc.* **2003**, *125*, 1162-1163.
79. Palmer, J. H.; Durrell, A. C.; Gross, Z.; Winkler, J. R.; Gray, H. B. Near-IR Phosphorescence of Iridium(III) Corroles at Ambient Temperature. *J. Am. Chem. Soc.* **2010**, *132*, 9230-9231.
80. Wagnert, L.; Berg, A.; Stavitski, E.; Berthold, T.; Kothe, G.; Goldberg, I.; Mahammed, A.; Simkhovich, L.; Gross, Z.; Levanon, H. Exploring the Photoexcited Triplet States of Aluminum and Tin Corroles by Time-Resolved Q-band EPR. *Appl. Magn. Reson.* **2006**, *30*, 591-604.
81. Wagnert, L.; Rubin, R.; Berg, A.; Mahammed, A.; Gross, Z.; Levanon, H. Photoexcited Triplet State Properties of Brominated and Nonbrominated Ga(III)-Corroles as Studied by Time-Resolved Electron Paramagnetic Resonance. *J. Phys. Chem. B* **2010**, *114*, 14303-14308.
82. (a) Du, R. B.; Liu, C.; Shen, D. M.; Chen, Q. Y. Partial Bromination and Fluoroalkylation of 5,10,15-Tris(pentafluorophenyl)-Corrole. *Synlett* **2009**, *2009*, 2701−2705. (b) Lemon, C. M.; Halbach, R. L.; Huynh, M.; Nocera, D. G. Photophysical Properties of *β*-Substituted Free-Base Corroles. *Inorg. Chem.* **2015**, *54*, 2713-2725. (c) Nardis, S.; Pomarico, G.; Stefanelli, M.; Lentini, S.; Cicero, D. O.; Fronczek, F. R.; Smith, K. M.; Paolesse, R. The Scope of the *β*-Halogenation of Triarylcorroles. *J. Porphyrins Phthalocyanines* **2016**, *20*, 465-474.
83. (a) Scrivanti, A.; Beghetto, V.; Matteoli, U.; Antonaroli, S.; Marini, A.; Mandoj, F.; Paolesse, R.; Crociani, B. Iminophosphine–Palladium (0) Complexes as Highly Active Catalysts in the Suzuki reaction. Synthesis of Undecaaryl Substituted Corroles. *Tetrahedron Lett.* **2004**, *45*, 5861-5864. (b) Gao, D.; Canard, G.; Giorgi, M.; Balaban, T. S. Synthesis and Characterization of Copper Undecaarylcorroles and the First Undecaarylcorrole Free Base. *Eur. J. Inorg. Chem.* **2012**, *2012*, 5915-5920. (c) Berg, S.; Thomas, K. E.; Beavers, C. M.; Ghosh, A. Undecaphenylcorroles. *Inorg. Chem.* **2012**, *51*, 9911-9916.
84. (a) Gao, D.; Canard, G.; Giorgi, M.; Vanloot, P.; Balaban, T. S. Electronic and Steric Effects of the Peripheral Substitution in Deca- and Undecaaryl Metallocorroles. *Eur. J. Inorg. Chem.* **2014**, *2014*, 279-287. (b) Gao, D.; Andeme Edzang, J.; Diallo, A. K.; Dutronc, T.; Balaban, T. S.; Videlot-Ackermann, C.; Terazzi, E.; Canard, G. Light Absorption and Hole-Transport Properties of Copper Corroles: from Aggregates to a Liquid Crystal Mesophase. *New J. Chem.* **2015**, *39*, 7140-7146. (c) Capar, J.; Zonneveld, J.; Berg, S.; Isaksson, J.; Gagnon, K. J.; Thomas, K. E.; Ghosh, A. Demetalation of Copper Undecaarylcorroles: Molecular Structures of a Free-Base Undecaarylisocorrole and a Gold Undecaarylcorrole. *J. Inorg. Biochem.* **2016**, *162*, 146-153.
85. (a) Pomarico, G.; Nardis, S.; Paolesse, R.; Ongayi, O. C.; Courtney, B. H.; Fronczek, F. R.; Vicente, M. G. H. Synthetic Routes to 5,10,15-Triaryl-tetrabenzocorroles. *J. Org. Chem.* **2011**, *76*, 3765-3773. (b) Pomarico, G.; Nardis, S.; Stefanelli, M.; Cicero, D. O.; Vicente, M. G. H.; Fang, Y.; Chen, P.; Kadish, K. M.; Paolesse, R. Synthesis and Characterization of Functionalized *meso*-Triaryltetrabenzocorroles. *Inorg. Chem.* **2013**, *52*, 8834-8844.
86. Stefanelli, M.; Naitana, M. L.; Chiarini, M.; Nardis, S.; Ricci, A.; Fronczek, F. R.; Lo Sterzo, C.; Smith, K. M.; Paolesse, R. Efficient Synthesis of *β*-Alkynylcorroles. *Eur. J. Org. Chem.* **2015**, *2015*, 6811-6816.

87. (a) Capar, C.; Hansen, L.-K.; Conradie, J.; Ghosh, A. *β*-Octabromo-*Meso*-Tris(pentafluorophenyl)Corrole: Reductive Demetalation-based Synthesis of a Heretofore Inaccessible, Perhalogenated Free-Base Corrole. *J. Porphyrins Phthalocyanines* **2010**, *14*, 509-512. (b) Capar, J.; Berg, S.; Thomas, K. E.; Beavers, C. M.; Gagnon, K. J.; Ghosh, A. Improved Syntheses of *β*-Octabromo-*Meso*-Triarylcorrole Derivatives. *J. Inorg. Biochem.* **2015**, *153*, 162-166.
88. Schechter, A.; Stanevsky, M.; Mahammed, A.; Gross, Z. Four-Electron Oxygen Reduction by Brominated Cobalt Corrole. *Inorg. Chem.* **2012**, *51*, 22-24.
89. (a) Vestfrid, J.; Botoshansky, M.; Palmer, J. H.; Durrell, A. C.; Gray, H. B.; Gross, Z. Iodinated Aluminum(III) Corroles with Long-Lived Triplet Excited States. *J. Am. Chem. Soc.* **2011**, *133*, 12899-12901. (b) Vestfrid, J.; Goldberg, I.; Gross, Z. Tuning the Photophysical and Redox Properties of Metallocorroles by Iodination. *Inorg. Chem.* **2014**, *53*, 10536-10542.
90. Vestfrid, J.; Kothari, R.; Kostenko, A.; Goldberg, I.; Tumanskii, B.; Gross, Z. Intriguing Physical and Chemical Properties of Phosphorus Corroles. *Inorg. Chem.* **2016**, *55*, 6061-6067.
91. Soll, M.; Sudhakar, K.; Fridman, N.; Müller, A.; Röder, B.; Gross, Z. One-Pot Conversion of Fluorophores to Phosphorophores. *Org. Lett.* **2016**, *18*, 5840-5843.
92. (a) Paolesse, R.; Nardis, S.; Venanzi, M.; Mastroianni, M.; Russo, M.; Fronczek, F. R.; Vicente, M. G. H. Vilsmeier Formylation of 5,10,15-Triphenylcorrole: Expected and Unusual Products. *Chem. Eur. J.* **2003**, *9*, 1192-1197. (b) Saltsman, I.; Mahammed, A.; Goldberg, I.; Tkachenko, E.; Botoshansky, M.; Gross, Z. Selective Substitution of Corroles: Nitration, Hydroformylation, and Chlorosulfonation. *J. Am. Chem. Soc.* **2002**, *124*, 7411-7420.
93. (a) Saltsman, I.; Goldberg, I.; Gross, Z. One-step Conversions of a Simple Corrole into Chiral and Amphiphilic Derivatives. *Tetrahedron Lett.* **2003**, *44*, 5669-5673. (b) Sudhakar, K.; Velkannan, V.; Giribabu, L. Synthesis, ElectroChemical and Photophysical Properties of *β*-Carboxy Triaryl Corroles. *Tetrahedron Lett.* **2012**, *53*, 991-993.
94. Hiroto, S.; Hisaki, I.; Shinokubo, H.; Osuka, A. Synthesis of Corrole Derivatives through Regioselective Ir-Catalyzed Direct Borylation. *Angew. Chem. Int. Ed.* **2005**, *44*, 6763-6766.
95. (a) Mahammed, A.; Gross, Z. Chlorosulfonated Corrole: A Versatile Synthon for Advanced Materials. *J. Porphyrins Phthalocyanines* **2010**, *14*, 911-923. (b) Mahammed, A.; Goldberg, I.; Gross, Z. Highly Selective Chlorosulfonation of Tris(pentafluorophenyl)corrole as a Synthetic Tool for the Preparation of Amphiphilic Corroles and Metal Complexes of Planar Chirality. *Org. Lett.* **2001**, *3*, 3443-3446. (c) Gross, Z.; Mahammed, A. Selective Sulfonation and Deuteration of Free-Base Corroles. *J. Porphyrins Phthalocyanines* **2002**, *06*, 553-555. (d) Naitana, M. L.; Nardis, S.; Lentini, S.; Cicero, D. O.; Paolesse, R. Widening the Scope of the Corrole Sulfonation. *J. Porphyrins Phthalocyanines* **2015**, *19*, 735-744.
96. (a) Pomarico, G.; Fronczek, F. R.; Nardis, S.; Smith, K. M.; Paolesse, R. Synthetic Protocols for the Nitration of Corroles. *J. Porphyrins Phthalocyanines* **2011**, *15*, 1085-1092. (b) Stefanelli, M.; Nardis, S.; Fronczek, F. R.; Smith, K. M.; Paolesse, R. Copper *β*-Trinitrocorrolates. *J. Porphyrins Phthalocyanines* **2013**, *17*, 440-446. (c) Stefanelli, M.; Mastroianni, M.; Nardis, S.; Licoccia, S.; Fronczek, F. R.; Smith, K. M.; Zhu, W.; Ou, Z.; Kadish, K. M.; Paolesse, R. Functionalization of Corroles: The Nitration Reaction. *Inorg. Chem.* **2007**, *46*, 10791-10799. (d) Stefanelli, M.; Pomarico, G.; Tortora, L.; Nardis, S.; Fronczek, F. R.; McCandless, G. T.; Smith, K. M.; Manowong, M.; Fang, Y.; Chen, P.; Kadish, K. M.; Rosa, A.; Ricciardi, G.;

Paolesse, R. *β*-Nitro-5,10,15-Tritolylcorroles. *Inorg. Chem.* **2012**, *51*, 6928-6942. (e) Stefanelli, M.; Mandoj, F.; Mastroianni, M.; Nardis, S.; Mohite, P.; Fronczek, F. R.; Smith, K. M.; Kadish, K. M.; Xiao, X.; Ou, Z.; Chen, P.; Paolesse, R. Amination Reaction on Copper and Germanium *β*-Nitrocorrolates. *Inorg. Chem.* **2011**, *50*, 8281-8292.

97. Chirik, P. J. Preface: Forum on Redox-Active Ligands. *Inorg. Chem.* **2011**, *50*, 9737-9740.
98. Jørgensen, C. K. Differences between the Four Halide Ligands, and Discussion Remarks on Trigonal-Bipyramidal Complexes, on Oxidation States, and on Diagonal Elements of One-Electron Energy. *Coord. Chem. Rev.* **1966**, *1*, 164-178.
99. Butin, K. P.; Beloglazkina, E. K.; Zyk, N. V. Metal complexes with Non-Innocent Ligands. *Russian Chem. Rev.* **2005***, 74(6)*, 531-553.
100. Eisenberg, R.; Gray, H. B. Noninnocence in Metal Complexes: A Dithiolene Dawn. *Inorg. Chem.* **2011**, *50*, 9741-9751.
101. (a) Schrauzer, G. N.; Mayweg, V. Reaction of Diphenylacetylene with Nickel Sulfides. *J. Am. Chem. Soc.* **1962**, *84*, 3221-3221. (b) Stiefel, E. I.; Waters, J. H.; Billig, E.; Gray, H. B. The Myth of Nickel(III) and Nickel(IV) in Planar Complexes. *J. Am. Chem. Soc.* **1965**, *87*, 3016-3017.
102. Gray, H. B.; Williams, R.; Bernal, I.; Billig, E. A Spin-Free Square Planar Cobaltous Complex. *J. Am. Chem. Soc.* **1962**, *84*, 3596-3597.
103. Lim, B. S.; Fomitchev, D. V.; Holm, R. H. Nickel Dithiolenes Revisited: Structures and Electron Distribution from Density Functional Theory for the Three-Member Electron-Transfer Series $[Ni(S_2C_2Me_2)_2]^{0,1-,2-}$. *Inorg. Chem.* **2001**, *40*, 4257-4262.
104. (a) Romao, M. J. Molybdenum and Tungsten Enzymes: a Crystallographic and Mechanistic Overview. *Dalton Trans.* **2009**, 4053-4068. (b) Hine, F. J.; Taylor, A. J.; Garner, C. D. Dithiolene Complexes and the Nature of Molybdopterin. *Coord. Chem. Rev.* **2010**, *254*, 1570-1579.
105. Pierpont, C. G. Studies on Charge Distribution and Valence Tautomerism in Transition Metal Complexes of Catecholate and Semiquinonate Ligands. *Coord. Chem. Rev.* **2001**, *216*, 99-125.
106. Pierpont, C. G. Ligand Redox Activity and Mixed Valency in First-Row Transition-Metal Complexes Containing Tetrachlorocatecholate and Radical Tetrachlorosemiquinonate Ligands. *Inorg. Chem.* **2011**, *50*, 9766-9772.
107. Downs, H. H.; Buchanan, R. M.; Pierpont, C. G. Multistep Redox Series of the Tris(o-semiquinone)chromium(III) Complexes. *Inorg. Chem.* **1979**, *18*, 1736-1740.
108. (a) Bugg, T. D. H.; Ramaswamy, S. Non-Heme Iron-Dependent Dioxygenases: Unravelling Catalytic Mechanisms for Complex Enzymatic Oxidations. *Current Opinion in Chemical Biology* **2008**, *12*, 134-140. (b) Pau, M. Y. M.; Davis, M. I.; Orville, A. M.; Lipscomb, J. D.; Solomon, E. I. Spectroscopic and Electronic Structure Study of the Enzyme−Substrate Complex of Intradiol Dioxygenases: Substrate Activation by a High-Spin Ferric Non-heme Iron Site. *J. Am. Chem. Soc.* **2007**, *129*, 1944-1958.
109. Bart, S. C.; Chłopek, K.; Bill, E.; Bouwkamp, M. W.; Lobkovsky, E.; Neese, F.; Wieghardt, K.; Chirik, P. J. Electronic Structure of Bis(imino)pyridine Iron Dichloride, Monochloride, and Neutral Ligand Complexes: A Combined Structural, Spectroscopic, and Computational Study. *J. Am. Chem. Soc.* **2006**, *128*, 13901-13912.
110. (a) Lyaskovskyy, V.; de Bruin, B. Redox Non-Innocent Ligands: Versatile New Tools to Control Catalytic Reactions. *ACS Catal.* **2012**, *2*, 270-279. (b) Luca, O. R.; Crabtree, R. H. Redox-Active Ligands in Catalysis. *Chem. Soc. Rev.* **2013**, *42*, 1440-1459.

111. (a) de Bruin, B.; Bill, E.; Bothe, E.; Weyhermüller, T.; Wieghardt, K. Molecular and Electronic Structures of Bis(pyridine-2,6-diimine)metal Complexes $[ML_2](PF_6)_n$ (n = 0, 1, 2, 3; M = Mn, Fe, Co, Ni, Cu, Zn). *Inorg. Chem.* **2000**, *39*, 2936-2947. (b) Budzelaar, P. H. M.; de Bruin, B.; Gal, A. W.; Wieghardt, K.; van Lenthe, J. H. Metal-to-Ligand Electron Transfer in Diiminopyridine Complexes of Mn−Zn. A Theoretical Study. *Inorg. Chem.* **2001**, *40*, 4649-4655.
112. Kaim, W.; Schwederski, B. Non-Innocent Ligands in BioInorganic Chemistry—An Overview. *Coord. Chem. Rev.* **2010**, *254*, 1580-1588.
113. (a) Weiss, J. J. Nature of the Iron-Oxygen Bond in Oxyhaemoglobin. *Nature* **1964**, *202*, 83-84. (b) Weiss, J. J. Nature of the Iron-Oxygen Bond in Oxyhaemoglobin. *Nature* **1964**, *203*, 183-183.
114. Pauling, L. Nature of the Iron-Oxygen Bond in Oxyhaemoglobin. *Nature* **1964**, *203*, 182-183.
115. Chen, H.; Ikeda-Saito, M.; Shaik, S. Nature of the Fe−O_2 Bonding in Oxy-Myoglobin: Effect of the Protein. *J. Am. Chem. Soc.* **2008**, *130*, 14778-14790.
116. (a) Manoharan, P. T.; Gray, H. B. Electronic Structure of Nitroprusside Ion. *J. Am. Chem. Soc.* **1965**, *87*, 3340-3348. (b) Manoharan, P. T.; Gray, H. B. Electronic Structures of Metal Pentacyanonitrosyls. *Inorg. Chem.* **1966**, *5*, 823-839. (c) Manoharan, P. T.; Hamilton, W. C. The Crystal Structure of Sodium Nitroprusside. *Inorg. Chem.* **1963**, *2*, 1043-1047
117. (a) Enemark, J. H.; Feltham, R. D. Principles of Structure, Bonding, and Reactivity for Metal Nitrosyl Complexes. *Coord. Chem. Rev.* **1974**, *13*, 339-406. (b) Enemark, J. H.; Feltham, R. D. Stereochemical Control of Valence. II. Behavior of the $\{MNO\}^n$ [Metal Mononitrosyl] Group in Ligand Fields. *J. Am. Chem. Soc.* **1974**, *96*, 5002-5004.
118. Ghosh, A. Metalloporphyrin-NO Bonding: Building Bridges with Organometallic Chemistry. *Acc. Chem*. Res. **2005**, 38, 943−954.
119. (a) Ellison, M. K.; Schulz, C. E.; Scheidt, W. R. Syntheses, Characterization, and Structural Studies of Several (Nitro)(nitrosyl)iron(III) Porphyrinates: $[Fe(Porph)(NO_2)(NO)]$. *Inorg. Chem.* **1999**, *38*, 100-108. (b) Tetsuhiko, Y. Substituent Effects on the Electronic Absorption and MCD Spectra of Five- and Six-Coordinate Nitrosyl(tetraphenylporphyrinato)iron(II) Complexes. *Bull. Chem. Soc. Jpn.* **1990**, *63*, 3689-3691. (c) Conradie, J.; Ghosh, A. Correlation between the FeNO Angle and d−p Mixing in $\{FeNO\}^7$ Complexes. *Inorg. Chem.* **2011**, *50*, 4223-4225.
120. Conradie, J.; Quarless, D. A.; Hsu, H.-F.; Harrop, T. C.; Lippard, S. J.; Koch, S. A.; Ghosh, A. Electronic Structure and FeNO Conformation of Nonheme Iron−Thiolate−NO Complexes: An Experimental and DFT Study. *J. Am. Chem. Soc.* **2007**, 129, 10446− 10456.
121. Ghosh, A.; Steene, E. High-Valent Transition Metal Centers and Noninnocent Ligands in Metalloporphyrins and Related Molecules: a Broad Overview Based on Quantum Chemical Calculations. *J. Bio. Inorg. Chem.* **2001**, *6*, 739-752.
122. (a) Hessenauer-Ilicheva, N.; Franke, A.; Meyer, D.; Woggon, W.-D.; van Eldik, R. Mechanistic Insight into Formation of Oxo-Iron(IV) Porphyrin π-Cation Radicals from Enzyme Mimics of Cytochrome P450 in Organic Solvents. *Chem. Eur. J.* **2009**, *15*, 2941-2959. (b) Schlichting, I.; Berendzen, J.; Chu, K.; Stock, A. M.; Maves, S. A.; Benson, D. E.; Sweet, R. M.; Ringe, D.; Petsko, G. A.; Sligar, S. G. The Catalytic Pathway of Cytochrome P450cam at Atomic Resolution. *Science (New York, N.Y.)* **2000**, *287*, 1615.
123. (a) Rittle, J.; Green, M. T. Cytochrome P450 compound I: Capture, Characterization, and C-H Bond Activation Kinetics. *Science (New York, N.Y.)* **2010**, *330*, 933-937. (b)

Roiban, G.-D.; Reetz, M. T. Expanding the Toolbox of Organic Chemists: Directed Evolution of P450 Monooxygenases as Catalysts in Regio- and Stereoselective Oxidative Hydroxylation. *Chem. Commun.* **2015**, *51*, 2208-2224.
124. Rigby, S. E. J.; Muhiuddin, I. P.; Santabarbara, S.; Evans, M. C. W.; Heathcote, P. Proton ENDOR Spectroscopy of the Anion Radicals of the Chlorophyll Primary Electron Acceptors in Type I Photosynthetic Reaction Centres. *Chem. Phys.* **2003**, *294*, 319-328.
125. Walker, F. A.; Licoccia, S.; Paolesse, R. Iron corrolates: Unambiguous Chloroiron(III) (corrolate)$^{2-}$ π-cation radicals. *J. Inorg. Biochem.* **2006**, *100*, 810-837.
126. Cai, S.; Licoccia, S.; Walker, F. A. Cyanide Complexes of Iron Corrolates: Spin Delocalization and Autoreduction. *Inorg. Chem.* **2001**, *40*, 5795-5798.
127. Autret, M.; Will, S.; Caemelbecke, E. V.; Lex, J.; Gisselbrecht, J.-P.; Gross, M.; Vogel, E.; Kadish, K. M. Synthesis and Electrochemistry of Iron(III) Corroles Containing a Nitrosyl Axial Ligand. Spectral Characterization of $[(OEC)FeIII(NO)]^n$ where n = 0, 1, 2, or -1 and OEC is the Trianion of 2,3,7,8,12,13,17,18-Octaethylcorrole. *J. Am. Chem. Soc.* **1994**, *116*, 9141-9149.
128. (a) Joseph, C. A.; Ford, P. C. The Remarkable Axial Lability of Iron(III) Corrole Complexes. *J. Am. Chem. Soc.* **2005**, *127*, 6737-6743. (b) Joseph, C. A.; Lee, M. S.; Iretskii, A. V.; Wu, G.; Ford, P. C. Substituent Effects on Nitrosyl Iron Corrole Complexes $Fe(Ar_3C)(NO)$. *Inorg. Chem.* **2006**, *45*, 2075-2082.
129. Nardis, S.; Stefanelli, M.; Mohite, P.; Pomarico, G.; Tortora, L.; Manowong, M.; Chen, P.; Kadish, K. M.; Fronczek, F. R.; McCandless, G. T.; Smith, K. M.; Paolesse, R. *β*-Nitro Derivatives of Iron Corrolates. *Inorg. Chem.* **2012**, *51*, 3910-3920.
130. Singh, P.; Saltsman, I.; Mahammed, A.; Goldberg, I.; Tumanskii, B.; Gross, Z. Iron Complexes of Tris(4-nitrophenyl)corrole, with Emphasis on the (Nitrosyl)iron Complex. *J. Porphyrins Phthalocyanines* **2012**, *16*, 663-673.
131. Sinha, W.; Deibel, N.; Agarwala, H.; Garai, A.; Schweinfurth, D.; Purohit, C. S.; Lahiri, G. K.; Sarkar, B.; Kar, S. Synthesis, Spectral Characterization, Structures, and Oxidation State Distributions in $[(corrolato)FeIII(NO)]^n$ (n = 0, +1, −1) Complexes. *Inorg. Chem.* **2014**, *53*, 1417-1429.
132. Vazquez-Lima, H.; Norheim, H.-K.; Einrem, R. F.; Ghosh, A. Cryptic noninnocence: FeNO Corroles in a New Light. *Dalton Trans.* **2015**, *44*, 10146-10151.
133. Norheim, H.-K.; Capar, J.; Einrem, R. F.; Gagnon, K. J.; Beavers, C. M.; Vazquez-Lima, H.; Ghosh, A. Ligand noninnocence in FeNO Corroles: Insights From *β*-Octabromocorrole Complexes. *Dalton Trans.* **2016**, *45*, 681-689.
134. Ghosh, A. Electronic Structure of Corrole Derivatives: Insights from Molecular Structures, Spectroscopy, Electrochemistry, and Quantum Chemical Calculations. *Chem. Rev.* **2017**, *117*, 3798-3881.
135. Bougher, C. J.; Liu, S.; Hicks, S. D.; Abu-Omar, M. M. Valence Tautomerization of High-Valent Manganese(V)-Oxo Corrole Induced by Protonation of the Oxo Ligand. *J. Am. Chem. Soc.* **2015**, *137*, 14481-14487.
136. Zdilla, M. J.; Abu-Omar, M. M. Mechanism of Catalytic Aziridination with Manganese Corrole: The Often Postulated High-Valent Mn(V) Imido Is Not the Group Transfer Reagent. *J. Am. Chem. Soc.* **2006**, *128*, 16971-16979.
137. Edwards, N. Y.; Eikey, R. A.; Loring, M. I.; Abu-Omar, M. M. High-Valent Imido Complexes of Manganese and Chromium Corroles. *Inorg. Chem.* **2005**, *44*, 3700-3708.
138. Yukito, M.; Yoshihisa, M.; Kazunori, S.; Sunao, Y.; Yasuhiro, T.; Yasuhiro, A. Transition-Metal Complexes of Pyrrole Pigments. XVII. Preparation and

Spectroscopic Properties of Corrole Complexes. *Bull. Chem. Soc. Jpn.* **1981**, *54*, 163-169.
139. Will, S.; Lex, J.; Vogel, E.; Schmickler, H.; Gisselbrecht, J.-P.; Haubtmann, C.; Bernard, M.; Gorss, M. Nickel and Copper Corroles: Well-Known Complexes in a New Light. *Angew. Chem. Int. Ed.* **1997**, *36*, 357-361.
140. Alemayehu, A. B.; Vazquez-Lima, H.; Beavers, C. M.; Gagnon, K. J.; Bendix, J.; Ghosh, A. Platinum Corroles. *Chem. Commun.* **2014**, *50*, 11093-11096.
141. Brückner, C.; Briñas, R. P.; Krause Bauer, J. A. X-ray Structure and Variable Temperature NMR Spectra of [*meso*-Triarylcorrolato]copper(III). *Inorg. Chem.* **2003**, *42*, 4495-4497.
142. Luobeznova, I.; Simkhovich, L.; Goldberg, I.; Gross, Z. Electronic Structures and Reactivities of Corrole−Copper Complexes. *Eur. J. Inorg. Chem.* **2004**, *2004*, 1724-1732.
143. Bröring, M.; Brégier, F.; Cónsul Tejero, E.; Hell, C.; Holthausen, M. C. Revisiting the Electronic Ground State of Copper Corroles. *Angew. Chem. Int. Ed.* **2007**, *46*, 445-448.
144. Alemayehu, A. B.; Gonzalez, E.; Hansen, L. K.; Ghosh, A. Copper Corroles Are Inherently Saddled. *Inorg. Chem.* **2009**, *48*, 7794-7799.
145. Pierloot, K.; Zhao, H.; Vancoillie, S. Copper Corroles: the Question of Noninnocence. *Inorg. Chem.* **2010**, *49*, 10316-10329.
146. Alemayehu, A. B.; Hansen, L. K.; Ghosh, A. Nonplanar, Noninnocent, and Chiral: A Strongly Saddled Metallocorrole. *Inorg. Chem.* **2010**, *49*, 7608-7610.
147. (a) Thomas, K. E.; Wasbotten, I. H.; Ghosh, A. Copper *β*-Octakis(trifluoromethyl)corroles: New Paradigms for Ligand Substituent Effects in Transition Metal Complexes. *Inorg. Chem.* **2008**, *47*, 10469-10478. (b) Thomas, K. E.; Conradie, J.; Hansen, L. K.; Ghosh, A. A Metallocorrole with Orthogonal Pyrrole Rings. *Eur. J. Inorg. Chem.* **2011**, *2011*, 1865-1870.
148. Alemayehu, A.; Conradie, J.; Ghosh, A. A First TDDFT Study of Metallocorrole Electronic Spectra: Copper meso-Triarylcorroles Exhibit Hyper Spectra. *Eur. J. Inorg. Chem.* **2011**, *2011*, 1857-1864.
149. Alemayehu, A.; Conradie, M. M.; Ghosh, A. Electronic Absorption Spectra of Copper Corroles: Unexpected Substituent Effects in Trans-*meso*-A_2B-Triarylcorrole Complexes. *J. Porphyrins Phthalocyanines* **2012**, *16*, 695-704.
150. Brückner, C.; Barta, C. A.; Briñas, R. P.; Krause Bauer, J. A. Synthesis and Structure of [*meso*-Triarylcorrolato]silver(III). *Inorg. Chem.* **2003**, *42*, 1673-1680.
151. Thomas, K. E.; Alemayehu, A. B.; Conradie, J.; Beavers, C.; Ghosh, A. Synthesis and Molecular Structure of Gold Triarylcorroles. *Inorg. Chem.* **2011**, *50*, 12844-12851.
152. Thomas, K. E.; Vazquez-Lima, H.; Fang, Y.; Song, Y.; Gagnon, K. J.; Beavers, C. M.; Kadish, K. M.; Ghosh, A. Ligand Noninnocence in Coinage Metal Corroles: A Silver Knife-Edge. *Chem. Eur. J.* **2015**, *21*, 16839-16847.
153. Sarangi, R.; Giles, L. J.; Thomas, K. E.; Ghosh, A. Ligand Noninnocence in Silver Corroles: A XANES Investigation. *Eur. J. Inorg. Chem.* **2016**, *2016*, 3225-3227.
154. (a) Bendix, J.; Dmochowski, I. J.; Gray, H. B.; Mahammed, A.; Simkhovich, L.; Gross, Z. Structural, Electrochemical, and Photophysical Properties of Gallium(III) 5,10,15-Tris(pentafluorophenyl)corrole. *Angew. Chem. Int. Ed.* **2000**, *39*, 4048-4051. (b) Liu, X.; Mahammed, A.; Tripathy, U.; Gross, Z.; Steer, R. P. Photophysics of Soret-Excited Tetrapyrroles in Solution. III. Porphyrin Analogues: Aluminum and Gallium Corroles. *Chem. Phys. Lett.* **2008**, *459*, 113-118.
155. (a) Nardis, S.; Mandoj, F.; Paolesse, R.; Fronczek, F. R.; Smith, K. M.; Prodi, L.; Montalti, M.; Battistini, G. Synthesis and Functionalization of Germanium

Triphenylcorrolate: The First Example of a Partially Brominated Corrole. *Eur. J. Inorg. Chem.* **2007**, *2007*, 2345-2352. (b) Mastroianni, M.; Zhu, W.; Stefanelli, M.; Nardis, S.; Fronczek, F. R.; Smith, K. M.; Ou, Z.; Kadish, K. M.; Paolesse, R. *β*-Nitro Derivatives of Germanium(IV) Corrolates. *Inorg. Chem.* **2008**, *47*, 11680-11687.

156. (a) Kadish, K. M.; Will, S.; Adamian, V. A.; Walther, B.; Erben, C.; Ou, Z.; Guo, N.; Vogel, E. Synthesis and Electrochemistry of Tin(IV) Octaethylcorroles, (OEC)Sn(C_6H_5) and (OEC)SnCl. *Inorg. Chem.* **1998**, *37*, 4573-4577. (b) Tsay, O. G.; Kim, B.-K.; Luu, T. L.; Kwak, J.; Churchill, D. G. Synthetic, ^{119}Sn NMR Spectroscopic, Electrochemical, and Reactivity Study of Organotin A_3 Corrolates Including Chiral and Ferrocenyl Derivatives. *Inorg. Chem.* **2013**, *52*, 1991-1999.
157. (a) Ghosh, A.; Ravikanth, M. Synthesis, Structure, Spectroscopic, and Electrochemical Properties of Highly Fluorescent Phosphorus(V)–meso-Triarylcorroles. *Chem. Eur. J.* **2012**, *18*, 6386-6396. (b) Kadish, K. M.; Ou, Z.; Adamian, V. A.; Guilard, R.; Gros, C. P.; Erben, C.; Will, S.; Vogel, E. Corroles with Group 15 Ions. 2. Synthesis and Characterization of Octaethylcorroles Containing a Phosphorus Central Atom. *Inorg. Chem.* **2000**, *39*, 5675-5682.
158. Kadish, K. M.; Erben, C.; Ou, Z.; Adamian, V. A.; Will, S.; Vogel, E. Corroles with Group 15 Metal Ions. Synthesis and Characterization of Octaethylcorroles Containing As, Sb, and Bi Ions in +3, +4, and +5 Oxidation States. *Inorg. Chem.* **2000**, *39*, 3312-3319.
159. Alemayehu, A. B.; Gagnon, K. J.; Terner, J.; Ghosh, A. Oxidative Metalation as a Route to Size-Mismatched Macrocyclic Complexes: Osmium Corroles. *Angew. Chem. Int. Ed.* **2014**, *53*, 14411-14414.
160. Einrem, R. F.; Gagnon, K. J.; Alemayehu, A. B.; Ghosh, A. Metal–Ligand Misfits: Facile Access to Rhenium–Oxo Corroles by Oxidative Metalation. *Chem. Eur. J.* **2016**, *22*, 517-520.
161. Einrem, R. F.; Braband, H.; Fox, T.; Vazquez-Lima, H.; Alberto, R.; Ghosh, A. Synthesis and Molecular Structure of ^{99}Tc Corroles. *Chem. Eur. J.* **2016**, *22*, 18747-18751.
162. Alemayehu, A. B.; Vazquez-Lima, H.; Gagnon, K. J.; Ghosh, A. Stepwise Deoxygenation of Nitrite as a Route to Two Families of Ruthenium Corroles: Group 8 Periodic Trends and Relativistic Effects. *Inorg. Chem.* **2017**, *56*, 5285-5294.
163. Johansen, I.; Norheim, H.-K.; Larsen, S.; Alemayehu, A. B.; Conradie, J.; Ghosh, A. Substituent Effects on Metallocorrole Spectra: Insights from Chromium-Oxo and Molybdenum-Oxo Triarylcorroles. *J. Porphyrins Phthalocyanines* **2011**, *15*, 1335-1344.
164. (a) Alemayehu, A. B.; Vazquez-Lima, H.; Gagnon, K. J.; Ghosh, A. Tungsten Biscorroles: New Chiral Sandwich Compounds. *Chem. eur. J.* **2016**, *22*, 6914-6920. (b) Alemayehu, A. B.; Vazquez-Lima, H.; McCormick, L. J.; Ghosh, A. Relativistic Effects in Metallocorroles: Comparison of Molybdenum and Tungsten Biscorroles. *Chem. Commun.* **2017**, *53*, 5830-5833.
165. Rabinovich, E.; Goldberg, I.; Gross, Z. Gold(I) and Gold(III) Corroles. *Chem. Eur. J.* **2011**, *17*, 12294-12301.
166. Thomas, K. E.; Beavers, C. M.; Ghosh, A. Molecular Structure of a Gold *β*-Octakis(trifluoromethyl)-*meso*-Triarylcorrole: an 85° Difference in Saddling Dihedral Relative to Copper. *Mol. Phys.* **2012**, *110*, 2439-2444.
167. Alemayehu, A. B.; Ghosh, A. Gold corroles. *J. Porphyrins Phthalocyanines* **2011**, *15*, 106-110.
168. Liu, H.-Y.; Mahmood, M. H. R.; Qiu, S.-X.; Chang, C. K. Recent developments in Manganese Corrole Chemistry. *Coord. Chem. Rev.* **2013**, *257*, 1306-1333.

169. Broring, M.; Hell, C. Manganese as a Template: a New Synthesis of Corrole. *Chem. Commun.* **2001**, 2336-2337.
170. Gross, Z.; Golubkov, G.; Simkhovich, L. Epoxidation Catalysis by a Manganese Corrole and Isolation of an Oxomanganese(V) Corrole. *Angew. Chem. Int. Ed.* **2000**, *39*, 4045-4047.
171. Liu, H.-Y.; Lai, T.-S.; Yeung, L.-L.; Chang, C. K. First Synthesis of Perfluorinated Corrole and Its MnO Complex. *Org. Lett.* **2003**, *5*, 617-620.
172. Gershman, Z.; Goldberg, I.; Gross, Z. DNA Binding and Catalytic Properties of Positively Charged Corroles. *Angew. Chem. Int. Ed.* **2007**, *46*, 4320-4324.
173. Fryxelius, J.; Eilers, G.; Feyziyev, Y.; Magnuson, A.; Sun, L.; Lomoth, R. Synthesis and Redox Properties of a [*meso*-Tris(4-nitrophenyl) Corrolato]Mn(III) Complex. *J. Porphyrins Phthalocyanines* **2005**, *09*, 379-386.
174. Ou, Z.; Erben, C.; Autret, M.; Will, S.; Rosen, D.; Lex, J.; Vogel, E.; Kadish, K. M. Manganese(III) and Manganese(IV) Corroles: Synthesis, Spectroscopic, Electrochemical and X-ray Structural Characterization. *J. Porphyrins Phthalocyanines* **2005**, *09*, 398-412.
175. Bendix, J.; Gray, H. B.; Golubkov, G.; Gross, Z. High-field (High-Frequency) EPR Spectroscopy and Structural Characterization of a Novel Manganese(III) Corrole. *Chem. Commun.* **2000**, 1957-1958.
176. Kumar, A.; Goldberg, I.; Botoshansky, M.; Buchman, Y.; Gross, Z. Oxygen Atom Transfer Reactions from Isolated (Oxo)manganese(V) Corroles to Sulfides. *J. Am. Chem. Soc.* **2010**, *132*, 15233-15245.
177. Krzystek, J.; Telser, J.; Hoffman, B. M.; Brunel, L.-C.; Licoccia, S. High-Frequency and Field EPR Investigation of (8,12-Diethyl-2,3,7,13,17,18-Hexamethylcorrolato)manganese(III). *J. Am. Chem. Soc.* **2001**, *123*, 7890-7897.
178. Licoccia, S.; Morgante, E.; Paolesse, R.; Polizio, F.; Senge, M. O.; Tondello, E.; Boschi, T. Tetracoordinated Manganese(III) Alkylcorrolates. Spectroscopic Studies and the Crystal and Molecular Structure of (7,13-Dimethyl-2,3,8,12,17,18-Hexaethylcorrolato)manganese(III). *Inorg. Chem.* **1997**, *36*, 1564-1570.
179. Gao, B.; Ou, Z.; Chen, X.; Huang, S.; Li, B.; Fang, Y.; Kadish, K. M. Spectroelectrochemical Characterization of *meso* Triaryl-Substituted Mn(IV), Mn(III) and Mn(II) corroles. Effect of Solvent and Oxidation State on UV-visible Spectra and Redox Potentials in Nonaqueous Media. *J. Porphyrins Phthalocyanines* **2014**, *18*, 1131-1144.
180. Shen, J.; El Ojaimi, M.; Chkounda, M.; Gros, C. P.; Barbe, J.-M.; Shao, J.; Guilard, R.; Kadish, K. M. Solvent, Anion, and Structural Effects on the Redox Potentials and UV−visible Spectral Properties of Mononuclear Manganese Corroles. *Inorg. Chem.* **2008**, *47*, 7717-7727.
181. Golubkov, G.; Bendix, J.; Gray, H. B.; Mahammed, A.; Goldberg, I.; DiBilio, A. J.; Gross, Z. High-Valent Manganese Corroles and the First Perhalogenated Metallocorrole Catalyst. *Angew. Chem. Int. Ed.* **2001**, *40*, 2132-2134.
182. Bröring, M.; Hell, C.; Steiner, M.; Brandt, C. D. Halogenido and Pseudohalogenido Complexes of (2,3,7,8,12,13,17,18-Octaethyl-5,15-Di-*p*-tolylcorrolato)manganese(IV). *Z. Anorg. Allg. Chem.* **2007**, *633*, 1082-1086.
183. Singh, P.; Dutta, G.; Goldberg, I.; Mahammed, A.; Gross, Z. Expected and Unexpected Transformations of Manganese(III) Tris(4-nitrophenyl)corrole. *Inorg. Chem.* **2013**, *52*, 9349-9355.
184. Broring, M.; Hell, C.; Brandt, C. D. Iodomanganesecorrole - a Stable Mn^{IV}-I Species. *Chem. Commun.* **2007**, 1861-1862.

185. (a) Steene, E.; Wondimagegn, T.; Ghosh, A. Electrochemical and Electronic Absorption Spectroscopic Studies of Substituent Effects in Iron(IV) and Manganese(IV) Corroles. Do the Compounds Feature High-Valent Metal Centers or Noninnocent Corrole Ligands? Implications for Peroxidase Compound I and II Intermediates. *J. Phys. Chem. B* **2001**, *105*, 11406-11413. (b) Additions and Corrections: *J. Phys. Chem. B* **2002**, *106*, 5312-5312.
186. Steene, E.; Wondimagegn, T.; Ghosh, A. Resonance Raman spectroscopy and density functional theoretical calculations of manganese corroles. *J. of Inorg. Biochem.* **2002**, *88*, 113-118.
187. Bröring, M.; Cordes, M.; Köhler, S. Manganese(IV) Corroles with σ-Aryl Ligands. *Z. Anorg. Allg. Chem.* **2008**, *634*, 125-130.
188. Kadish, K. M.; Adamian, V. A.; Van Caemelbecke, E.; Gueletii, E.; Will, S.; Erben, C.; Vogel, E. Electrogeneration of Oxidized Corrole Dimers. Electrochemistry of (OEC)M Where M = Mn, Co, Ni, or Cu and OEC Is the Trianion of 2,3,7,8,12,13,17,18-Octaethylcorrole. *J. Am. Chem. Soc.* **1998**, *120*, 11986-11993.
189. Fang, Y.; Ou, Z.; Kadish, K. M. Electrochemistry of Corroles in Nonaqueous Media. *Chem. Rev.* **2017**, *117*, 3377-3419.
190. Vogel, E.; Will, S.; Tilling, A. S.; Neumann, L.; Lex, J.; Bill, E.; Trautwein, A. X.; Wieghardt, K. Metallocorroles with Formally Tetravalent Iron. *Angew. Chem. Int. Ed.* **1994**, *33*, 731-735.
191. Simkhovich, L.; Mahammed, A.; Goldberg, I.; Gross, Z. Synthesis and Characterization of Germanium, Tin, Phosphorus, Iron, and Rhodium Complexes of Tris(pentafluorophenyl)corrole, and the Utilization of the Iron and Rhodium Corroles as Cyclopropanation Catalysts. *Chem. Eur. J.* **2001**, *7*, 1041-1055.
192. Walker, F. A. In *The Porphyrin Handbook*; Kadish, K. M., Smith, K. M., Guilard, R., Eds.; Academic Press: San Diego, CA, 2000; Vol. 5, Chapter 36, pp 81-183.
193. Simkhovich, L.; Goldberg, I.; Gross, Z. Iron(III) and Iron(IV) Corroles: Synthesis, Spectroscopy, Structures, and No Indications for Corrole Radicals. *Inorg. Chem.* **2002**, *41*, 5433-5439.

194. Hocking, R. K.; George, S. D.; Gross, Z.; Walker, F. A.; Hodgson, K. O.; Hedman, B.; Solomon, E. I. Fe L- and K-edge XAS of Low-Spin Ferric Corrole: Bonding and Reactivity Relative to Low-Spin Ferric Porphyrin. *Inorg. Chem.* **2009**, *48*, 1678-1688.
195. Simkhovich, L.; Galili, N.; Saltsman, I.; Goldberg, I.; Gross, Z. Coordination Chemistry of the Novel 5,10,15-Tris(pentafluorophenyl)corrole: Synthesis, Spectroscopy, and Structural Characterization of Its Cobalt(III), Rhodium(III), and Iron(IV) Complexes. *Inorg. Chem.* **2000**, *39*, 2704-2705.
196. Simkhovich, L.; Gross, Z. Halogeno-Coordinated Iron Corroles. *Inorg. Chem.* **2004**, *43*, 6136-6138.
197. Cai, S.; Walker, F. A.; Licoccia, S. NMR and EPR Investigations of Iron Corrolates: Iron(III) Corrolate π Cation Radicals or Iron(IV) Corrolates? *Inorg. Chem.* **2000**, *39*, 3466-3478.
198. Zakharieva, O.; Schünemann, V.; Gerdan, M.; Licoccia, S.; Cai, S.; Walker, F. A.; Trautwein, A. X. Is the Corrolate Macrocycle Innocent or Noninnocent? Magnetic Susceptibility, Mössbauer, ^{1}H NMR, and DFT Investigations of Chloro- and Phenyliron Corrolates. *J. Am. Chem. Soc.* **2002**, *124*, 6636-6648.
199. Cai, S.; Licoccia, S.; D'Ottavi, C.; Paolesse, R.; Nardis, S.; Bulach, V.; Zimmer, B.; Shokhireva, T. K.; Ann Walker, F. Chloroiron *meso*-Triphenylcorrolates: Electronic Ground State and Spin Delocalization. *Inorg. Chim. Acta* **2002**, *339*, 171-178.

200. Nardis, S.; Paolesse, R.; Licoccia, S.; Fronczek, F. R.; Vicente, M. G. H.; Shokhireva, T. K.; Cai, S.; Walker, F. A. NMR and Structural Investigations of a Nonplanar Iron Corrolate: Modified Patterns of Spin Delocalization and Coupling in A Slightly Saddled Chloroiron(III) Corrolate Radical. *Inorg. Chem.* **2005**, *44*, 7030-7046.
201. Yatsunyk, L.; Walker, F. A. ^{19}F Isotropic Shifts in Paramagnetic Iron(III) Octaethyltetraphenylporphyrinate and Tetraphenylporphyrinate Complexes of a Variety of Electronic Ground States: Implications for the Electron Configuration of Chloroiron Tri-(pentafluorophenyl)corrolate. *Inorg. Chim. Acta* **2002**, *337*, 266-274.
202. (a) Ghosh, A.; Steene, E. High-valent transition Metal Centers versus Noninnocent Ligands in Metallocorroles: Insights from Electrochemistry and Implications for High-Valent Heme Protein Intermediates. *J. Inorg. Biochem.* **2002**, *91*, 423-436. (b) Ghosh, A.; Vangberg, T.; Gonzalez, E.; Taylor, P. Molecular Structures and Electron Distributions of Higher-Valent Iron and Manganese Porphyrins. Density Functional Theory Calculations and some Preliminary Open-Shell Coupled-Cluster Results. *J. Porphyrins Phthalocyanines* **2001**, *5*, 345-356.
203. Roos, B. O.; Veryazov, V.; Conradie, J.; Taylor, P. R.; Ghosh, A. Not Innocent: Verdict from Ab Initio Multiconfigurational Second-Order Perturbation Theory on the Electronic Structure of Chloroiron Corrole. *J. Phys. Chem. B* **2008**, *112*, 14099-14102.
204. Ye, S.; Tuttle, T.; Bill, E.; Simkhovich, L.; Gross, Z.; Thiel, W.; Neese, F. The Electronic Structure of Iron Corroles: A Combined Experimental and Quantum Chemical Study. *Chem. Eur. J.* **2008**, *14*, 10839-10851.
205. Nardis, S.; Cicero, D. O.; Licoccia, S.; Pomarico, G.; Berionni Berna, B.; Sette, M.; Ricciardi, G.; Rosa, A.; Fronczek, F. R.; Smith, K. M.; Paolesse, R. Phenyl Derivative of Iron 5,10,15-Tritolylcorrole. *Inorg. Chem.* **2014**, *53*, 4215-4227.
206. Nakano, K.; Kobayashi, K.; Ohkawara, T.; Imoto, H.; Nozaki, K. Copolymerization of Epoxides with Carbon Dioxide Catalyzed by Iron–Corrole Complexes: Synthesis of a Crystalline Copolymer. *J. Am. Chem. Soc.* **2013**, *135*, 8456-8459.
207. Stefanelli, M.; Nardis, S.; Tortora, L.; Fronczek, F. R.; Smith, K. M.; Licoccia, S.; Paolesse, R. Nitration of Iron Corrolates: Further Evidence for Non-Innocence of the Corrole Ligand. *Chem. Commun.* **2011**, *47*, 4255-4257.
208. Zhang, Y.; Wen, J.-y.; Wang, X.-l.; Mahmood, M. H. R.; Liu, Z.-Y.; Wang, H.; Ji, L.-n.; Liu, H.-y. DNA Binding and Nuclease Activity of Cationic Iron(IV) and Manganese(III) Corrole Complexes. *Appl. Organometal. Chem.* **2014**, *28*, 559-566.
209. (a) Schwalbe, M.; Dogutan, D. K.; Stoian, S. A.; Teets, T. S.; Nocera, D. G. Xanthene-Modified and Hangman Iron Corroles. *Inorg. Chem.* **2011**, *50*, 1368-1377. (b) Zyska, B.; Schwalbe, M. Synthesis of Sterically Hindered Xanthene-Modified Iron Corroles with Catalase-Like Activity. *Chem. Commun.* **2013**, *49*, 3799-3801.
210. Mahammed, A.; Gross, Z. Highly Efficient Catalase Activity of Metallocorroles. *Chem. Commun.* **2010**, *46*, 7040-7042.
211. (a) Chen, T.-H.; Kwong, K. W.; Carver, A.; Luo, W.; Zhang, R. Enhanced iron(III) Corrole-Catalyzed Oxidations with Iodobenzene Diacetate: Synthetic and Mechanistic Investigations. *Appl. Catal. A: General* **2015**, *497*, 121-126. (b) Chen, T.-H.; Kwong, K. W.; Lee, N. F.; Ranburger, D.; Zhang, R. Highly Efficient and Chemoselective Oxidation of Sulfides catalyzed by Iron(III) Corroles with Iodobenzene Diacetate. *Inorg. Chim. Acta* **2016**, *451*, 65-72.
212. (a) Harischandra, D. N.; Lowery, G.; Zhang, R.; Newcomb, M. Production of a Putative Iron(V)−Oxocorrole Species by Photo-Disproportionation of a Bis-Corrole−Diiron(IV)−μ-Oxo Dimer: Implication for a Green Oxidation Catalyst. *Org. Lett.* **2009**, *11*, 2089-2092. (b) Zhang, R.; Vanover, E.; Chen, T.-H.; Thompson, H.

Visible Light-Driven Aerobic Oxidation Catalyzed by a Diiron(IV) μ-oxo Biscorrole Complex. *Appl. Catal. A: General* **2013**, *464*, 95-100.
213. (a) Paolesse, R.; Licoccia, S.; Fanciullo, M.; Morgante, E.; Boschi, T. Synthesis and Characterization of Cobalt(III) Complexes of *Meso*-Phenyl-Substituted Corroles. *Inorg. Chim. Acta* **1993**, *203*, 107-114. (b) Licoccia, S.; Tassoni, E.; Paolesse, R.; Boschi, T. The Effect of Steric Hindrance in the Synthesis of Corrolates via the Cobalt Catalyzed Cyclization of 2-(α-hydroxyalkyl)pyrroles. *Inorg. Chim. Acta* **1995**, *235*, 15-20.
214. Mahammed, A.; Giladi, I.; Goldberg, I.; Gross, Z. Synthesis and Structural Characterization of a Novel Covalently-Bound Corrole Dimer. *Chem. Eur. J.* **2001**, *7*, 4259-4265.
215. Simkhovich, L.; Goldberg, I.; Gross, Z. Easy Preparation of Cobalt Corrole and Hexaphyrin and Isolation of New Oligopyrroles in the Solvent-Free Condensation of Pyrrole with Pentafluorobenzaldehyde. *Org. Lett.* **2003**, *5*, 1241-1244.
216. (a) Thomas, K. E.; Conradie, J.; Hansen, L. K.; Ghosh, A. Corroles Cannot Ruffle. *Inorg. Chem.* **2011**, *50*, 3247-3251. (b) Goldschmidt, R.; Goldberg, I.; Balazs, Y.; Gross, Z. Synthesis and Properties of a Corrole with Small and Electron-Withdrawing Substitutents, 5,15-bis(trifluoromethyl)-10-Pentafluorophenylcorrole. *J. Porphyrins Phthalocyanines* **2006**, *10*, 76-86.
217. Tang, J.; Ou, Z.; Ye, L.; Yuan, M.; Fang, Y.; Xue, Z.; Kadish, K. M. *Meso*-Dichlorophenyl Substituted Co(III) Corrole: A selective Electrocatalyst for the Two-Electron Reduction of Dioxygen in Acid Media, X-ray Crystal Structure Analysis and Electrochemistry. *J. Porphyrins Phthalocyanines* **2014**, *18*, 891-898.
218. Chen, C.; Zhu, Y.-Z.; Fan, Q.-J.; Song, H.-B.; Zheng, J.-Y. Syntheses of Corrole Derivatives and their Supramolecular Interactions with Fullerenes in Solution and the Solid State. *Tetrahedron Lett.* **2013**, *54*, 4143-4147.
219. Li, B.; Ou, Z.; Meng, D.; Tang, J.; Fang, Y.; Liu, R.; Kadish, K. M. Cobalt Triarylcorroles Containing One, Two or Three Nitro Groups. Effect of NO_2 Substitution on Electrochemical Properties and Catalytic Activity for Reduction of Molecular Oxygen in Acid Media. *J. Inorg. Biochem.* **2014**, *136*, 130-139.
220. Sun, J.; Ou, Z.; Guo, R.; Fang, Y.; Chen, M.; Song, Y.; Kadish, K. M. Synthesis and Electrochemistry of Cobalt Tetrabutanotriarylcorroles. Highly Selective Electrocatalysts for Two-Electron Reduction of Dioxygen in Acidic and Basic Media. *J. Porphyrins Phthalocyanines* **2016**, *20*, 456-464.
221. (a) Huang, S.; Fang, Y.; Lü, A.; Lu, G.; Ou, Z.; Kadish, K. M. Synthesis, Characterization and Solvent/Structural Effects on Spectral and Redox Properties of Cobalt Triphenylcorroles in Nonaqueous Media. *J. Porphyrins Phthalocyanines* **2012**, *16*, 958-967.(b) Ou, Z.; Lü, A.; Meng, D.; Huang, S.; Fang, Y.; Lu, G.; Kadish, K. M. Molecular Oxygen Reduction Electrocatalyzed by *meso*-Substituted Cobalt Corroles Coated on Edge-Plane Pyrolytic Graphite Electrodes in Acidic Media. *Inorg. Chem.* **2012**, *51*, 8890-8896.
222. Adamian, V. A.; D'Souza, F.; Licoccia, S.; Di Vona, M. L.; Tassoni, E.; Paolesse, R.; Boschi, T.; Kadish, K. M. Synthesis, Characterization, and Electrochemical Behavior of (5,10,15-Tri-X-phenyl-2,3,7,8,12,13,17,18-octamethylcorrolato)cobalt(III) Triphenylphosphine Complexes, Where X = *p*-OCH_3, *p*-CH_3, *p*-Cl, *m*-Cl, *o*-Cl, *m*-F, or *o*-F. *Inorg. Chem.* **1995**, *34*, 532-540.
223. Zhu, W.; Huang, T.; Qin, M.; Li, M.; Mack, J.; Liang, X. Tuning the Synthetic Cobalt(III)corroles Electroreductive Catalyzed Lindane Dehalogenation Reactivity through *meso*-Substituents. *J. Electroanalytical Chem.* **2016**, *774*, 58-65.

224. Grodkowski, J.; Neta, P.; Fujita, E.; Mahammed, A.; Simkhovich, L.; Gross, Z. Reduction of Cobalt and Iron Corroles and Catalyzed Reduction of CO_2. *J. Phys. Chem. A* **2002**, *106*, 4772-4778.
225. Wang, Y.; Ou, Z.; Fang, Y.; Guo, R.; Tang, J.; Song, Y.; Kadish, K. M. Synthesis and Electrochemistry of A_2B type Mono- and Bis-Cobalt Triarylcorroles and their Electrocatalytic Properties for Reduction of Dioxygen in Acid Media. *J. Porphyrins Phthalocyanines* **2016**, *20*, 1284-1295.
226. Saltsman, I.; Goldberg, I.; Gross, Z. Porphyrins and Corroles with 2,6-Pyrimidyl Substituents. *Org. Lett.* **2015**, *17*, 3214-3217.
227. Maiti, N.; Lee, J.; Kwon, S. J.; Kwak, J.; Do, Y.; Churchill, D. G. Synthetic, Crystallographic and Electrochemical studies of Thienyl-Substituted Corrole Complexes of Copper and Cobalt. *Polyhedron* **2006**, *25*, 1519-1530.
228. (a) Ooi, S.; Tanaka, T.; Osuka, A. Cobalt(III) and Gallium(III) Complexes of *meso*-Free Corroles with Distinct Position-Dependent Substituent Effects. *J. Porphyrins Phthalocyanines* **2016**, *20*, 274-281. (b) Ooi, S.; Tanaka, T.; Osuka, A. Metal Complexes of *meso–meso* Linked Corrole Dimers. *Inorg. Chem.* **2016**, *55*, 8920-8927.
229. Mahammed, A.; Botoshansky, M.; Gross, Z. Chlorinated Corroles. *Dalton Trans.* **2012**, *41*, 10938-10940.
230. Rhoda, H. M.; Crandall, L. A.; Geier, G. R.; Ziegler, C. J.; Nemykin, V. N. Combined MCD/DFT/TDDFT Study of the Electronic Structure of Axially Pyridine Coordinated Metallocorroles. *Inorg. Chem.* **2015**, *54*, 4652-4662.
231. Lei, H.; Han, A.; Li, F.; Zhang, M.; Han, Y.; Du, P.; Lai, W.; Cao, R. Electrochemical Spectroscopic and Theoretical Studies of a Simple Bifunctional Cobalt Corrole Catalyst for Oxygen Evolution and Hydrogen Production. *Phys. Chem. Chem. Phys.* **2014**, *16*, 1883-1893.
232. Wang, Z.; Lei, H.; Cao, R.; Zhang, M. Cobalt Corrole on Carbon Nanotube as a Synergistic Catalyst for Oxygen Reduction Reaction in Acid Media. *Electrochim. Acta* **2015**, *171*, 81-88.
233. Lei, H.; Liu, C.; Wang, Z.; Zhang, Z.; Zhang, M.; Chang, X.; Zhang, W.; Cao, R. Noncovalent Immobilization of a Pyrene-Modified Cobalt Corrole on Carbon Supports for Enhanced Electrocatalytic Oxygen Reduction and Oxygen Evolution in Aqueous Solutions. *ACS Catal.* **2016**, *6*, 6429-6437.
234. Mahammed, A.; Tumanskii, B.; Gross, Z. Effect of Bromination on the Electrochemistry, Frontier Orbitals, and Spectroscopy of Metallocorroles. *J. Porphyrins Phthalocyanines* **2011**, *15*, 1275-1286.
235. Mahammed, A.; Mondal, B.; Rana, A.; Dey, A.; Gross, Z. The Cobalt Corrole Catalyzed Hydrogen Evolution Reaction: Surprising Electronic Effects and Characterization of Key Reaction Intermediates. *Chem. Commun.* **2014**, *50*, 2725-2727.
236. Mondal, B.; Sengupta, K.; Rana, A.; Mahammed, A.; Botoshansky, M.; Dey, S. G.; Gross, Z.; Dey, A. Cobalt Corrole Catalyst for Efficient Hydrogen Evolution Reaction from H_2O under Ambient Conditions: Reactivity, Spectroscopy, and Density Functional Theory Calculations. *Inorg. Chem.* **2013**, *52*, 3381-3387.
237. Mittra, K.; Mondal, B.; Mahammed, A.; Gross, Z.; Dey, A. Dioxygen Bound Cobalt Corroles. *Chem. Commun.* **2017**, *53*, 877-880.
238. (a) Guilard, R.; Gros, C. P.; Bolze, F.; Jérôme, F.; Ou, Z.; Shao, J.; Fischer, J.; Weiss, R.; Kadish, K. M. Alkyl and Aryl Substituted Corroles. 1. Synthesis and Characterization of Free Base and Cobalt Containing Derivatives. X-ray Structure of $(Me_4Ph_5Cor)Co(py)_2$. *Inorg. Chem.* **2001**, *40*, 4845-4855. (b) Kadish, K. M.; Shao, J.; Ou, Z.; Gros, C. P.; Bolze, F.; Barbe, J.-M.; Guilard, R. Alkyl- and Aryl-Substituted

Corroles. 4. Solvent Effects on the Electrochemical and Spectral Properties of Cobalt Corroles. *Inorg. Chem.* **2003**, *42*, 4062-4070.
239. Lemon, C. M.; Dogutan, D. K.; Nocera, D. G. Porphyrin and Corrole Platforms for Water Oxidation, Oxygen Reduction, and Peroxide Dismutation. *In* Handbook of Porphyrin Science. Kadish, K. M.; Smith, K. M.; Guilard, R. (eds). 2012, vol. 21, pp. 1–143. DOI: 10.1142/9789814397605_0001.
240. Barbe, J.-M.; Canard, G.; Brandes, S.; Jerome, F.; Dubois, G.; Guilard, R. Metallocorroles as Sensing Components for Gas Sensors: Remarkable Affinity and Selectivity of Cobalt(III) Corroles for CO vs. O_2 and N_2. *Dalton Trans.* **2004**, 1208-1214.
241. (a) Barbe, J.-M.; Canard, G.; Brandès, S.; Guilard, R. Organic–Inorg. Hybrid Sol–Gel Materials Incorporating Functionalized Cobalt(III) Corroles for the Selective Detection of CO. *Angew. Chem. Int. Ed.* **2005**, *44*, 3103-3106. (b) Barbe, J.-M.; Canard, G.; Brandès, S.; Guilard, R. Selective Chemisorption of Carbon Monoxide by Organic–Inorganic Hybrid Materials Incorporating Cobalt(III) Corroles as Sensing Components. *Chem. Eur. J.* **2007**, *13*, 2118-2129.
242. Vazquez-Lima, H.; Conradie, J.; Ghosh, A. Metallocorrole Interactions with Carbon Monoxide, Nitric Oxide, and Nitroxyl—A DFT Study of Low-Energy Bound States. *Inorg. Chem.* **2016**, *55*, 8248-8250.
243. (a) Grigg, R.; Trocha-Grimshaw, J.; Viswanatha, V. Rhodium (I) Complexes of Olypyrrole Macrocycles. *Tetrahedron Lett.* **1976**, *17*, 289-292. (b) Abeysekera, A. M.; Grigg, R.; Trocha-Grimshaw, J.; Viswanatha, V. Dicarbonylrhodium(I) Complexes of Polypyrrole Macrocycles. Part 1. Preparation and Oxidative Addition Reactions with Alkyl Halides and Carboxylic Acid Anhydrides. *J. Chem. Soc., Perkin Trans. 1* **1977**, 36-44. (c) Abeysekera, A. M.; Grigg, R.; Trocha-Grimshaw, J.; King, T. J. Dicarbonylrhodium(I) Complexes of Polypyrrole Macrocycles. Part 3. Synthesis and Crystal Structures of Complexes of N-Methylcorroles, N-Methylporphyrins, and Acyclic Polypyrroles. *J. Chem. Soc., Perkin Trans. 1* **1979**, 2184-2192.
244. Simkhovich, L.; Goldberg, I.; Gross, Z. The Effects of Bulky *ortho*-Aryl Substituents in Corroles, tested by X-ray Crystallography of the Rhodium Complexes and Catalysis thereby. *J. Porphyrins Phthalocyanines* **2002**, *06*, 439-444.
245. Palmer, J. H.; Mahammed, A.; Lancaster, K. M.; Gross, Z.; Gray, H. B. Structures and Reactivity Patterns of Group 9 Metallocorroles. *Inorg. Chem.* **2009**, *48*, 9308-9315.
246. Dong, S. S.; Nielsen, R. J.; Palmer, J. H.; Gray, H. B.; Gross, Z.; Dasgupta, S.; Goddard, W. A. Electronic Structures of Group 9 Metallocorroles with Axial Ammines. *Inorg. Chem.* **2011**, *50*, 764-770.
247. Kadish, K. M.; Koh, W.; Tagliatesta, P.; Sazou, D.; Paolesse, R.; Licoccia, S.; Boschi, T. Electrochemistry of Rhodium and Cobalt corroles. Characterization of (OMC)Rh(PPh_3) and (OMC)Co(PPh_3) where OMC is the Trianion of 2,3,7,8,12,13,17,18-octamethylcorrole. *Inorg. Chem.* **1992**, *31*, 2305-2313.
248. Kurahashi, T. Reverse Catalase Reaction: Dioxygen Activation via Two-Electron Transfer from Hydroxide to Dioxygen Mediated by a Manganese(III) Salen Complex. *Inorg. Chem.* **2015**, *54*, 8356-8366.

List of Papers

(a) Ganguly, S.; Vazquez-Lima, H.; Ghosh, A. Wolves in Sheep's Clothing: *μ*-Oxo-Diiron Corroles Revisited. *Chem. Eur. J.* **2016**, *22*, 10336-10340.

(b) Ganguly, S.; Giles, L. J.; Thomas, K. E.; Sarangi, R.; Ghosh, A. Ligand Noninnocence in Iron Corroles: Insights from Optical and X-ray Absorption Spectroscopies and Electrochemical Redox Potentials. *Chem. Eur. J.* **2017**, 23, 1-10.

(c) Ganguly, S.; Renz, D.; Giles, L. J.; Gagnon, K.J.; McCormick, L. J.; Conradie, J.; Sarangi, R.; Ghosh, A. Cobalt- and Rhodium-Corrole-Triphenylphosphine Complexes Revisited: The Question of a Noninnocent Corrole. Submitted to *Inorg. Chem*.

(d) Ganguly, S.; Conradie, J.; Bendix. J.; Gagnon, K.J.; McCormick, L. J.; Ghosh, A. Electronic Structure of Cobalt-Corrole-Pyridine Complexes: Noninnocent Five-coordinate Co(II) Corrole-Radical States. Submitted to *J. Phys. Chem. A.*